Development of chemically functionalized oligonucleotides for DNA-binding proteins labeling and DNA cross-linking

博士論文

Development of chemically functionalized oligonucleotides for DNA-binding proteins labeling and DNA cross-linking

(DNA 結合蛋白をラベル化及び DNA 架橋反応性を持つ機能性オリゴヌクレオチドの開発)

Ahmed Mostafa Ahmed Ibrahim Abdel Hady

令和 4 年

Tohoku University
Graduate School of Science
Department of Chemistry
Sendai 980-8578, Japan

APPROVAL SHEET

This is to certify that this Ph.D. thesis entitled "**Development of chemically functionalized oligonucleotides for DNA-binding proteins labeling and DNA cross-linking**" **(DNA 結合蛋白をラベル化及び DNA 架橋反応性を持つ機能性オリゴヌクレオチドの開発)** prepared by Mr. **Ahmed Mostafa Ahmed Ibrahim Abdel Hady** in partial fulfillment of the requirements for the degree of "**Doctor of Philosophy**" is an official copy of the original Ph.D. thesis that has been examined and approved by the following Examination Committee:

_____

Prof. Fumi NAGATSUGI, Chairman of the Examination Committee

_____

Prof. Takehiko WADA

_____

Prof. Minoru UEDA

Approved

Date: 2023 / 03 / 03

_____

Prof. Masahiro TERADA

Dean, Graduate School of Science, Tohoku University
6-3, Aramaki Aza-Aoba, Aoba-ku, Sendai 980-8578, Japan

FRONTISPIECE

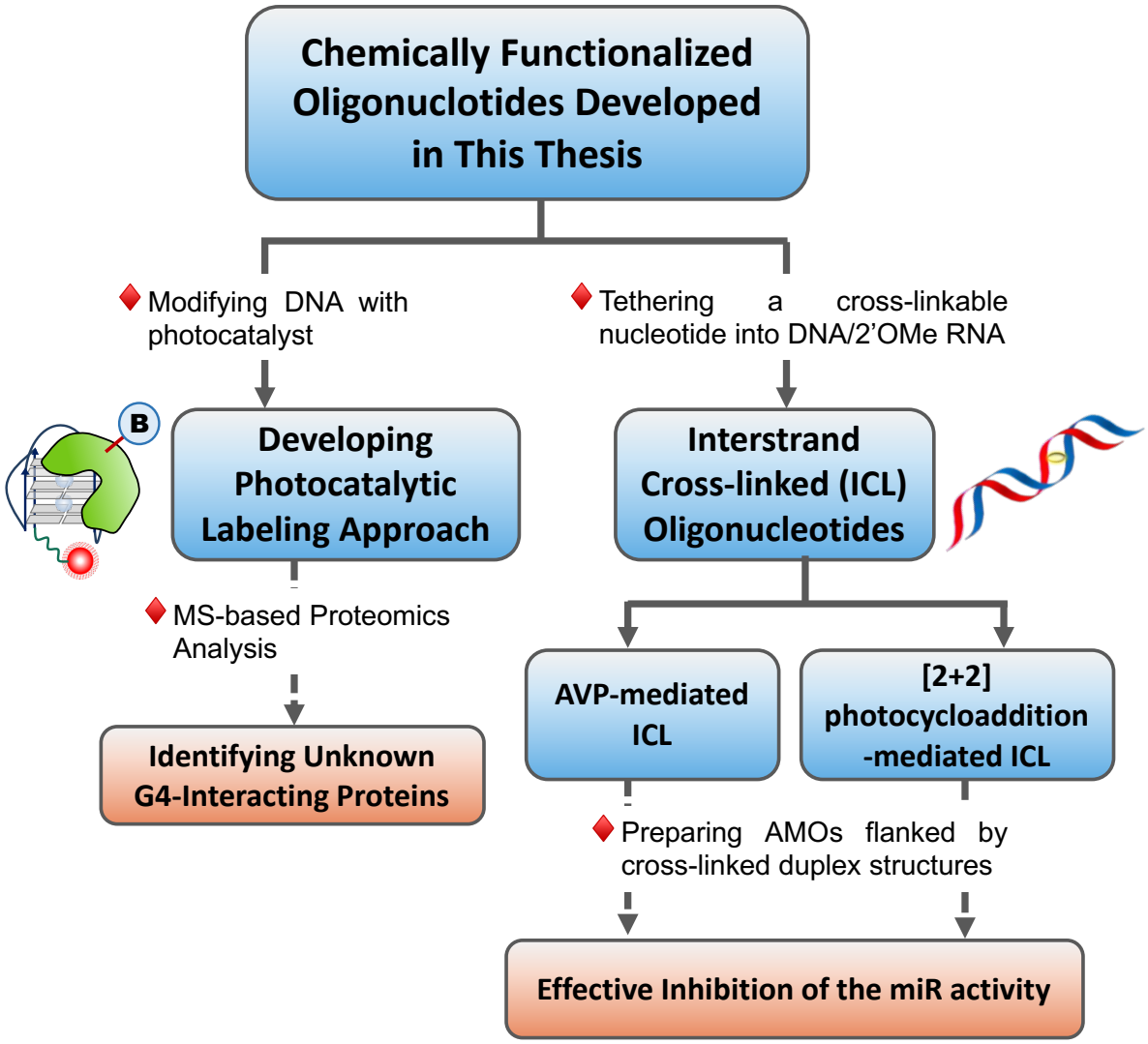

DECLARATION AND COPYRIGHTS

I, Ahmed Mostafa Ahmed Ibrahim Abdel Hady, declare that this thesis is my own original work and that it has not been presented and will not be presented to any other university for a similar or any other degree award.

Signature: _____Date: 2023 / 02 / 13

(Say, "Indeed, my prayer, my rites of sacrifice, my living and my dying are for Allah, Lord of the worlds.)

Sura: Al-An'aam – Aya: 162

ACKNOWLEDGMENT

Foremost, I would like to express my sincere gratitude to my supervisor, Prof. Fumi Nagatsugi, for her enormous support during all steps of my Ph.D. time, starting from the grand application (one year before my Ph.D.) until the end of my Ph.D. study. In my research, her wide and deep knowledge, and remarkable comments and recommendations helped me greatly to successfully achieve my Ph.D. research. Apart from research, I would like to thank her for being kind and encouraging me to enjoy my life in Japan, for unforgettable memories, and for her delicious homemade cake and traditional Japanese food.

It is really hard to find words to express my sincere gratitude to my amazing Ph.D. mentor, Dr. Kazumitsu Onizuka. I would like to say thank you, ありがとうございます, شكرًا (shkran means thank you in Arabic) to him for all that he did for me. He helped me to enjoy my projects through his smart and plentiful ideas, deep and wide knowledge, passion, and nice vision. I was so lucky to get the opportunity to learn a lot from him. What I have learned from him helped me enormously to grow rapidly and change into a better version of myself as a researcher. He really did a lot of effort in teaching me how to think, solve problems, and observe the data in a different and useful way, and offering me a suitable environment to think and dream. He was a great mentor not only for my Ph.D. but also a great mentor for life. I think after graduation his way of minoring just started.

I would like to thank Dr. Hidenori Okamura for his kind advice and comments on the seminars, and presentations which helped me to improve a lot. He gave me a piece of genuine and kind advice during discussing my research and career plans with him. He was very active in lab management and organization which helped me to do my experiments properly.

I would like to thank Dr. Yuuhei Yamano for his help and support during the time we shared in the lab. I have never hesitated to ask him for help because I know that he will be happy. As he is a nice photochemistry specialist, I really enjoyed discussing related topics with him.

I would like to thank my lab mate, Kawahara-san for his help and support in many things, e.g., document translation and supporting my proteomics experiments. I really enjoyed the time between us.

I would like to thank my lab mate, Chen-san, for the good time, for being positive and helpful. We maintained a very good relationship for more than three years. As I sat next to her, she was the most person I talk to in the lab. We had the opportunity to share the information, discuss about new trends in our field of study, and even exchange the differences in the culture between Egypt and China.

I would like to thank my friend and lab mate Nagasawa-san. I frequently had a dinner with him. He knows many thinks about me, including the food that I can or cannot eat. Most of the time that we shared we were just laughing. There was a chemistry between us. For example, he was the only person that I can discuss anything with him. I would like to thank him of the good time, teaching me “slang” Japanese and for translation of many Japanese documents into English.

I would like to thank many students graduated during my Ph.D. study. I cannot mention all of them. But I should say thank you for Yajima-san for teaching me how to use many instruments in Nagatsugi lab during my early Ph.D. time. She also gave me a lot of Japanese food with brief description about the name and ingredients. Also, I cannot forget my friend Dong-kun for the nice discussions and for the technical support regarding electronics. He was exceptional.

I would like to thank Uchida-san, Iwata-san, Yao-san and Kawamori-san for organizing our lab events, kindly considering my special food and for the nice time, we shared.

I would like to thank Kanyama-san, Nadia-san, Fan-kun, and Lan-san for the nice time. Also, I would like to thank Okan-san and Jamila-san for their help during my final defense and for the nice time we shared.

Many thanks to our lab technicians for their help and support, especially to Ozawa-san for conducting the dual luciferase assay for me and preparing gel for us.

I would like to thank our amazing and energetic secretariat, Kimura-san for the countless support. I cannot mention all things, but I cannot forget her help during my early days in Sendai, finding a dorm and private apartment for me, going to hospital with me to support me and bringing a very delicious fish to us every year.

In addition, I would like to express my deep and sincere gratitude to the Culture, Education and Science Bureau in Tokyo, Cultural Affairs and Missions Sector, Ministry of Higher Education & Scientific Research, Egypt for their financial support through the fully funded Ph.D. scholarship of the Egypt-Japan Education Partnership (EJEP) program. Also, I would like to express my sincere gratitude to my home university, Al-Azhar University, Egypt for their support. Many thanks to my previous mentor and the Head of the Chemistry Department, Faculty of Science, Al-Azhar University, Cairo Egypt, Prof. Ahmed Halawa, for his support during my Ph.D.

Finally, I would like to thank my family for their prayers, and I hope with the successful defense of my thesis I could partially relieve the fears and stress I cause them during my Ph.D. I dedicate this thesis to my wife, Sarah, and my two guys, Anas (Annos) and Mohamed (Mody)

for holding me during the journey supporting me, not complaining, and surviving alone without my help and care. They bear a lot only to see my success.

ABSTRACT

Oligonucleotides (ONs) can be chemically modified with functional reactive moieties so that various specific chemical reactions can be accelerated through the proximity effect between the reaction points. In addition, some oligos with higher-order structure motifs can also be recognized by proteins. The introduced functional moieties into these ONs can be used as a tool to study the interaction between these ONs and proteins. In my research, I designed and synthesized three kinds of chemically functionalized ONs and evaluated their properties.

Firstly, …….

Secondly, I developed a highly efficient AVP-mediated 2'-OMe-RNA interstrand cross-linked (CL) anti-miRNA ONs (AMOs). It has been reported that miRNAs are overexpressed in many diseases, such as cancer. Chemically modified AMOs can interfere with these disease-relevant miRNAs and block them from binding to their mRNA targets. Komatsu's group reported that cross-linked duplexes flanking the single-stranded AMO inhibited the miRNA function more efficiently than AMOs with normal single or double strands. Here, I designed and synthesized AMOs flanked by native-like and less-distorted structures of interstrand cross-linked duplexes using the ONs containing 2-amino-6-vinylpurine (AVP) (Figure B). These AMOs inhibited the miRNA function at a low nM concentration.

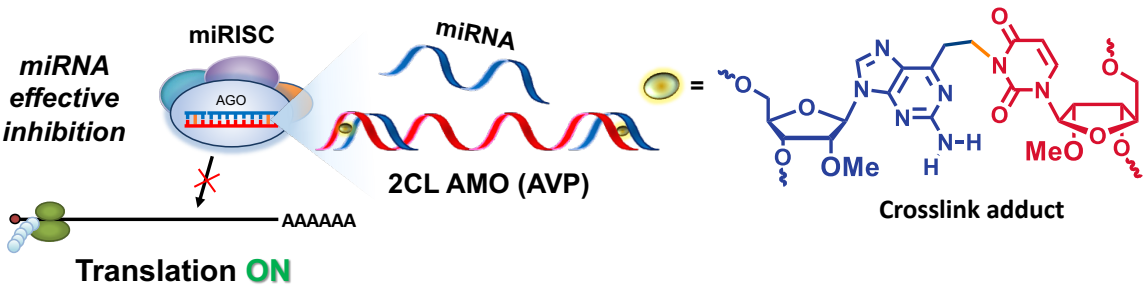

Figure B. The inhibition of miRNA activity by AVP-mediated CL AMO.

Finally, I designed and synthesized the artificial ON to induce the base flipping and accelerate the interstrand photo-cross-linking within the DNA duplex. The ONs containing properly designed artificial nucleic acids can induce base flipping and create specific fields for various chemical reactions. Previously, our group found that the alkyne–alkyne photo-cross-linking rapidly proceeded by the use of the base-flipping-out field where two alkynes overlap each other. In this study, I designed the alkene-type analog having a 5-methyl pyridone derivative linked to Ph or An groups with an alkene linker at the C3 position. The specific field created by the designed alkene analogs accelerated the [2+2] photocycloaddition reaction in duplex

DNA. The Ph-Ph combination provided a high yield, where 10 sec was enough to achieve more than 80% cross-link yield calculated from HPLC analysis (Figure C). As the Ph-Ph cross-link

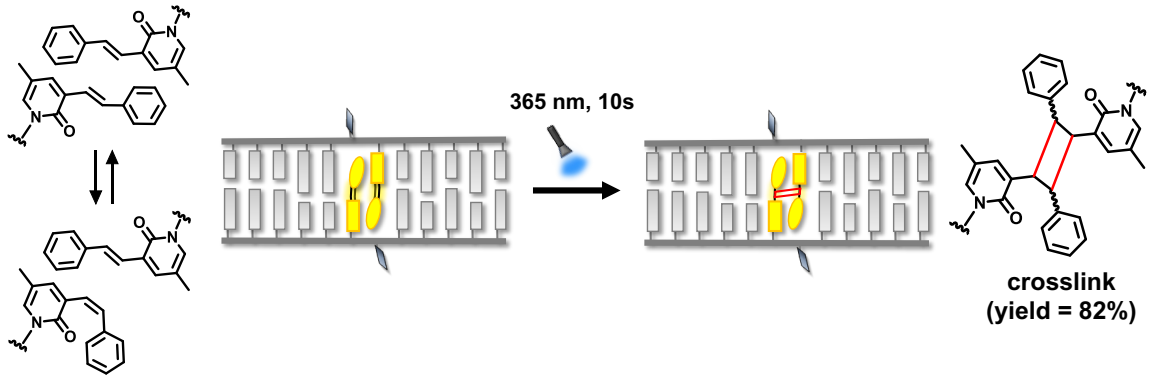

Figure C Schematic representation of the photo-cross-linking reaction within DNA duplex.

was found to be stable under thermal and irradiation conditions, I synthesized the Ph-Ph crosslinked AMO to investigate the inhibition of miRNA activity. The flip-out CL AMO showed similar activity with AVP-containing AMOs, suggesting that cross-linking is essential regardless of the structures.

LIST OF CONTENTS

LIST OF TABLES

LIST OF FIGURES

LIST OF APPENDICES

LIST OF ABBREVIATIONS

$^1O_2$	Singlet oxygen
A	Adenine
An	Anthracenyl
Anhyd.	Anhydrous
Aq.	aqueous
AVP	2-Amino-6-vinylpurine
C	Cytosine
Calcd.	Calculated
cat	catalyst
ds	Double strand
Eq.	equivalent
ESI-MS	Electrospray ionization mass spectroscopy
FAM	6-Carboxyfluorescence aminohexyl
Fluc	firefly luciferase
G	Guanine
G4	G-quadruplex
h	hour
HOBt	1-Hydroxybenzotriazole
HPLC	High performance liquid chromatography
hRluc	Renilla luciferase
HRMS	High resolution mass spectroscopy
HT	Human telomeric
L	liter
M	Molar (mol/L)
MALDI	Matrix-assisted laser desorption ionization
Me	Methyl
MES	2-(*N*-morpholino)ethanesulfonic
min	minute
MMPP	Monoperoxyphthalic acid magnesium salt hexahydrate

mol	Mole
NMR	Nuclear magnetic resonance
ODN	Oligodeoxyribonucleotide
ORN	Oligoribonucleotide
PAGE	Polyacrylamide gel electrophoresis
PDB	Protein data bank
Ph	Phenyl
PH	photocatalyst
RNA	Ribonucleic acid
RP-HPLC	Reverse phase high performance liquid chromatography
rt	Room temperature
Ru	Ruthenium
sec	Second
SET	Single electron transfer
Soln.	Solution
ss	Single strand
T	Thymine
$t_{½}$	Half-life
TBE	Tris-borate-EDTA buffer
TEA	Triethylamine
TEAA	Triethylammonium acetate
TFA	Trifluoroacetic acid
T_m	Melting temperature
TOF-MS	Time-of-flight mass spectroscopy
U	Uracil
UV	Ultraviolet spectrum
Vis	Visible spectrum

Chapter 1

General Introduction

1. Chemical modification of oligonucleotides and their applications

Genetic information is transcribed from DNA to RNA and translated into proteins in only one direction, as stated by a theory in molecular biology called central dogma (Figure 1).

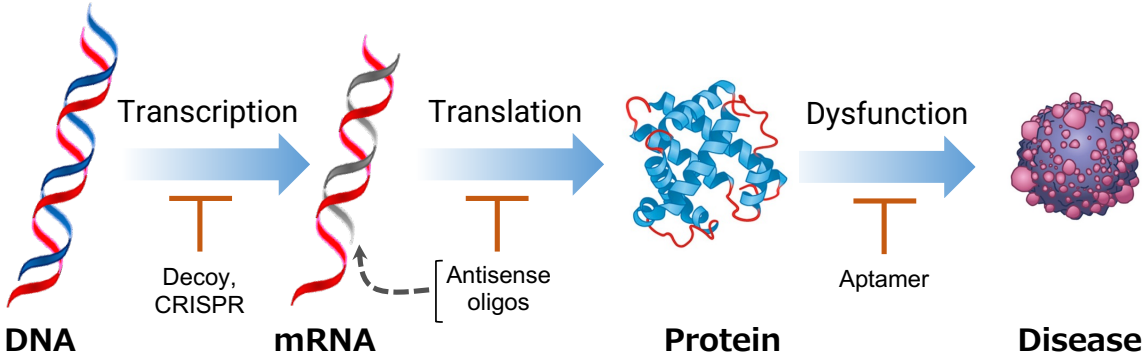

Figure 1. Gene expression (central dogma) and ONs-mediated regulations.

Genetic disorders give rise to many types of diseases, and one strategy for treating these diseases is the use of oligonucleotides. The oligonucleotide therapeutics include decoys, antisense oligonucleotide (ASO), anti-microRNA oligonucleotide (AMO), small interfering RNA (siRNA), and aptamers.

Oligonucleotides (ONs) are short and single-stranded oligomers of nucleic acid that can recognize their complementary target gene by forming a duplex structure in a sequence-selective manner. ONs that can form higher-order structure motifs bind to target proteins with high specificity and affinity. Due to their high specificity, ONs have numerous utilities ranging from research to diagnostic applications and, recently, therapeutics. However, the chemical

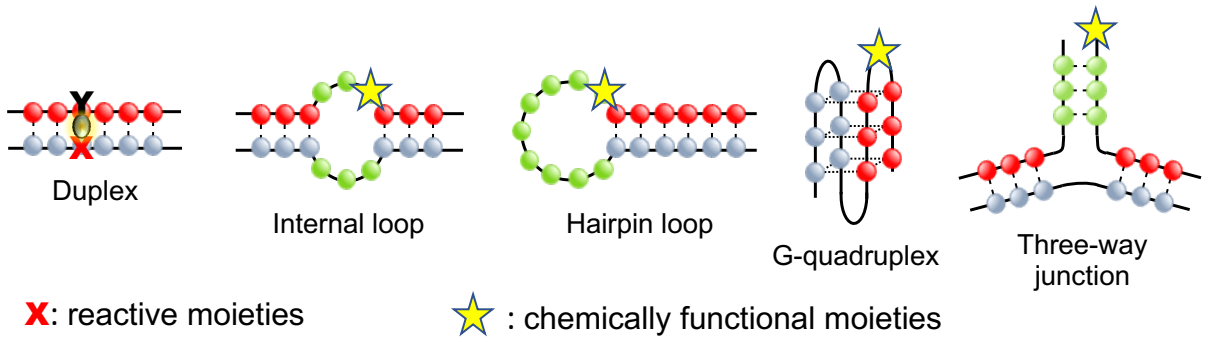

Figure 2. Representative higher-order structure motifs of oligonucleotides and their chemical modifications

modification of ONs with reactive moieties can significantly expand their tasks and applications. The kind of modification depends on the purpose for which ONs will be used. The chemically modified ONs with functional reactive moieties can accelerate various specific chemical

reactions through the proximity effect between the reaction points (Figure 2). The introduced functional moieties into some higher-order structure motifs of ONs can be used as probes or a tool to study the interaction between these ONs and proteins and probe their binding proteins.

2. Crosslink forming modified oligonucleotides

2.1 Cross-linking of oligonucleotides with their interacting proteins

Interaction between protein complexes and nucleic acids is extremely important in regulating plentiful essential nucleic acid-dependent cellular processes.[1] Thus, the study of these interactions is highly demanded to discover their roles and further understand the unrevealed mechanism underlying raised number of diseases.[2,3] In oligonucleotide therapeutics, administrated ASO exhibited an off-target binding to some cellular proteins that can affect their efficacy, and identifying those proteins would help increase their potency[4]. Recently, many methods have been developed to investigate these interactions. The oligonucleotides, which are modified with reactive crosslinkers, can crosslink with their interacting proteins.[5] This nucleic acid-protein cross-linking is one of the most efficient methods for the identification of weakly bound proteins that cannot be detected by conventional pull-down assays.

2.1.1 Cross-linking using oligonucleotides containing photo-activable moieties

Although nucleic acid-protein cross-linking using UV irradiation[6–8] or additive photocrosslinkers, e.g., formaldehyde,[8] has been reported. The oligonucleotides bearing a photo-activable reactive unit were frequently used to perform the nucleic acid-protein photo-crosslinking.[9–18] For example, in some of these methods, a diazirine photo-responsive crosslinker was tethered into an oligonucleotide strand to investigate the interactome of N^6-Methyladenosine (m^6A)-containing RNA[12,14] or siRNA.[10,11] Aryl azide group-bearing RNA was used to crosslink with RNA polymerase subunits.[9] However, the damage caused by the UV light, the low efficiency of the crosslinking reaction, and the off-target cross-linking hindered the applicability of these methods for mapping the nucleic acid-protein interactions.

2.1.1 Cross-linking using oligonucleotides bearing amino acid-specific reactive groups

Several methods utilizing enzymatically modified nucleic acids with reactive groups to crosslink with specific amino acids on the interacting protein have been developed.[19–32] Due to the high selectivity of the reactive groups and the proximity effect between the reactive points,

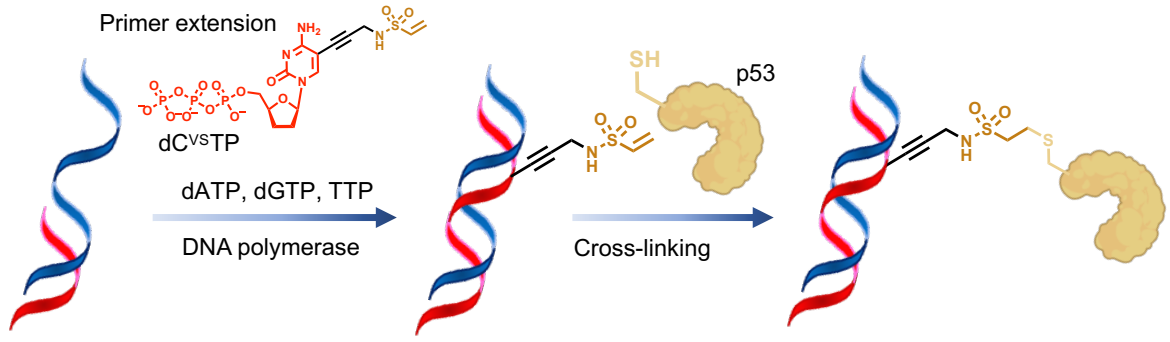

Figure 3. Cross-linking reaction between vinylsulfonamide-bearing DNA probe and a Cys-containing protein.[19]

effective cross-linking has been achieved by these methods. Vinylsulfonamide group incorporation into the DNA probe allowed cross-linking with cysteines (Cys)-containing proteins through Michael addition (Figure 3).[19] The Cys or Histidins (His)-containing protein were cross-linked with both DNA[20] and RNA[33] probes bearing chloroacetamide group (Figure 4). However, the chloroacetamide showed an extremely slow reactivity with His. For lysines (Lys), squaramate[27] and aldehydes[21–26]-modified DNA probes were used. Also arginines (Arg)-selective cross-linking with 1,3-diketones[29] and glyoxal[28] have been reported.

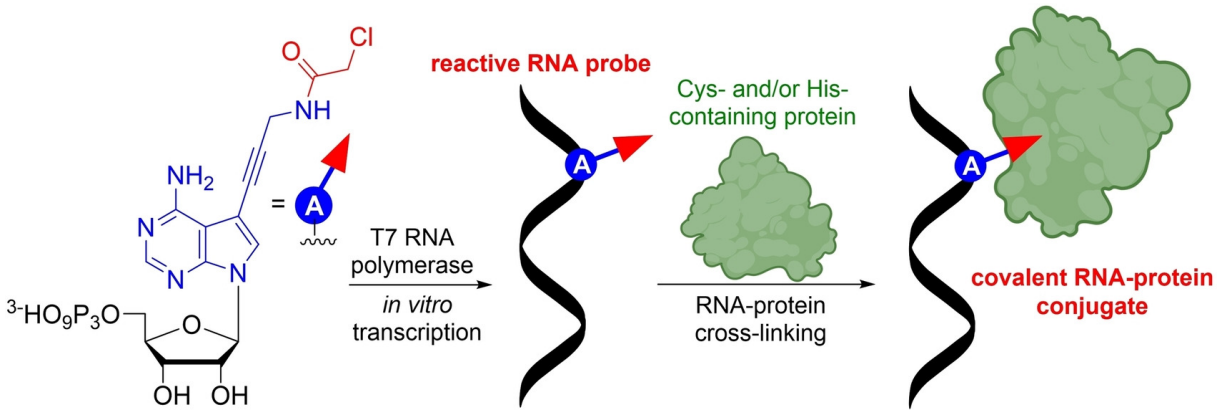

Figure 4. Cross-linking reaction between chloroacetamide-bearing RNA probe and a Cys or His-containing protein.[33]

2.2 Interstrand cross-linking of oligonucleotides with nucleic acid

Interstrand cross-linking of nucleic acids has high potential in oligonucleotide therapeutics,

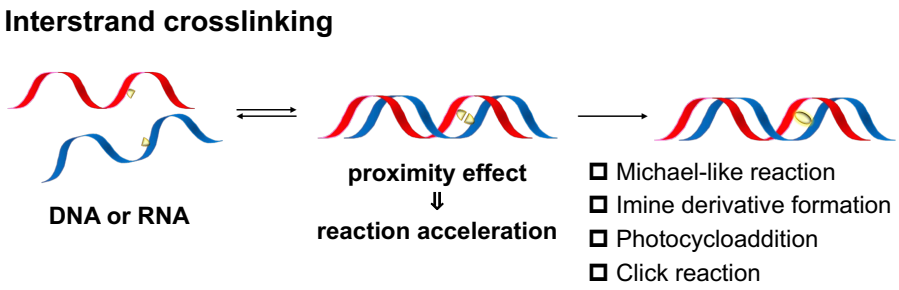

Figure 5. Illustration of interstrand cross-linking.

chemical biology, and nanotechnology. For interstrand cross-linking, various reactions based on Michael-like reactions, imine derivative formation, the click reaction, and photocycloaddition have been utilized (Figure 5).[34]

2.2.1 Interstrand cross-linking using Michael-like reaction

Our group has developed cross-linking reactions using vinyl chemistry for many years (Figure 6).[35–48] They initially developed 2-amino-6-vinylpurine (AVP) as a covalent warhead (Figure 6A). [35–38] The AVP base has a reactive vinyl group and reacts with T and U in the complementary position of the duplex under neutral conditions (Figure 6A). In the duplex between AVP-containing 2'-OMe RNA and native RNA, the vinyl group can approach the N3 atom of the U base, and Michael-type addition efficiently proceeds. At the monomer level, such efficient reactions were not observed, suggesting that the proximity effect is significant for the vinyl reaction. Additionally, vinyl reactivity and selectivity can be modulated by changing the base and sugar structure of the vinyl compound.[41–48] For example, 4-amino-6-oxo-2-vinylpyrimidine (AOVP) with an ethylene linker in the sugar component selectively reacted at the complementary sites of T in DNA and U in RNA (Figure 6B). Conversely, AOVP with an acyclic linker produced adducts with the G and T bases in DNA and the G base in RNA (Figure 6C).[46] These results suggest that selective cross-linking reactions can be achieved by the proper arrangement of vinyl groups, even with pyrimidine derivatives. This vinyl chemistry can also be applied to develop reactive small molecules, and they have reported several

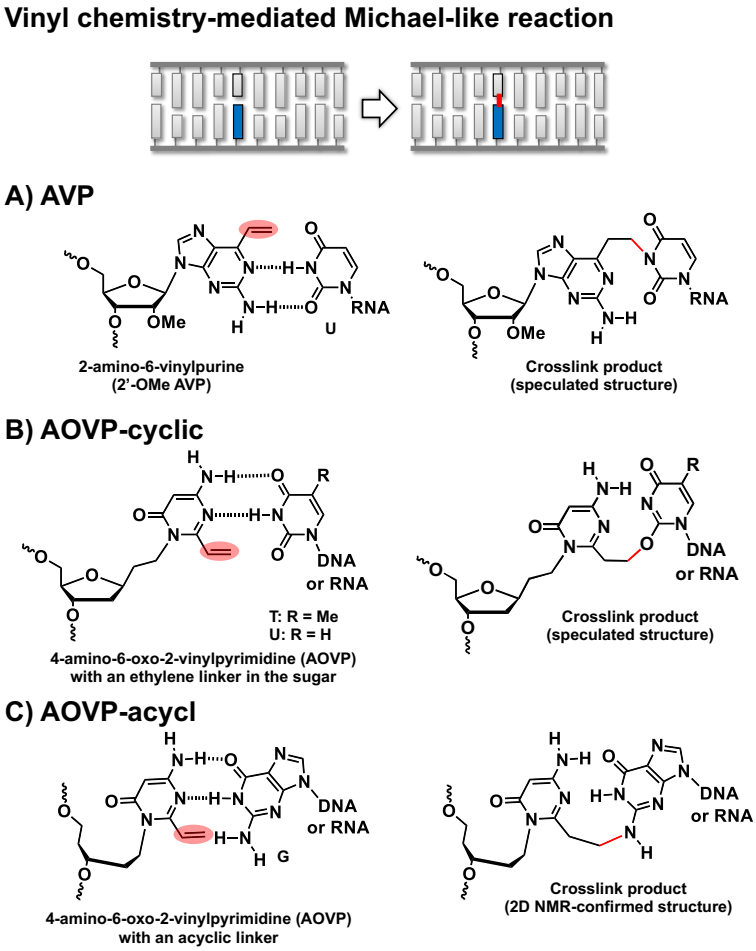

Figure 6. Interstrand cross-linking reactions by the Michael-like reaction using A) AVP. B) AOVP with an ethylene linker, and C) AOVP with an acyclic linker.

compounds.[49–55] The vinyl derivative-containing oligonucleotides were developed to control gene expression by cross-linking formation. To create a functional cross-linking structure, they used vinyl chemistry to synthesize cross-linked RNA duplexes.[56]

2.2.2 Interstrand cross-linking using oxime formation

Cross-linked duplex structures were prepared using a short bifunctional crosslinker containing bis-aminooxy groups and a pair of apurinic/apyrimidinic (AP) sites (Figure 7).[57,58] The bifunctional linker could intercalate in the AP sites and efficiently form cross-linked duplex

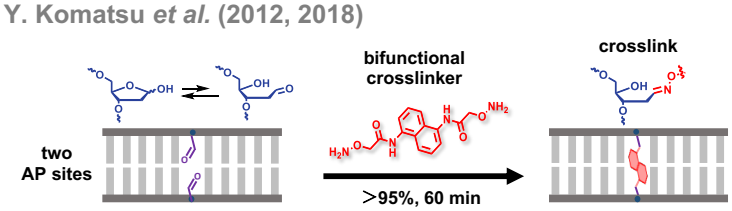

Figure 7. Interstrand cross-linking through oxime formation using two AP sites.

DNA and 2'-OMe RNA by the oxime formation reaction between oxyamine and the aldehyde of an AP site. Anti-microRNA oligonucleotides (AMOs) with flanking cross-linked duplex structures were prepared using this cross-linking reaction.[58,59] Compared with other structured AMOs, AMO flanking cross-linked duplex structures at the 5' and 3' termini exhibited higher inhibitory activity in cells. The 3'-side cross-linking improved nuclease resistance, whereas the 5'-side cross-linking contributed to binding with miRNA in Argonaute (Ago). These structure-function relationship analyses of AMOs provided essential insights into the function control of Ago-miRNA complexes. In addition, the crosslinked AMOs did not induce an immune response and showed no significant cytotoxicity in cells. Further structure-function relationship analysis of the crosslinked AMOs and a detailed investigation of the inhibition mechanism is desired.

2.2.3 Interstrand cross-linking using imine derivative formation

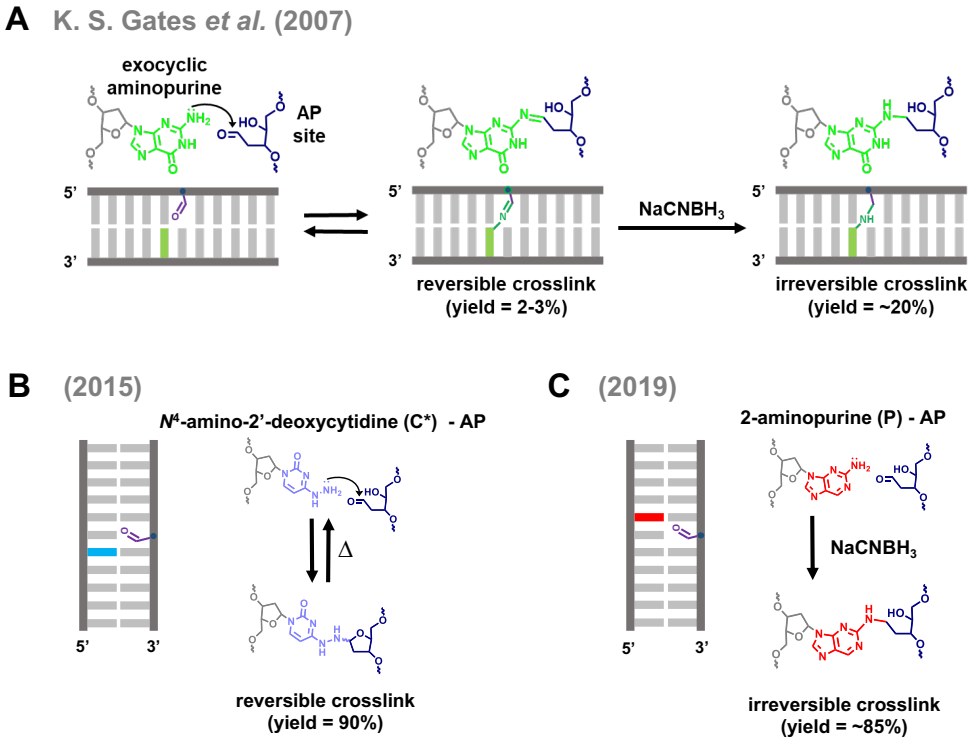

Figure 8. Interstrand cross-linking by imine derivative formation using an AP site. The reaction between the AP site and A) guanine base. B) N^4-amino-2'-deoxycytidine, or C) 2-aminopurine in the opposite strand.

Using an AP site, Gates's group reported another type of interstrand cross-linking reaction (Figure 8).[60–65] The aldehyde group of the AP site reacted with the exocyclic amino group of the purine base in the opposite strand of the duplex to provide an imine-derived linkage (Figure

8A).[60–64] Cross-linking occurred more efficiently when N4-amino-2'-deoxycytidine (C*)[61] and 2-aminopurine (P)[60] were utilized instead of the canonical purine bases (Figure 8B-C). These cross-linking products were reversible. However, reductive amination with sodium cyanoborohydride enabled irreversible cross-linking. It also should be noted that the optimum arrangement of the AP site and nucleobase differs for each nucleobase. For example, 5'-AP A/3'-A C* sequence is suitable for C*-AP crosslink (Figure 8B), while the P-AP crosslink prefers a differently arranged 5'-T AP/3'-P A sequence (Figure 8C). These reports not only provide insight into the variety of lesions that can occur via AP sites but also suggest that these crosslinks are promising candidates for creating interstrand cross-linking structures with minimal artificial modifications.

2.2.4 Interstrand cross-linking using click reaction

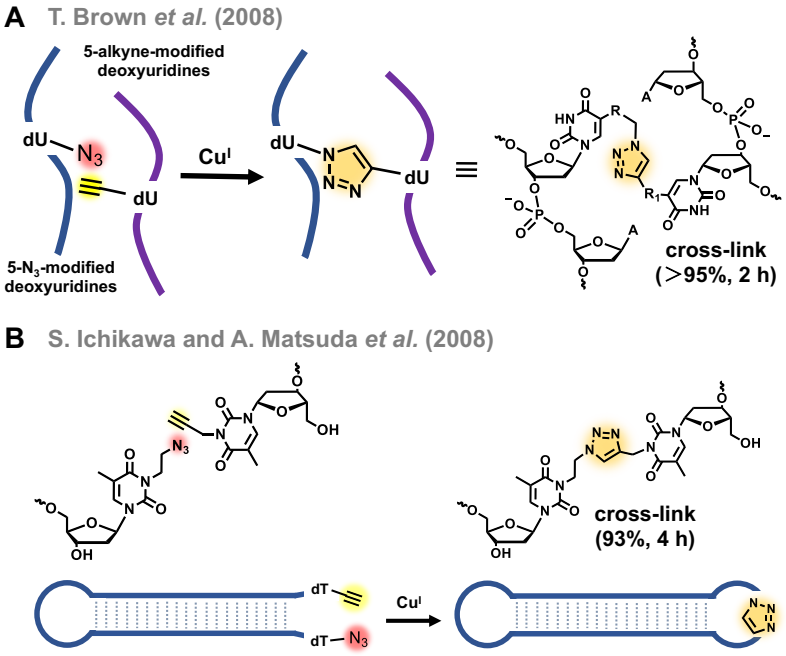

Figure 9. Cross-linking by CuAAC. A) The crosslinking of duplex and B) the dumbbell-shaped ODN were achieved by this reaction.

The click reaction, particularly copper-catalyzed azide–alkyne cycloaddition (CuAAC), is a powerful reaction. Many papers have reported nucleic acid conjugation and cross-linking via these reactions.[66–71] As an example of cross-linking reactions, rapid and efficient DNA cross-linking was achieved using two oligo DNAs (ODNs) containing 5-octadiynyl dU and 5-

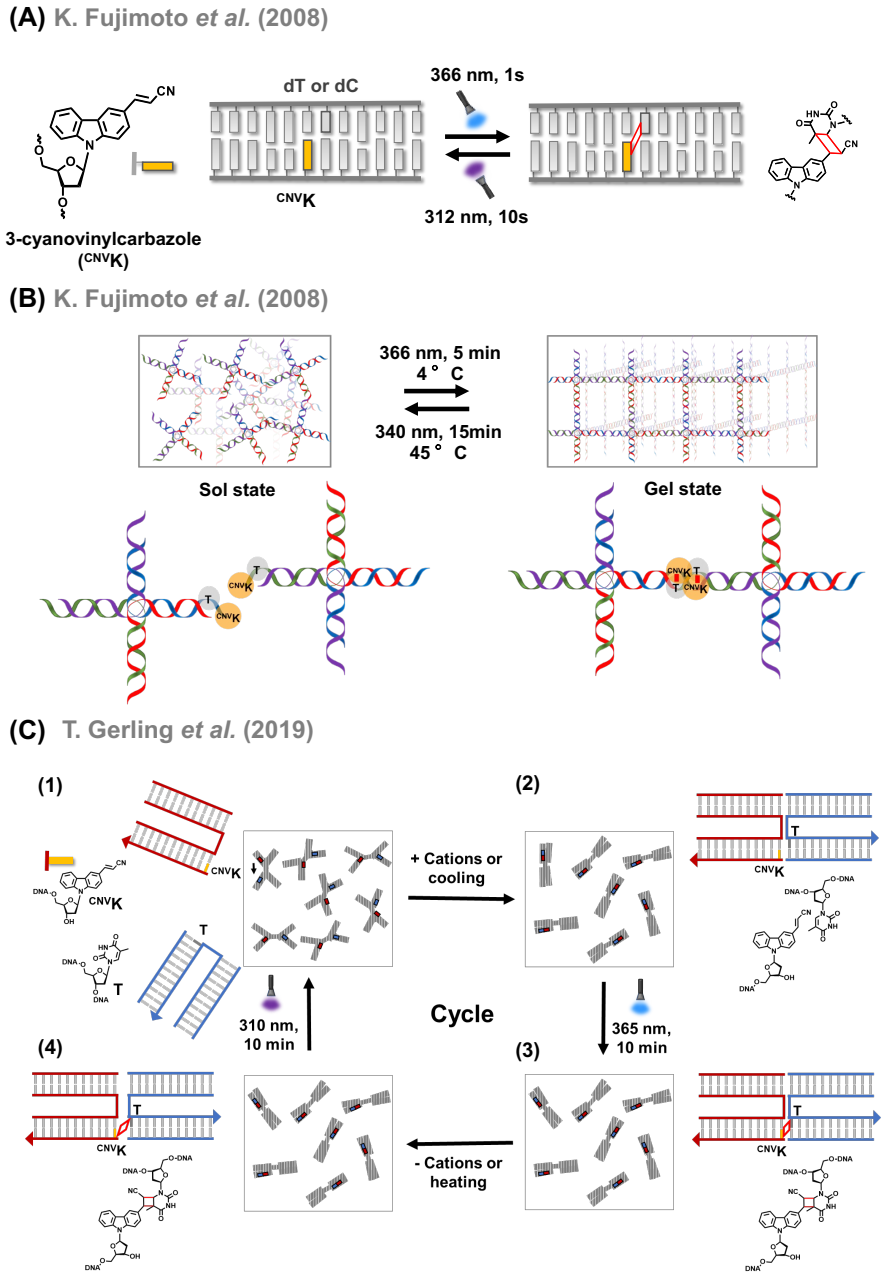

Figure 10. Reversible interstrand photo-cross-linking using 3-cyanovinylcarbazole (^{CNV}K). A) Upon 366 nm light irradiation, ^{CNV}K undergoes a [2+2] cycloaddition reaction with the pyrimidine base in the complementary strand. Cycloreversion proceeds with light irradiation at 312 nm light irradiation. B) Gel–sol transition of X-motif with ^{CNV}K. Transitions are triggered by photo-cross-linking and cleaving. C) Schematic of the photo-cross-linking and photo-cleavage of ^{CNV}K-modified nucleosides across stacking contacts for the DNA origami switch object.

azido modified dU (Figure 9A).[72] To create a functional structure, dumbbell-shaped clicked ODNs were synthesized using ODN containing N-3-(azidoethyl)thymidine and N-3-(propargyl)thymidine at the 3'- and 5'-termini (Figure 7B).[73] The dumbbell-shaped ODNs were thermally and enzymatically stable and showed the ability to bind to NF-κB p50

homodimers within a similar range to that of a control double-stranded decoy ODN. As both examples show, high reaction yield and relatively high flexibility of the reaction point distance are the advantages of CuAAC cross-linking.

2.2.5 Interstrand cross-linking using [2+2] photocycloaddition

Photocycloaddition is often used for cross-linking. Fujimoto's group developed many crosslinkers toward pyrimidine bases. The 3-cyanovinylcarbazole (^{CNV}K) base is one of the most potent photo-crosslinkers that crosslinks between the vinyl component of the ^{CNV}K base and the double bond of pyrimidine bases.[74] This [2+2] photocycloaddition reaction proceeded after only 1 s by photoirradiation at 366 nm (Figure 10A). Furthermore, the reverse reaction occurred by photoirradiation for 60 s by photoirradiation at 312 nm. Recently, the reaction rate[75] was further improved by changing the sugar structure, and the wavelength of the forward and reverse reactions[76] was lengthened by changing the vinylcarbazole base structure. The type of cross-linking has been used for many applications, such as the inhibition of translation,[77,78] RNA editing,[79,80] RNA fluorescence *in situ* hybridization[81–83], functional gel materials engineering,[84] and DNA origami.[85] In DNA nanotechnology, the photo-reversible crosslinking property of ^{CNV}K is one of the advantages of creating smart materials. For example, photo-responsive DNA gels, which undergo repetitive sol-gel transitions in response to different photo-irradiation wavelengths and temperatures, were developed using the property of ^{CNV}K in the suitable position at the sticky ends of the X-shaped DNA structure (Figure 10B).[84] This technique could have potential applications in medicine, e.g., drug delivery. Despite forming a stable DNA origami under different cation concentrations is challenging, the

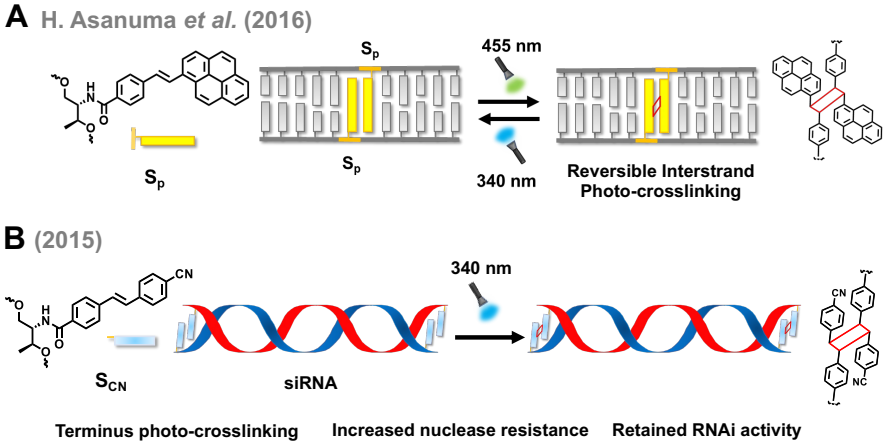

Figure 11. Reversible photo-cross-linking using stilbene derivatives tethered with an acyclic linker. A) Reversible interstrand photo-cross-linking using styrylpyrene (Sp). B) Preparation of terminus cross-linked siRNA using photo-cross-linking of *p*-cyanostilbene (S_{CN}).

^{CNV}K can offer a photo-chemical strategy for reversible covalent bond formation across stacking contacts of DNA origami (Figure 10C).[85] A coumarin analog can also be used for establishing reversible interstrand cross-linking to pyrimidine bases.[86]

On the other hand, Asanuma's group achieved reversible photo-cross-linking by developing photo-crosslinkers of stilbene derivatives tethered with a D-threoninol linker.[87,88] The photocycloaddition reaction between two overlapping styrylpyrene moieties on the DNA duplex was triggered by 455 nm visible-light irradiation (Figure 11A). The reverse reaction was realized with 340 nm UV-light irradiation. As an application of the photo-cross-linking reaction, a terminally photo-crosslinked siRNA with stilbene derivatives was prepared, and it showed high nuclease resistance while retaining RNAi activity (Figure 11B).[89] Additionally, the cross-linking reaction was utilized in the DNA-encoded dynamic library.[90] This cross-linking method that can additionally introduce photo-crosslink type molecules via acyclic linkers has the advantage that can create strong linkages with only the slight disturbance of nucleic acid structure.

2.2.6 Interstrand cross-linking induced by base-flipping out field

In addition, our group developed alkyne-type flipping-out-induced bases (Ph(alkyne) and An(alkyne)) with an alkyne linker instead of an alkene linker at the C3 position (Fig. 10).[91] In

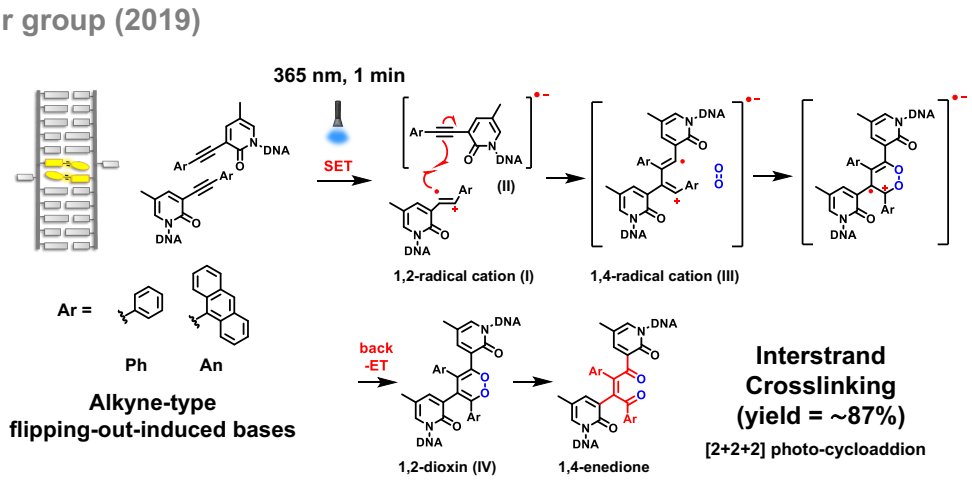

Figure 12. Postulated reaction mechanism of alkyne–alkyne photo-cross-linking on the flipping-out and base-stacked field.

this case, efficient alkyne–alkyne photo-cross-linking was realized using the heterocombination of Ph(alkyne) and An(alkyne) rather than a homocombination, such as Ph–Ph and An–An. The difference in the reaction rates between the hetero and homocombinations occurred because single electron transfer (SET) is essential for alkyne-type reactions, *i.e.*, SET occurs more readily for the heterocombinations than for the homocombinations because of the difference in

redox potential. In their postulated photoreaction mechanism based on several reports on the photoinduced [2+2+2] cycloaddition reactions (Fig. 12),[92–94] the first step is affected by the base combinations. One Ar base is excited, and SET occurs between the excited and unexcited Ar bases to give the 1,2-radical cation (I) and the reduced radical anion base (II) on the flipping-out and base-stacked field. The radical anion may delocalize on the DNA duplex. The 1,2-radical cation (I) reacts with the alkyne (II) to provide the 1,4-radical cation (III). The following cyclization with O_2 and the back electron transfer (back-ET) provide a neutral 1,2-dioxin (IV). After O–O bond cleavage, a 1,4-enedione crosslinked product is generated. Because these crosslinks provide a unique flipped-out structure, exploring the novel biological functions would be interesting. In nanotechnology applications, the flipped-out bases may be used as additional interaction and modification scaffolds to create new materials.

4. The objectives of this thesis

In this thesis, I focused my research on developing chemically modified oligonucleotides aiming to use them as a tool to interrogate nucleic acid interacting proteins, inhibiting the miRs function, and achieve efficient and rapid interstrand crosslinking induced by base flipping out.

In chapter 2, ….

In chapter 3, this vinyl cross-linking provided a native-like structure with high thermal stability. The native-like structure is advantageous for biochemical study and the development of nucleic acid medicine because the large artificial moiety often causes a decrease in enzyme affinity. In the native-like cross-linked duplex RNA study, the cross-linked duplex RNA had a slightly higher binding affinity with adenosine deaminase acting on RNA type 2 (ADAR2) than the natural duplex RNA.[56] In the study of the crosslinked 2'-OMe RNA duplexes, we synthesized anti-miRNA oligonucleotides (AMOs) with a flanking cross-linked duplex structure using AVP. These crosslinked AMOs containing the antisense targeting miR-21 showed markedly higher anti-miRNA activity than the commercially available miR-21 inhibitor, which has locked nucleic acid residues.[95]

In chapter 4, DNA cross-linking by the [2+2] photocycloaddition reaction was also achieved using flipping-out-induced ODNs.[96] In our group, several flipping-out-induced bases were developed based on the original alkylated-thymidine structure.[51] Alkene-type flipping-out-induced bases (Ph(alkene) and An(alkene)) are 5-methylpyridone derivatives linked to an aromatic compound with an alkene linker at the C3 position.[96] Ph(alkene), in particular, efficiently provided the cross-linked product in high yield after only 10 s of photoirradiation when the alkenes in the duplex DNA overlapped. Under photoirradiation, isomerization also

occurred to produce the crosslinked isomers. This highly efficient reaction provided a crosslinked product, even when a duplex with a low T_m value was used.

Chapter 2

Photocatalytic proximity labeling approach identifying the photocatalyst-modified DNA G-quadruplex-interacting proteins

Chapter 3

Synthesis of Crosslinked 2'-OMe RNA Duplexes and Their Application for Effective Inhibition of miRNA Function

1. A. M. Abdelhady, Y. Hirano, K. Onizuka, H. Okamura, *Bioorg Med Chem Lett* **2021**, *48*, 128257.
2. A. M. Abdelhady, Y. Hirano, K. Onizuka, H. Okamura, Y. Komatsu, F. Nagatsugi, *Curr Protoc* **2022**, e386.

Introduction

Micro RNAs (miRNAs) are a class of small non-coding endogenous RNA molecules that modulate gene expression at the post-transcription level.[97] MiRNA forms the RNA-induced silencing complex (RISC) with Argonaut (Ago) proteins and binds to the miRNA binding site in the 3'-UTR of the target mRNAs. This results in gene silencing by degradation of the mRNA or suppression of translation. MiRNAs regulate many biological processes, including differentiation,[98,99] apoptosis,[100,101] and proliferation.[102,103] Hence, the dysregulation of miRNAs can induce diverse pathologies, including cancer,[104,105] neurodegenerative disorders,[106,107] cardiovascular diseases,[108] and impairment of the immune system.[109] Therefore, miRNAs are valuable targets for therapeutic development.

One of the general strategies to inhibit miRNA activity is to use synthetic anti-miRNA oligonucleotides (AMOs), which have perfect complementarity to the mature miRNA target. Several chemically modified AMOs have been shown to increase the thermal stability of the complimentary hybridization and to improve the nuclease resistance. For example, the 2'-modified riboses, such as 2′-O-methyl (2′OMe), 2′-O-(methoxyethyl) (2′MOE), and 2′-fluoro (2′F), are used as chemically-modified oligonucleotide (ON) for inhibition of miRNA.[110,111] Recently, the ONs composed of acyclic serinol nucleic acid (SNA) have been reported to show high anti-miRNA activity.[112] Locked nucleic acids (LNAs), which strongly bind to RNA, have also been utilized for anti-miRNA applications. A short LNA-AMO of 8 nucleotides targeting the seed region was reported to exhibit the effective inhibition of miRNA.[113] In addition to the single-stranded chemically modified oligonucleotides, the structural modification of AMOs was shown to be effective for the improved anti-miRNA effect. For example, 2′OMe RNAs with double-stranded hairpin structures were shown to improve the inhibitory effects of miRNA.[114] Furthermore, the secondary-structured 2′OMe RNAs composed of two stem regions and two miRNA binding sites were revealed to exhibit a high anti-miRNA activity.[115]

In an alternative approach, 2′OMe-AMO containing the antisense sequence targeting miRNA and crosslinked duplexes at its terminal position showed a higher miRNA inhibitory effect than the double-stranded hairpin structures and oligonucleotides with two stem regions.[58] The crosslinked duplexes were prepared using a pair of reactive abasic sites, which was produced

from the enzymatic hydrolysis of deoxyuridines in the duplex by uracil DNA glycosylase (UDG), and a bifunctional cross-linker having two aminooxyacetyl groups.[57] The 2′OMe-AMO containing crosslinked duplex at the 5’ terminal position exhibited a higher inhibitory activity to the target miRNA than the AMO with the crosslinked duplex at the 3’ terminal position. It is suggested that the crosslinked duplex at the 5’ terminal position interacts with the Ago-miRNA complex. Accordingly, we envisioned that creating a less distorted structure of the crosslinked duplex might be important for a high inhibitory activity against miRNA.

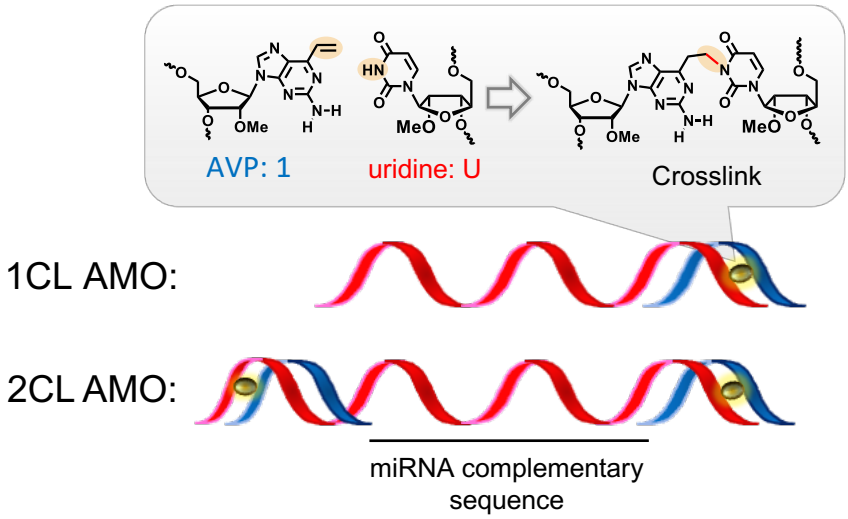

Figure 1. Schematic of AMO with flanking crosslinked-duplex structures. The crosslink was formed by the reaction between AVP (**1**) and uridine.

The interstrand crosslinking of nucleic acids is one of the strategies to create a stable complex. For example, various photo-activated crosslinking reactions were reported using modified oligonucleotides,[116] such as psoralen,[117,118] diaziridine,[119,120] carbazoles[75,78,121,122] and chloro-aldehyde.[123] In addition, reactive functional groups activated by a chemical reaction have been reported, such as quinone methides[124] and furan derivatives.[125–128] While the crosslinking formation by these strategies is useful to efficiently inhibit the target RNA function and label the target RNA by covalent bond formation, they are not suitable for creating a less distorted structure of the crosslinked duplex due to the large non-native structure of the reactive groups.

In previous studies, we developed interstrand crosslinking purine bases having a vinyl group as a small reactive group. The cross-linked duplex RNA prepared by using vinylpurine formed a less distorted native-like stable dsRNA and had nearly the same affinity as the native duplex RNA to the dsRNA-binding enzyme.[56] Moreover, we reported that the fully 2′OMe-ON

having 2-amino-6-vinylpurine (**1**: AVP) efficiently formed a covalent linkage with the complementary sequence of RNA at the uridine residue across from the AVP.[36,37] In this study,[95,129] we synthesized the modified 2′OMe-AMOs bearing crosslinked duplexes by using AVP (**1**) (Figure 1) and evaluated the miRNA inhibition in cells with these AMOs.

Results and discussion

The 2'-OMe-crosslink forming oligonucleotide (CFO) containing AVP (**1**) was synthesized as previously reported.[35] The sequence of CFO was complementary to the terminal sequence of the 2'-OMeRNA**1**. The structure was confirmed by MALDI-TOF MS (see the experimental data) measurements.

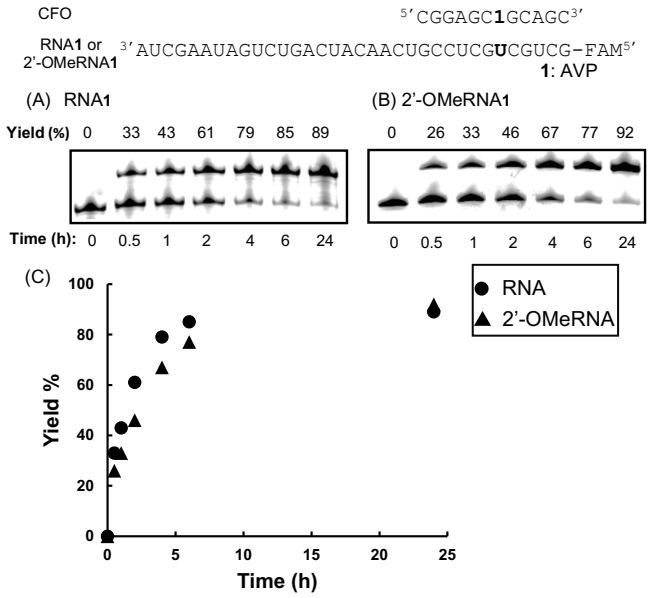

Figure 2. Time course for crosslink yields to FAM-labeled RNA or 2'-OMe RNA with CFO. Analysis of the crosslink reaction to RNA**1** (**A**) and 2'-OMe RNA**1** (**B**) using 16 % denaturing polyamide gel electrophoresis. Comparison of the crosslink yields to RNA and 2'-OMe RNA (**C**). The reaction was performed with 4 mM CFO and 2 mM RNAs in 100mM NaCl, 50 mM MES, pH 7.0 at 37 °C.

We first compared the crosslinking reactivity of CFO containing AVP to the RNA**1** and 2'-OMe RNA**1** because AVP has a sequence and sugar structure dependency.[36] The crosslinking reactivity of the CFO was evaluated using fluorescently (FAM)-labeled RNA and 2'-OMe RNA that are partly complementary to CFO. The CFO was incubated with the FAM-labeled RNA or 2'-OMe RNA, and the reaction mixture was analyzed by denaturing polyacrylamide gel electrophoresis. The crosslink yields at each reaction time were calculated based on the ratio

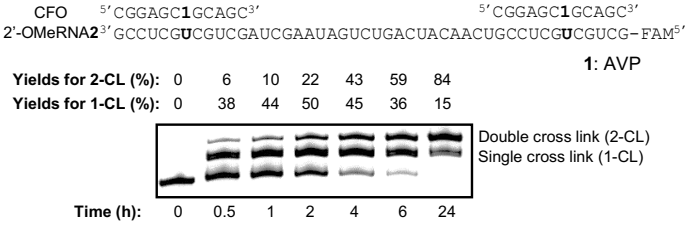

Figure 3. Analysis of the crosslink reaction to 2'-OMe RNA**2**. The reaction was performed with 4 mM CFO and 1 mM 2'-OMe RNA**2** in 100 mM NaCl, 50 mM MES, pH 7.0 at 37 °C.

between the crosslinked product and the remaining single-stranded RNA. As shown in Figure 2A, the CFO crosslinked to the native RNA**1** in good yield in 24 h. When the reaction was

performed against 2'-OMe RNA**1**, the formation of the crosslinked duplex was observed at a similar rate and yields over the same time period (Figure 2B). These results revealed that the

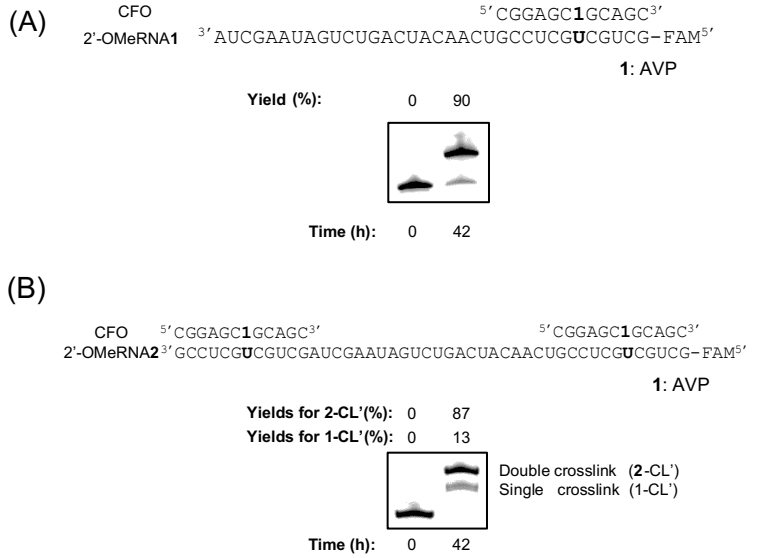

Figure 4. Analysis of the crosslink reaction to (**A**) target 2'-OMe RNA**1** and (**B**) target 2'-OMe RNA**2** using 16 % denaturing polyamide gel electrophoresis. The reaction was performed with 4 mM CFO and 1 mM target RNA**1** or RNA**2** in 100 mM NaCl, 50 mM MES, pH 7.0 at 37 °C.

CFO containing AVP (**1**) could crosslink not only with RNA but also with 2'OMe-RNA with a similar efficiency using this sequence.

We next evaluated the crosslinking reactivity of CFO to the 2'-OMe RNA**2** containing two target sites. The CFO (4 mM) was incubated with the FAM-labeled 2'-OMe RNA**2** (1 mM)

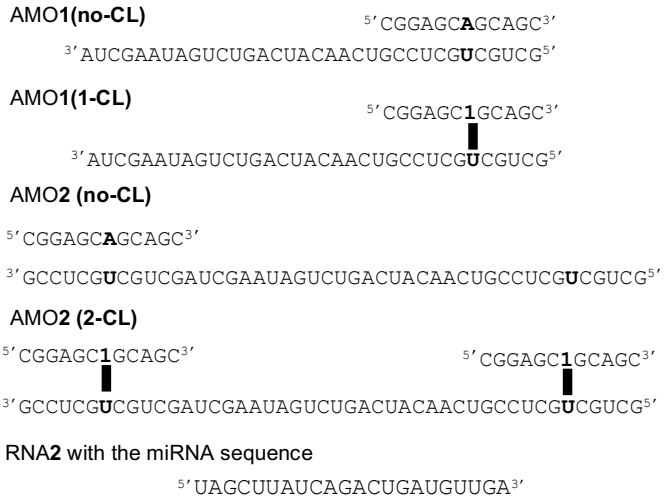

Figure 5. Sequence of 2'-OMe AMOs with or without crosslinked duplex and targeting miR-21 used in the present study.

and the progress of the cross-linking was monitored by gel electrophoresis (Figure 3). The first product band corresponding to the single crosslinked product was observed after 30 min and increased for 2 h. The second product with a slower mobility band gradually appeared and became the major one after 24 h. The reaction yields did not increase after 24 h (Figure 4).

These results indicated that the modified 2′OMe-AMOs bearing the double crosslinked duplex efficiently formed using the CFO containing AVP (**1**), and the appropriate reaction time was 24 h.

In a previous study, it was demonstrated that the AMOs containing the crosslinked duplex at both terminal positions and at the 5'-terminal one exhibited a higher inhibitory activity to miRNA than the non-crosslinked one.[58] Based on these results, we constructed AMO**1** (1-CL) and **2** (2-CL) containing the single-crosslinked duplex and double-crosslinked duplex using the above-described conditions as shown in Figure 5. The CFO was incubated with 2′OMe-RNA**1** or 2′OMe-RNA**2** without the FAM-label for 24 h and 1-CL or 2-CL 2′OMe-AMOs were purified by denaturing polyacrylamide gel electrophoresis. We confirmed each structure of the modified AMOs**1**, **2** by MALDI-TOF MS (see the experimental data) measurements.

The thermal stability of the crosslinked duplexes was compared to the corresponding non-crosslinked one by measuring the melting temperature (T_m). The increase in UV absorbance with AMO**1** (no-CL) was observed as the temperature rises above 70 ˚C, and the duplex

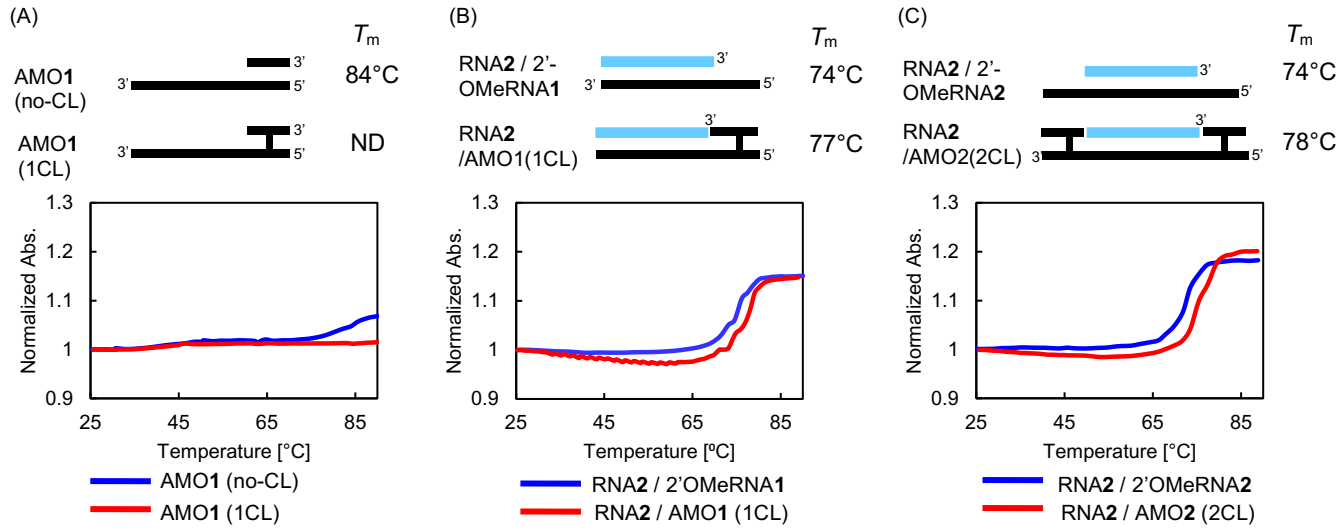

Figure 6. T_m measurement of AMO and AMO-target RNA with or without crosslinking. The T_m was measured using duplex (1.0 μM) in phosphate buffer (20 mM, pH 7.0) containing NaCl (100 mM).

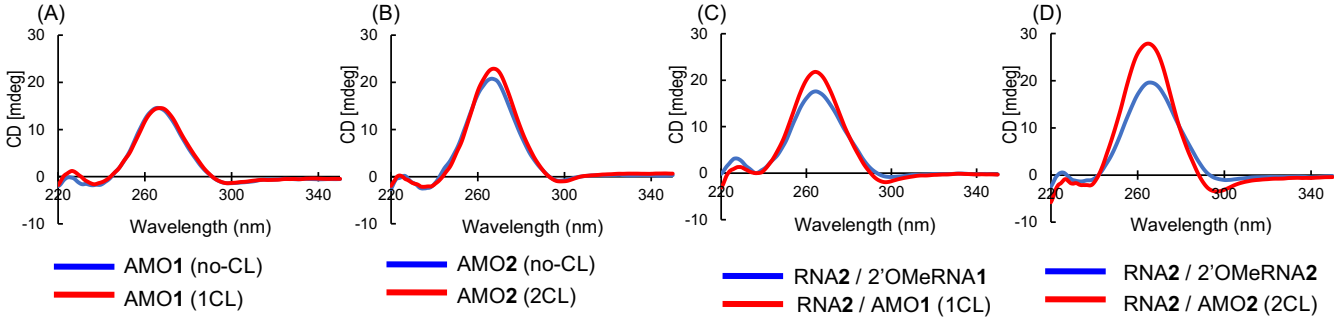

Figure 7. CD measurement of AMO and AMO-target RNA with or without crosslinking. The CD spectra were measured using duplex (1.0 μM) in phosphate buffer (20 mM, pH 7.0) containing NaCl (100 mM) at 25°C.

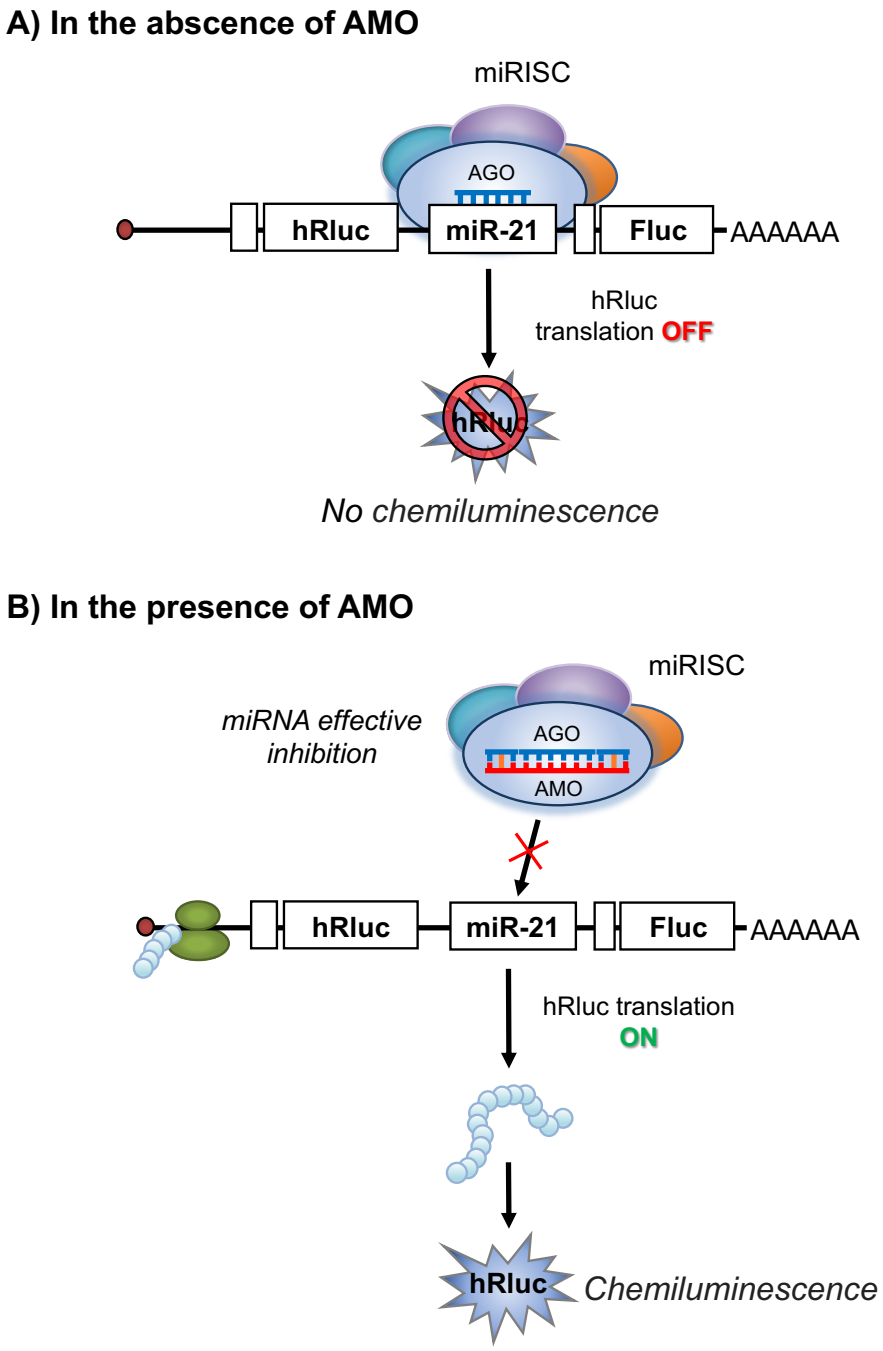

Figure 8. The dual luciferase system concept. (**A**) In the absence of AMOs, miR-21 binds to its target mRNA so that Renilla luciferase (hRluc) gene translation can be turned off. (**B**) Administration of AMO to the cells allows miR-21 inhibition, which leads to the hRluc enzyme being lighted up due to its translation.

between AMO**1** (no-CL) and 2'-OMe RNA was denatured over this temperature (Figure 6A). In contrast, the AMO**1** (1CL) did not show any significant absorbance change, indicating that denaturation of the crosslinked duplex to the single-stranded RNA did not occur at temperatures below 90 ˚C (Figure 6A). We next measured the T_m of the duplex formed between AMO**1** or **2** and the RNA**2** (Figures 6B and C)). The duplex AMO**1** (CL1)/RNA**2** showed a higher T_m

value (77 ˚C) than that of 2'-OMeRNA**1**/RNA**2** (74 ˚C) (Figure 6B). The T_m value of the AMO**2** (CL2)/RNA**2** duplex was also 4 ˚C higher than that of 2'-OMeRNA**2**/RNA**2** (Figure 6C). These results indicated that the crosslinked duplexes at the terminal position increased the duplex stability with the target miRNA due to the additional staking interaction with the CFO regions, as previously reported.[58] To gain insights into the structure, the circular dichroism (CD) spectra were measured using AMO**1**, **2**. A strong positive peak at 265 nm was observed in all the CD spectra, indicating a typical A-form structure for the crosslinked duplex in AMO. No significant differences in the CD spectra were observed between AMO**1**, **2** with and without crosslinking (Figures 7A and B), suggesting that this crosslinking formation does not disturb the duplex structure. The CD spectra of the RNA**2** annealed with AMO**1** (1CL) or AMO**2** (2CL) were also measured (Figures 7C and D). No significant shape differences in the spectra were observed between the duplexes with RNA**2**-2'-OMeRNA and RNA**2**-AMO (1 or 2-CL). These results suggest that the crosslinked duplex did not disturb the duplex structures between the AMO and target RNA.

We next evaluated the miR-21 inhibitory activity of the crosslinked AMOs in cultured cells. Each AMO was transfected into HeLa cells at concentrations ranging from 0 to 10 nM, and their inhibitory activities against miR-21 were evaluated using a dual luciferase assay system (Figure 8) composed of the Renilla luciferase (hRluc) gene with the miR-21 binding sequence and firefly luciferase (Fluc) gene as the internal control. The hRluc/Fluc ratios were normalized using the ratio obtained from the control cells that were transfected with a dual luciferase reporter without the miR-21 binding sequence. Surprisingly, AMO**2** (CL2) exhibited a dramatic inhibition of the miR-21 activity with only a 0.5 nM administration (Figure 9). The observed inhibition activity was significantly higher than that of the LNA-containing anti-miR-21, which is a commercially available miR-21 inhibitor. The inhibitory activity showed a slight decrease with AMO**1** (CL1), however, the activity was still higher than that of the LNA-containing anti-miR-21. These results indicated that the AVP-mediated crosslinked duplex structure is highly effective for increasing the miRNA inhibition activity of the AMOs. Previously, the crosslinked AMOs were reported to affect its binding efficiency to the Ago2-

RISC complex[58], and this interaction might be attributed to stronger inhibitory activity with crosslinked AMOs than that of LNA.

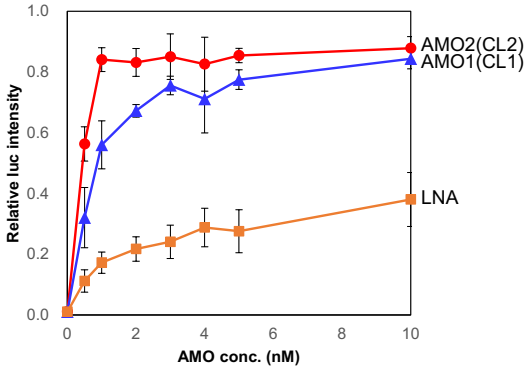

Figure 9. Inhibitory activity assays of AMOs. Relative luciferase intensities in dual luciferase assays at several AMO concentrations. Normalized intensities are represented as mean ±SD (n=3 independent experiments).

Conclusion

In summary, we established a chemical approach to efficiently synthesize the crosslinked 2'-OMe RNA duplexes using AVP (**1**) and prepared AMOs containing crosslinked duplexes at the terminal positions. The melting temperature of the crosslinked 2'-OMe RNA duplex was higher than 90 ˚C indicating that the crosslinked 2'-OMe RNA duplex is very stable and its dissociation to the single-stranded 2'-OMe RNA does not occur within the monitored temperature ranges. The stable hybridization with the target RNA was observed with the AMOs containing the crosslinked duplex. The structure of the hybridization was not disturbed by the crosslinked structure, as indicated by the CD spectra. We investigated the anti-miRNA activity using AMOs containing the crosslinked duplex. These AMOs inhibited the miRNA function at a low nM concentration. The AVP-mediated crosslinked duplexes have advantages in terms of easy preparation as well as their native-like duplex structure, providing the basis for preparing AMOs containing the crosslinked duplex with a high inhibitory potency against several miRNAs. We will investigate the detailed mechanism for high anti-miRNA activity with the AMOs containing crosslinked duplex and the structure-activity relationship of the crosslinked regions using this new and efficient synthesis.

Experimental data

General Materials and Methods. Reagents for synthesis, buffers, and salts were purchased from Wako, Aldrich, Sigma or Nakalai tesque. RNA and 2'-OMeRNA oligomers were purchased from Japan Bio Services Co., LTD. (Saitama, JAPAN). Locked nucleic acid (LNA) was purchased from Qiagen (miRCURY, LNA miRNA inhibitor (Exiqon4102261-001). Oligonucleotide synthesis was conducted by using Applied Biosystems 392 DNA/RNA synthesizer. Purification of oligonucleotides was performed on a Jasco HPLC system (PU2089Plus, UV-2075Plus, FP-2015Plus and CO-2065Plus) and Nakalai tesque COSMOSIL $5C_{18}$-MS-II (4.6ID or 10 x 250 mm). MALDI-TOF-MS was performed on a Bruker Autoflex speed instrument utilizing a 3-hydroxypicolinic acid/diammonium hydrogen citrate matrix. T_m curves were measured on a JASCO V-570-DS or a Beckman coulter DU800 spectrophotometer. CD spectra were recorded on a J-720WI (JASCO Co., Hachioji, Japan) equipped with a Peltier temperature controller.

Synthesis of 2-Phenoxyacetylamino-9-[5'-O-dimethoxytrityl-3-O-(N,N-diisopropyl-2 cyanoethylphosphoramidyl)-2'-deoxy-d-ribofranosyl]-6-(2-methylthioethyl)purine (3). The phosphoramidite adduct was synthesized following a previous report.[130] The synthesis was commenced with compound 1 which was co-evaporated in anhydrous acetonitrile (3.0 mL, 2×) followed by co-evaporation in anhydrous pyridine (3.0 mL, 1×). A solution of **1** (121 mg,

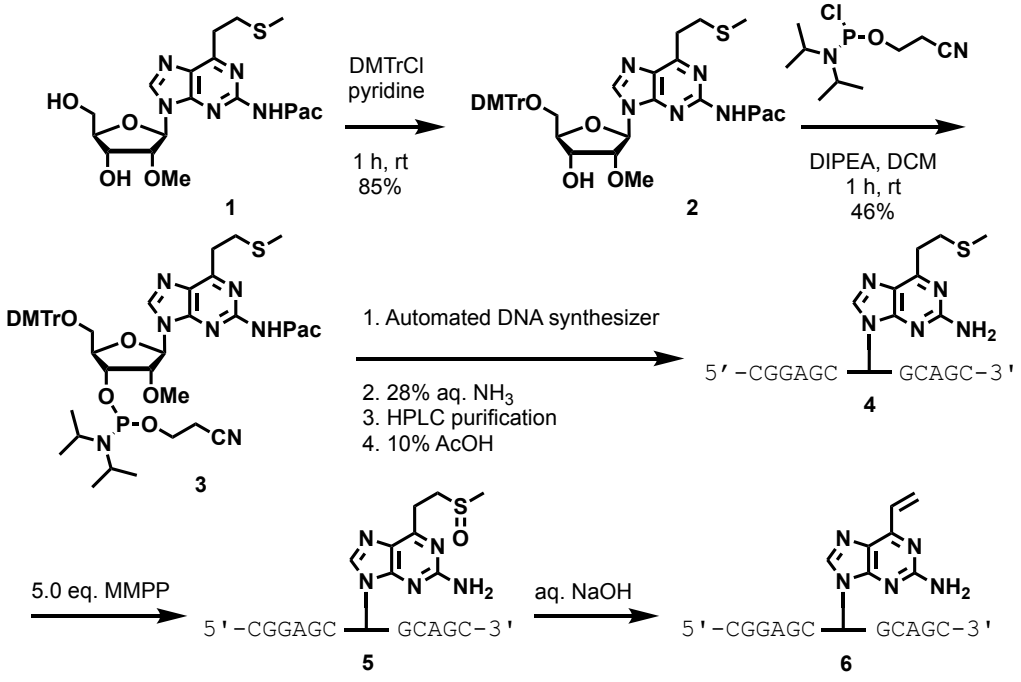

0.248 mmol) in dry pyridine (1.5 mL) was mixed with dimethoxytrityl chloride (242 mg, 0.496 mmol) and the mixture was stirred for 1 h. The resulting mixture was diluted with EtOAc (20 mL) and washed with H_2O (20 mL) and brine (20 mL). The organic layer was dried over anhydrous Na_2SO_4, filtered, and concentrated under reduced pressure. The residue was purified by silica gel chromatography (hexane−EtOAc 3:1, 1% pyridine, v/v) to afford 2-phenoxyacetylamino-9-(5-O-dimethoxytrityl-2‘-deoxy-d-ribofranosyl)-6-(2-methylthioethyl)-purine as a pale yellow foam (166 mg, 85%): ^{1}H NMR (400 MHz, $CDCl_3$): δ 8.62 (1H, br s), 8.20 (1H, s), 7.68−7.01 (14H, m), 6.81−6.78 (4H, m), 6.18 (1H, t, J = 6.3 Hz), 4.68 (2H, br s), 4.87 (1H, dt, J = 5.9, 3.0 Hz), 4.17 (1H, m), 3.78 (6H, s), 3.50−3.42 (4H, m), 3.09 (2H, t, J = 6.9 Hz), 2.62 (2H, m), 2.19 (3H, s); HRMS (ESI): *m/z* calcd for $C_{43}H_{46}N_5O_8S^+$ $[M+H]^+$, 792.3067; found, 792.3061.

To a solution of the above product (90 mg, 0.114 mmol) in dry dichloromethane (2.0 mL), diisopropylethylamine (0.118 mL, 0.682 mmol) and 2-cyanoethyl N,N-diisopropylchlorophosphoramidite (0.063 mL, 0.284 mmol) were added and then the resulting mixture was stirred for 1 h at the same temperature. The resulting mixture was diluted with ethyl acetate (20 mL) and washed with saturated aqueous $NaHCO_3$ and brine. The organic layer was dried over anhydrous Na_2SO_4, filtered, and concentrated under reduced pressure. The residue was purified by silica gel chromatography (hexanes−ethyl acetate 1:1, v/v) to afford **3** as a colorless oil (51.8 mg, 46%). ^{1}H NMR (400 MHz, $CDCl_3$): δ 8.80 (1H, br s), 8.15 (1H, s), 7.42−6.99 (14H, m), 6.78 (4H, dd, J = 6.8, 2.0 Hz), 6.17 (1H, t, J = 6.3 Hz), 4.23-4.11 (4H, m), 3.93−3.88 (2H, m), 3.86 (6H, s), 3.77−3.43 (6H, m), 3.09 (2H, t, J = 6.3 Hz), 2.78−2.75 (2H, m), 2.65 (2H, t, J = 6.3 Hz), 2.19 (3H, s), 1.17 (6H, d, J = 6.9 Hz), 1.04 (6H, d, J = 6.9 Hz); ^{31}P NMR (162 MHz, $CDCl_3$): δ 150.9, 150.4; HRMS (ESI): *m/z* calcd for $C_{52}H_{63}N_7O_9PS.Na^+$ $[M+Na]^+$, 1014.3967; found, 1014.3956.

Synthesis of crosslink forming oligonucleotides (CFOs). The sulphide-protected 2’-OMe ON was then synthesized from the phosphoramidite **3** precursor according to standard protocols (1.0 μmol scale) using an Applied Biosystems model 392 automated DNA synthesizer.

Deprotection and cleavage from the CPG support were carried out under a mild condition with 28% ammonia solution at room temperature for 4 h. Next, The DMTr-ON Oligonucleotides (**4**) were purified by HPLC. HPLC purification conditions: C-18 column (Nacalai tesque: COSMOSIL 5C_{18}-MS-II, 4.6ID x 250 mm) by a linear gradient of 10%-40%/20 min acetonitrile in TEAA buffer (0.1 M) at a flow rate of 4 mL/min at 35 °C. Peaks were monitored by UV detector (λ = 254 nm). The DMTr group was deprotected by

detritylation with 10% AcOH for 1 h. The concentration of the ONs was calculated by UV absorption at 260 nm. The ON (**4**) was then subjected to oxidation with magnesium monoperphthalate (MMPP) to produce **5**, followed by the elimination of the sulfoxide group under an alkaline condition to produce active CFO (**6**). The structures of CFO (**6**) were confirmed by MALDI-TOF MS as follows:

	Calcd	found
CFO (**6**)	4063.7407	4064.376

Quantification of crosslink reactivity of the CFO. CFO (**6**) (4 μM) was incubated with fluorescently (FAM)-labeled RNA and 2'-OMe RNA (2 μM) in 50 mM MES buffer containing 100 mM NaCl at 37°C. The solution (3 μl) was mixed with loading buffer (3 μl, 95% formamide containing 20 mM EDTA) and loaded to 16 % polyacrylamide and 20% formamide gel containing 45% urea. The electrophoresis was performed at 300V for 60 min. The gel was visualized by Fuji FLA-5100 fluoroscanner. The fluorescent band intensity was quantified by using MultiGauge software. The crosslink yield was calculated from the ratio of crosslinked product to the remaining single-stranded fluorescently (FAM)-labeled RNA and 2'-OMe RNA.

Preparation of AMO1 (1-CL) and 2 (2-CL). CFO (**6**) (4 μM) was incubated with 2′OMe-RNA**1** or 2′OMe-RNA**2** without FAM-labeling (2.66 μM) for 24 h in 50 mM MES buffer containing 100 mM NaCl at 37°C. 1-CL or 2-CL 2′OMe-AMOs were desalted by Sep-Pak® Plus C18-column then purified by denaturing polyacrylamide gel electrophoresis. The AMOs solution was mixed with an equal volume of loading buffer (95% formamide containing 20 mM EDTA) and loaded to 16 % polyacrylamide and 20% formamide gel containing 45% urea. The electrophoresis was performed at 400V for 2.5 h. The AMOs-containing gel was crashed, and AMOs was extracted from the gel by adding a solution containing (4 mL) EDTA (10 mM) and NaCl (0.2 M) and shaking overnight. 1-CL or 2-CL 2′OMe-AMOs products were filtered-off gel and desalted by Sep-Pak® Plus C18-column. Each product structure of modified AMOs**1**, **2** was confirmed by measuring MALDI-TOF MS as follows:

AMOs	Calcd	found
AMO1(1CL)	15330.552	15329.404
AMO2(2CL)	23387.24	23387.269

Melting temperature (T_m) measurement (UV) of AMO and AMO-target RNA with or without crosslinking. A mixture (100 μL) of the duplex (1.0 μM) in phosphate buffer (20 mM, pH 7.0) containing NaCl (100 mM) was transferred to a micro quartz cell with a 1-cm path length. The melting temperature was then measured under UV absorption at 260 nm from 25 to 90 °C at the rate of 0.5 °C/min. The measurements were carried out three times per each sample and averaged to obtain the final value.

CD measurements of AMO and AMO-target RNA with or without crosslinking. A mixture (100 μL) of the duplex (1.0 μM) in phosphate buffer (20 mM, pH 7.0) containing NaCl (100 mM) was transferred to a micro quartz cell with a 1-cm path length. The CD spectra were measured at 25 °C.

Luciferase assays. A target sequence complementary to mature microRNA-21 (miR-21) was inserted into the 3'-UTR of the Renilla luciferase (hRluc) gene of the psiCHECK-2 vector (Promega), yielding plasmid psiCHECK-2-miR21, which contained both hRluc and firefly luciferase genes. [*Mol Ther- Nucleic Acids*. 2018; **10**: 64–74] HeLa cells were seeded at densities of 1.5×10^4 cells per well in 96 well plates (Nunc) in DMEM (100 μL) containing 10% FBS the day before transfection. The cells were transfected in triplicate with optiMEM solution (10 μL) containing Lipofectamine® 2000 (Invitrogen; 0.3 μL per well), psiCHECK-2-miR21 (100 ng per well), and AMOs. The concentrations of AMOs were varied from 0 to 10 nM. Luciferase activity measurements were performed at 48 h post-transfection according to the manufacturer's instructions (Promega, Dual-Glo Luciferase Assay System). The ratios of Renilla luciferase to firefly luciferase (hRluc/Fluc) were first calculated from the average of triplicate wells. Then, all ratios were normalized using the ratio of psiCHECK-2-treated cells without AMO.

Chapter 4

Rapid Alkene–Alkene Photo-cross-linking on the Base Flipping-out Field in Duplex DNA

1. A. Abdelhady, K. Onizuka, K. Ishida, S. Yajima, E. Mano, F. Nagatsugi, *J Org Chem* **2022**, *87*, 2267–2276.

Introduction

The specific chemical reactions by enzymes acting on a nucleobase are realized by flipping the target base out of the helix (Figure 1). For example, RNA editing enzymes flip the target base out of the helix, take the base into an active site, and convert adenine and cytosine to inosine and uracil by accelerating the hydrolysis of the amino group of adenine and cytosine (Figure 1A).[131–133] Similarly, the artificial oligodeoxynucleotides (ODNs) can also induce base flipping (Figures 1B and 1C) and a specific chemical reaction. Sugimoto's group previously developed phenylcarbamoyl-modified dA-containing ODNs with the ability of base flipping and found that the base-flipping accelerated the RNA-cleaving reaction (Figure 1D).[134–137] In our previous study, as base flipping-inducing artificial bases,[51,91] we developed 5-methylpyridone derivatives linked to an aromatic compound with a rigid alkyne linker at the C3 position (Figures 1B and 1C). In addition, an efficient alkyne-alkyne photo-cross-linking was realized by taking advantage of the formed flipping-out field.[91]

The interstrand cross-linked products of nucleic acids have been synthesized by various reactions and utilized for various applications.[38,39,57,72,74,119,128,138–143] As the application for nucleic acid therapeutics, the cross-linked strand capping of anti-miRNA showed a highly efficient anti-miRNA effect.[58,95] A terminus-free cross-linked siRNA acquired a high nuclease resistance while retaining the RNAi activity.[89] The cross-linked dumbbell oligodeoxynucleotides were developed as potential decoy molecules with an NF-κB binding ability.[73] In addition, various types of cross-linking reactions to the native RNA have been developed to form the stable complex,[56] inhibit the gene expression,[77,78,123,144,145] capture the target RNA[116,120,126] and fluorescently label RNA.[81–83] As other applications, the cross-linking reaction was utilized in the DNA-encoded dynamic library[90] and DNA origami.[85,146,147]

In this study, we report an easily prepared and unique structure-providing photo-cross-linking reaction by taking advantage of the base-flipping out field formed by the alkene-type base flipping-inducing artificial bases (Figures 1E and 1F). Based on our previous alkyne-type base chemistry[91] and the reports regarding alkene-alkene photo-cross-linking in the duplex DNA by Letsinger's[148] and Asanuma's group,[87,88,149] we designed alkene-type phenyl (Ph) and anthracenyl (An) bases, 5-methylpyridone derivatives linked to an aromatic compound with an

alkene linker at the C3 position. We expected that the Ph and/or An bases flip the complimentary base out and create a specific field where the two alkenes overlap each other (Figure 1G). Since the two alkenes can keep approaching on the created field, the [2+2] photocycloaddition reaction was expected to efficiently proceed to provide the cross-linked product.

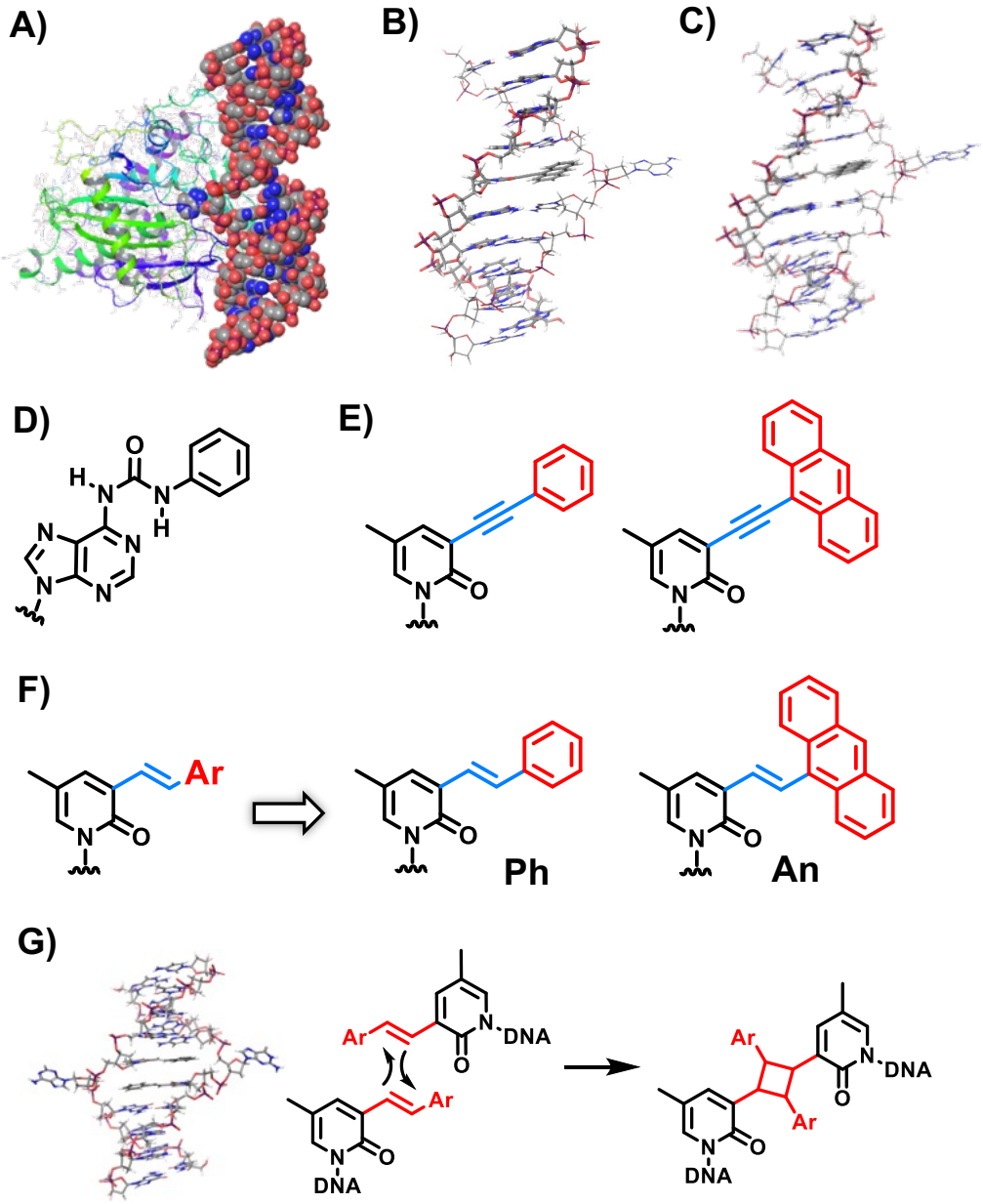

Figure 1. Molecular design of the base-flipping-inducing ODN. A) Base flipping by human ADAR2 (PDB: 5ED1).[169] B) Base flipping by alkyne-type ODN. The model was calculated using MacroModel software. C) Structure of alkyne-type Ph and An bases. D) Structure of phenylcarbamoyl-modified dA. E) Base flipping by alkene-type ODN. F) Structures of alkene-type Ph and An bases. G) [2+2] photocycloaddition reaction by the two alkene-type bases.

Results and Discussion

To incorporate Ph and An nucleotides into an ODN, phosphoramidites **3-Ph** and **3-An** were synthesized (Scheme 1). The synthesis commenced with the palladium-catalyzed Heck coupling of the formerly reported bromopyridone nucleoside (**1**)[91] with styrene and 9-vinyl

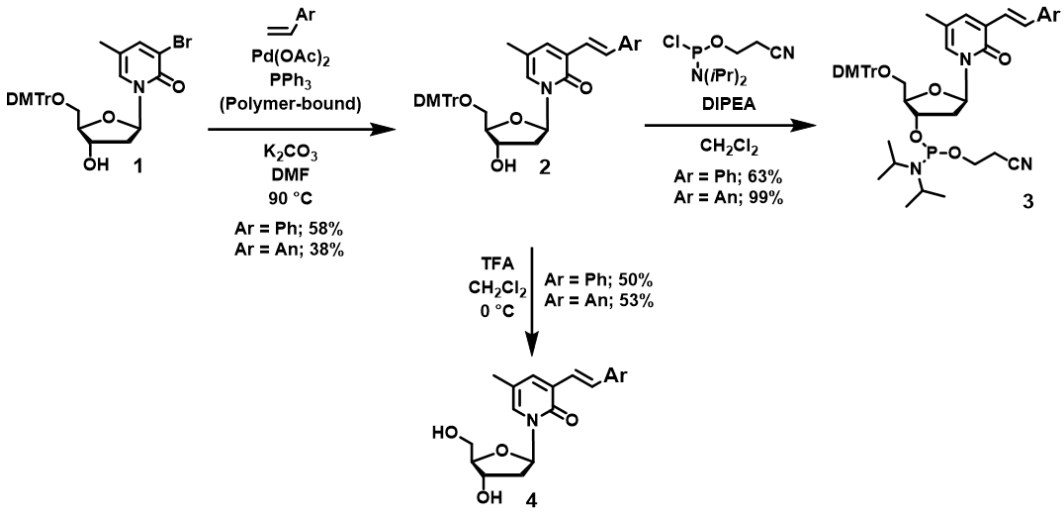

Scheme 1. Synthesis of phosphoramidites and diols.

anthracene in the presence of the triphenylphosphine polymer-bound to afford **2-Ph** and **2-An** in 58% and 38% yields, respectively. The relatively low yield of the Heck coupling with 9-vinyl anthracene may be due to the instability of the product (**2-An**) under the stated reaction

Entry	X or Z	[a]Calcd.	[b]Found
ODN**1**	X = Ph	3111.5	3110.8
ODN**1**	X = An	3211.5	3211.1
ODN**3**	Z = Ph	3126.5	3126.8
ODN**3**	Z = An	3226.5	3227.7
ODN**4**	Ph	3086.5	3087.0
ODN**5**	Ph	3086.5	3086.9

Table 1. MALDI-TOF MS data of the synthesized ODNs. [a] $[M–H]^-$, [b] all data were collected in negative mode.

conditions. Phosphitylations of the Heck coupling products produced the phosphoramidites (**3-Ph** and **3-An**). Using **3-Ph** and **3-An**, ODN**1** and **3-5** with Ph or An were prepared by a DNA synthesizer. The ODNs were purified by reversed-phase (RP) HPLC after deprotection and cleavage from the CPG support. Subsequent MALDI-TOF MS measurements were carried out

for the characterization of the ODNs (Table 1). To determine the molar extinction coefficients at 260 nm (ε_{260}) of Ph and An, the DMTr group of compound **2** was deprotected. The ε_{260} values were 9632 and 21265 $M^{-1}cm^{-1}$ for **4-Ph** and **4-An**, respectively (Figure 2).

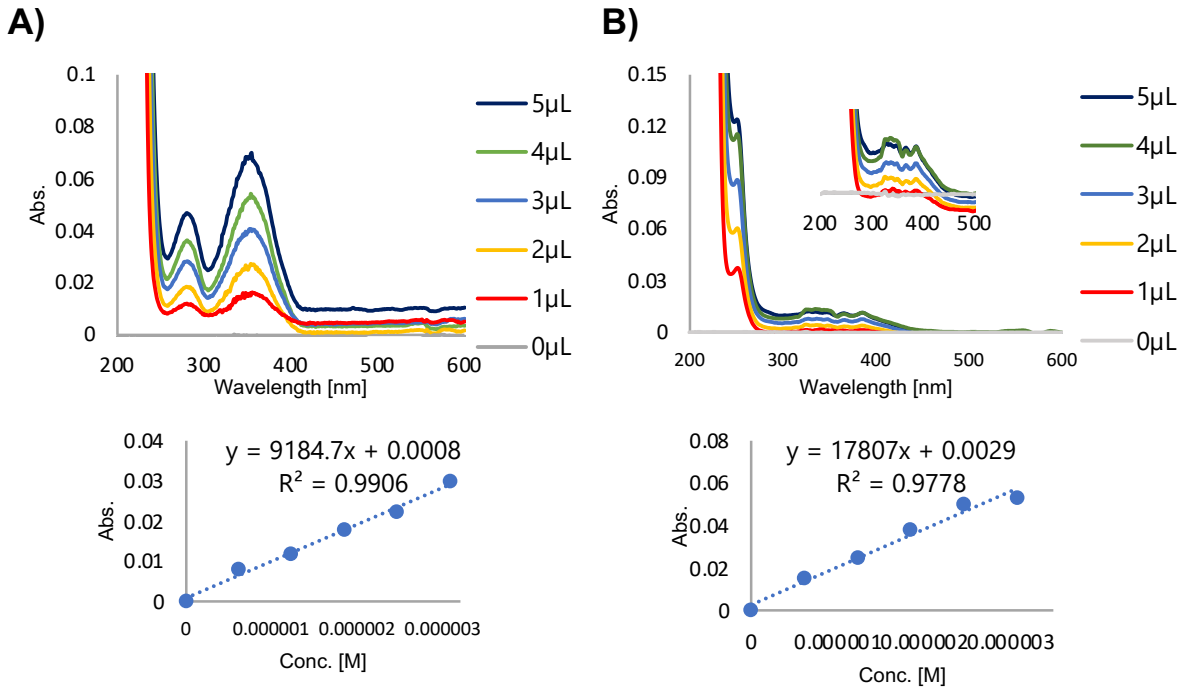

Figure 2. Calculation of the molar extinction coefficients at 260 nm (ε_{260}) of Ph and An. The UV spectra and titration graphs of A) **4-Ph** and B) **4-An**. The DMSO solution (200 μM) of the nucleoside was titrated to H_2O (325 μL). The molar extinction coefficients were calculated by the average of three individual titrations.

The flipping-out property was investigated by a fluorescence emission assay using the 2-aminopurine-containing ODN**2**(**Y** = AP) (Figure 3).[135,150] AP is a fluorescent probe that was efficiently quenched inside the duplex. The single-stranded ODN**2**(**Y** = AP) showed a high fluorescence intensity at 370 nm, in contrast, the fluorescence of AP in the ODN**1**(**X** = T)-ODN**2**(**Y** = AP) duplex was efficiently quenched (Figures 3A-C). For ODN**1**(**X** = Ph) (Figure 3B), the fluorescence intensity of AP in the ODN**1**(**X** = Ph)-ODN**2**(**Y** = AP) duplex slightly increased at 370 nm. Also, a hyperchromic shift in the fluorescence intensity of Ph base at 450 nm was observed compared to the ODN**1**(**X** = Ph)-ODN**2**(**Y** = A) duplex and single-stranded ODN**1**(**X** = Ph), suggesting that AP was flipped-out, then a Forster resonance energy transfer (FRET) would occur between the flipping AP and Ph bases.[151] Similarly, regarding ODN**1**(**X** = An) (Figure 3C), a slight increase in the fluorescence of AP at 370 nm and a large hyperchromic shift in the fluorescence intensity of the An base at 530 nm were recorded using the ODN**1**(**X** = An)-ODN**2**(**Y** = AP) duplex.

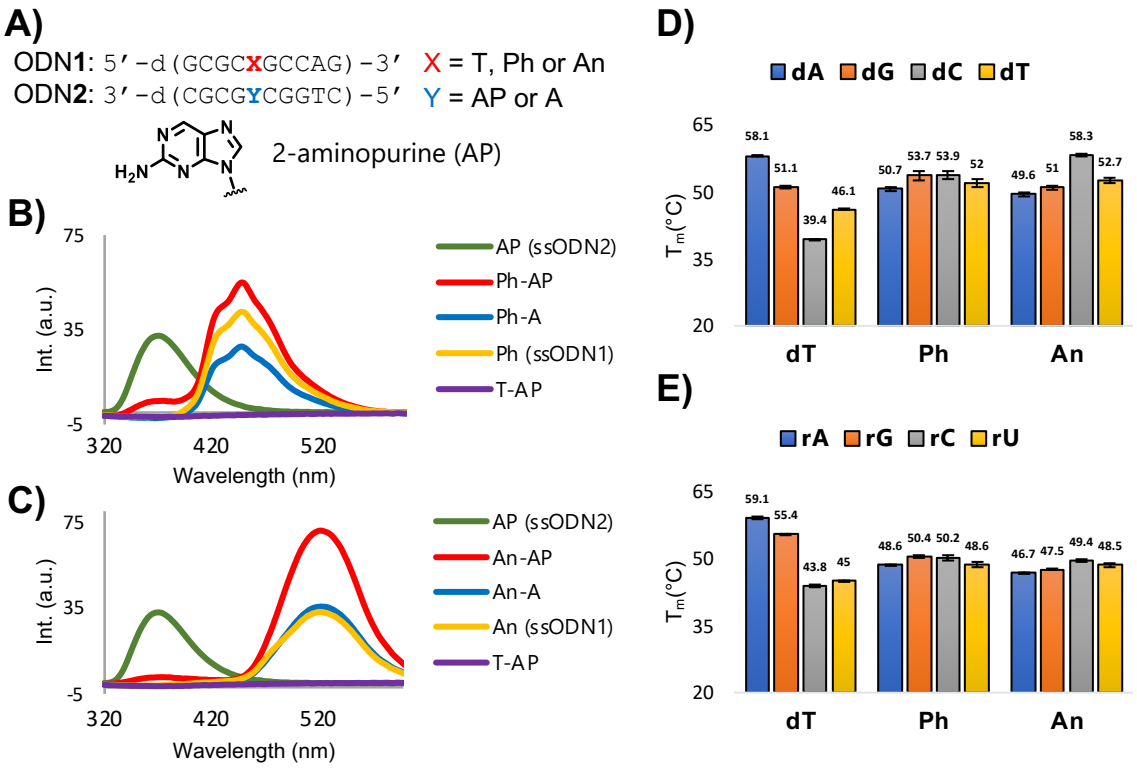

Figure 3. Investigation of base-flipping ability using a 2-aminopurine base and T_m measurement of Ph and An. A) Sequence of duplex. B) Fluorescence emission spectra for ODN**1**(**X** = Ph). C) Fluorescence emission spectra for ODN**1**(**X** = An). All measurements were carried out using the duplex or single strand (5.0 μM) in phosphate buffer (20 mM, pH 7.0) containing 100 mM NaCl at 25 °C. All spectra were excited at 310 nm. AP (ssODN**2**) indicates the single-stranded ODN**2**(**Y** = AP) D) T_m values of ODN**1**(**X** = dT, Ph or An)-ODN**2**(**Y** = dN) duplex. E) T_m values of ODN**1**(**X** = dT, Ph or An)-ORN**1**(**Y** = rN) duplex. The T_m values were measured using the duplex (4.0 μM) in phosphate buffer (20 mM, pH 7.0) containing NaCl (100 mM).

The thermal stability and base dependency of the Ph and An-containing duplex was next investigated by T_m measurements (Figures 3D, 3E, 4 and 5). Figures 3D and 3E show the T_m values of the ODN**1**(**X** = T, Ph or An)- ODN**2**(**Y** = dN) and ODN**1**(**X** = T, Ph or An)-ORN**1**(**Y** = rN) duplexes, respectively. The T_m values of the native ODN**1**(**X** = T)-ODN**2**(**Y** = dN) duplexes were in the range from 58.1 to 39.4 °C ($\Delta T_m = T_{m,max} - T_{m,min} = 18.7$ °C), while those of ODN**1**(**X** = Ph)-ODN**2**(**Y** = dN) and ODN**1**(**X** = An)-ODN**2**(**Y** = dN) were from 53.9 to 50.7 °C ($\Delta T_m = 3.2$ °C) and from 58.3 to 49.6 °C ($\Delta T_m = 8.7$ °C), respectively. The large base

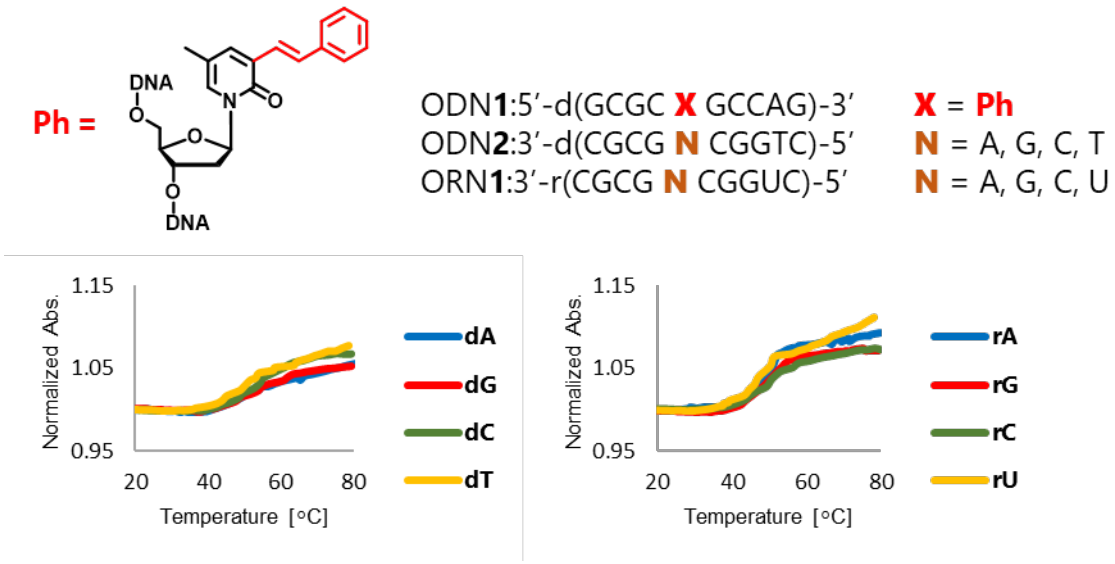

Figure 4. T_m measurement of Ph. UV-melting curves of ODN**1**(**X** = Ph)-ODN**2** and ODN**1**(**X** = Ph)-ORN**1** duplex. The T_m were measured using duplex (4.0 μM) in phosphate buffer (20 mM, pH 7.0) containing NaCl (100 mM).

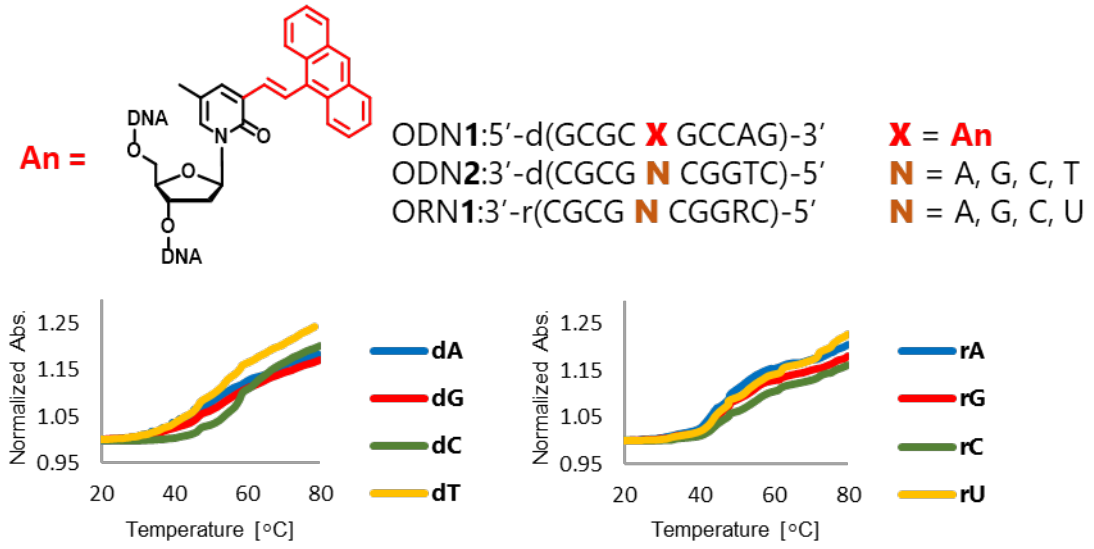

Figure 5. T_m measurement of An. UV-melting curves of ODN**1**(**X** = An)-ODN**2** and ODN**1**(**X** = An)-ORN**1** duplex. The T_m were measured using duplex (4.0 μM) in phosphate buffer (20 mM, pH 7.0) containing NaCl (100 mM).

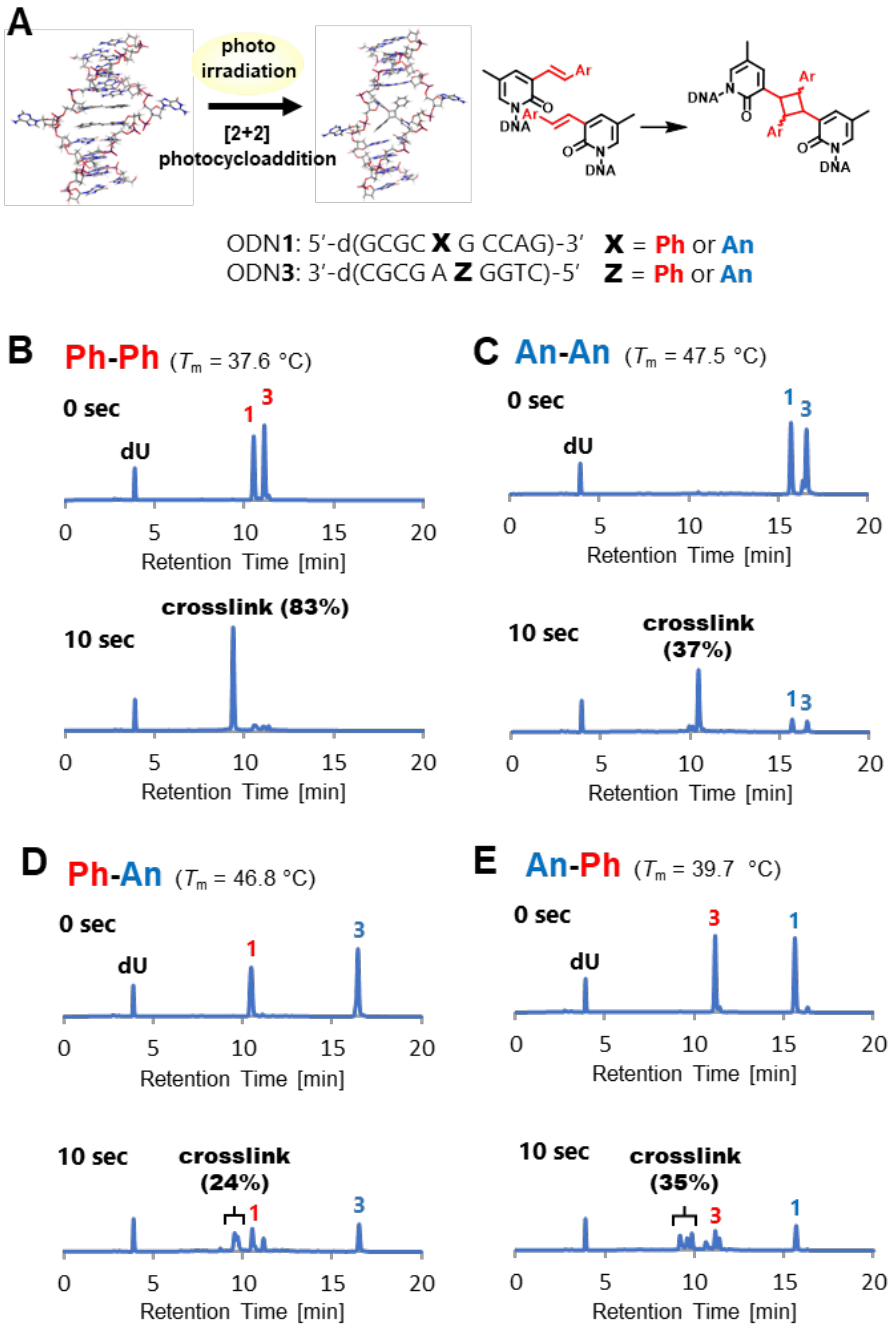

Figure 6. HPLC analysis for photo-cross-linking reaction of the ODN**1**–ODN**3** duplex. The photo reaction was carried out with ODN (5.0 μM) in phosphate buffer (20 mM, pH 7.0) containing NaCl (100 mM) by 365 nm UV lamp for 10 sec at 25 °C. (A) Scheme and sequences. (B) ODN**1**(**X** = Ph)–ODN**3**(**Z** = Ph) duplex. (C) ODN**1**(**X** = An)–ODN**3**(**Z** = An) duplex. (D) ODN**1**(**X** = Ph)–ODN**3**(**Z** = An) duplex. (E) ODN**1**(**X** = An)–ODN**3**(**Z** = Ph) duplex. The dU was used as an internal standard.

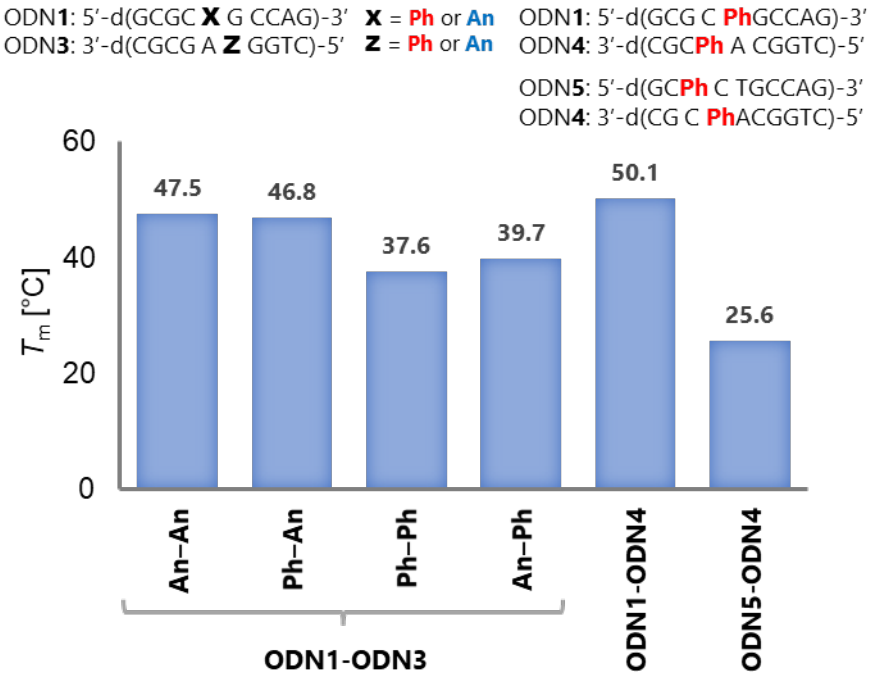

Figure 7. T_m measurement. UV-melting values of ODN**1**(**X** = Ph or An)-ODN**3**(**X** = Ph or An), ODN**1**(**X** = Ph)-ODN**4**(**X** = Ph) and ODN**5**(**X** = Ph)-ODN**4**(**X** = Ph) duplexes. The T_m were measured using duplex (4.0 μM) in Phosphate buffer (20 mM, pH 7.0) containing NaCl (100 mM).

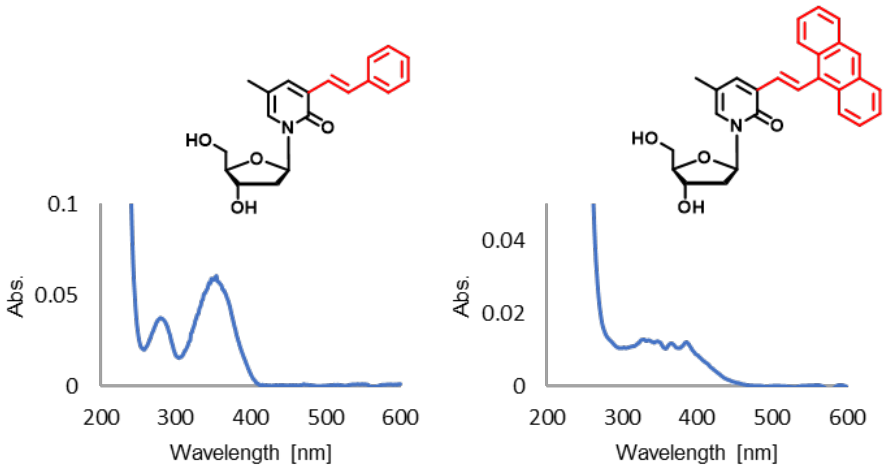

Figure 8. UV absorption measurement of Ph and An monomers. Absorbance measurement conditions: Diol (5 μL; 200 μM in DMSO) was added to H_2O (325 μL).

dependence of Ph and An was not observed except for the unexpectedly high T_m value of ODN**1**(**X** = An)-ODN**2**(**Y** = dC), and their values were comparable to that of the T-G mismatched duplex (51.1 °C). These results suggest that the displacement of T by Ph or An maintains the duplex stability by a stacking interaction of the aromatic moiety inside the duplex and flips the complementary base into the unstacked position. Similarly, as for the DNA-RNA

duplex, the T_m values of ODN**1**(**X** = T)- ORN**1**(**Y** = rN) were in the range from 59.1 to 43.8 °C (ΔT_m = 15.3 °C), while those of ODN**1**(**X** = Ph)-ORN**1**(**Y** = rN) and ODN**1**(**X** = An)-ORN**1**(**Y** = rN) were from 50.4 to 48.6 °C (ΔT_m = 1.8 °C) and from 49.4 to 46.7 °C (ΔT_m = 2.7 °C), respectively. No significant base dependence of Ph and An was observed for the DNA-RNA duplexes as well as for the DNA-DNA duplexes, and the values were higher than those of the T-C and T-U mismatched duplex (43.8 and 45.0 °C, respectively), indicating that the Ph and An bases worked as a flipping-out-induced base not only toward DNA but also RNA.

Table 2. MALDI-TOF mass data of the cross-linked products:

Entry	[a]Calcd	Assignment	[b]Found
ODN**1**(Ph)-ODN**3**(Ph)	6239.0	cross-link	6239.1
ODN**1**(An)-ODN**3**(An)	6436.7	cross-link	6437.9
ODN**1**(Ph)-ODN**3**(An)	6337.1	cross-link1	6338.7
		cross-link2	6337.7
ODN**1**(An)-ODN**3**(Ph)	6336.7	cross-link1	6336.7
		cross-link2	6337.9
		cross-link3	6337.7
ODN**1**(Ph)-ODN**4**(Ph)	6199.0	cross-link1	6199.4
		cross-link2	6199.4
ODN**5**(Ph)-ODN**4**(Ph)	6172.0	cross-link1	6173.5
		cross-link2	6173.9
		cross-link3	6174.3

[a] $[M\text{-}H]^-$, [b] All data were collected in negative mode.

Besides our previous attempt of alkyne—alkyne photo-cross-linking to realize a specific reaction by taking advantage of the flipping-out field,[91] in this study, we attempted alkene—alkene photo-cross-linking (Figure 6). We reciprocally arranged the Ph and/or An on ODN**1**-ODN**3** duplex and expected that Ph and/or An would flip the complementary base out and create a specific field where the photocycloaddition reaction occurs between the alkene-alkene, leading to the cross-linking of the duplex (Figure 6A). Before the photo-cross-linking reaction, we confirmed the thermal stability of the duplex for the photo-cross-linking (Figure 7). Regarding the ODN**1**-ODN**3** duplex, the T_m values of all combinations, *i.e.*, Ph-Ph, An-An,

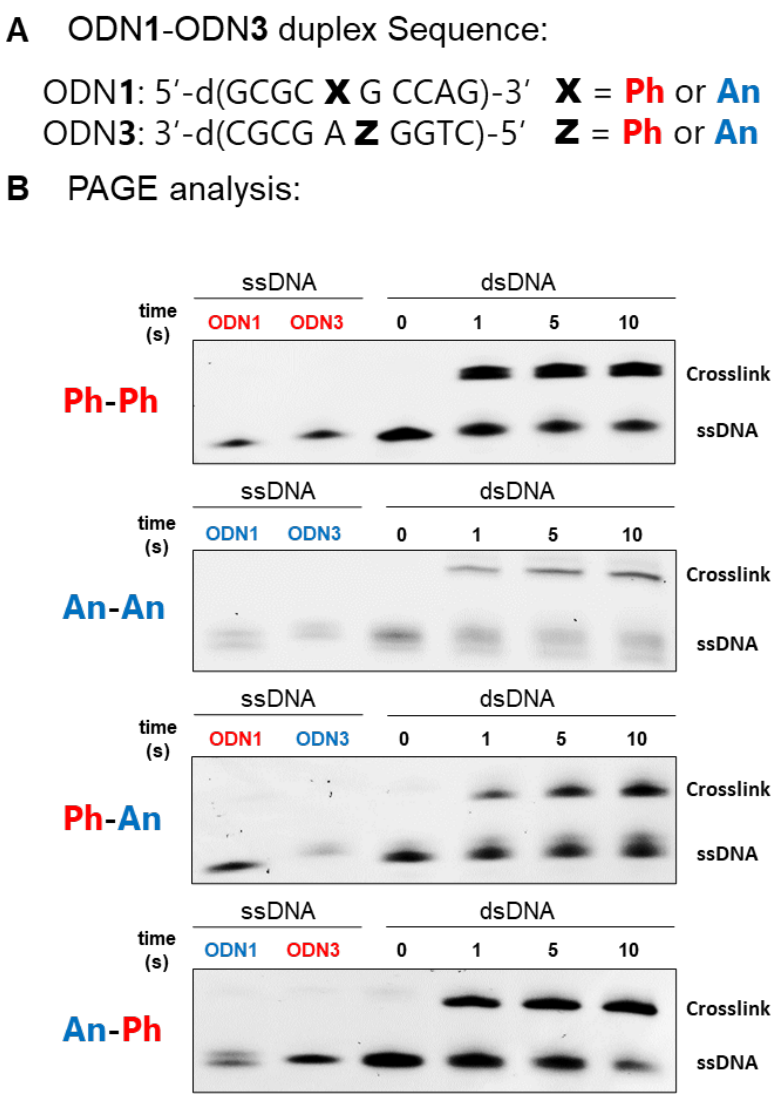

Figure 9. Photo-cross-linking reaction. The reaction was carried out with ODN**1**(**X** = Ph or An) (1.0 μM) and ODN**3**(**X** = Ph or An) (1.0 μM) in phosphate buffer (20 mM, pH 7.0) containing NaCl (100 mM) under 365 nm photoirradiation at 25 °C. (A) ODN**1**-ODN**3** duplex sequence. (B) PAGE analysis. The electrophoresis was performed on a 20% denaturing polyacrylamide gel. The DNAs were stained by SYBR gold.

Ph-An and An-Ph, were measured. The An-An and Ph-An combinations maintained relatively high T_m values (47.5 and 46.8 °C, respectively), while the Ph-Ph and An-Ph combinations reduced the T_m values to less than 40 °C (37.6 and 39.7 °C, respectively). A significant position dependency was observed when combined with the T_m values of the ODN**1**(**X** = Ph)-ODN**4** (50.1 °C) and ODN**5**-ODN**4** (25.6 °C) duplexes. Since these duplexes were sufficiently stable at 25 °C, except for the ODN5-ODN4 duplex, the photo reaction temperature was determined to be 25 °C.

The alkene–alkene photo-cross-linking was carried out by 365 nm UV light irradiation. The wavelength was determined from the UV-Vis spectra of the Ph and An nucleosides (Figure 8). HPLC analysis before and after the photoirradiation revealed that the Ph-Ph combination was the most effective, and a 10-sec photoirradiation was sufficient to achieve an 83% crosslinked product (Figure 6B). The MALDI-TOF MS measurements (Table 2) and polyacrylamide gel electrophoresis (PAGE) analysis (Figure 9) clearly showed that the product was the cross-linked one. In order to verify the structure of the Ph-Ph cross-linked product, the purified cross-linked ODN**1**(**X** = Ph)-ODN**3**(**Y** = Ph) was enzymatically digested down to the individual

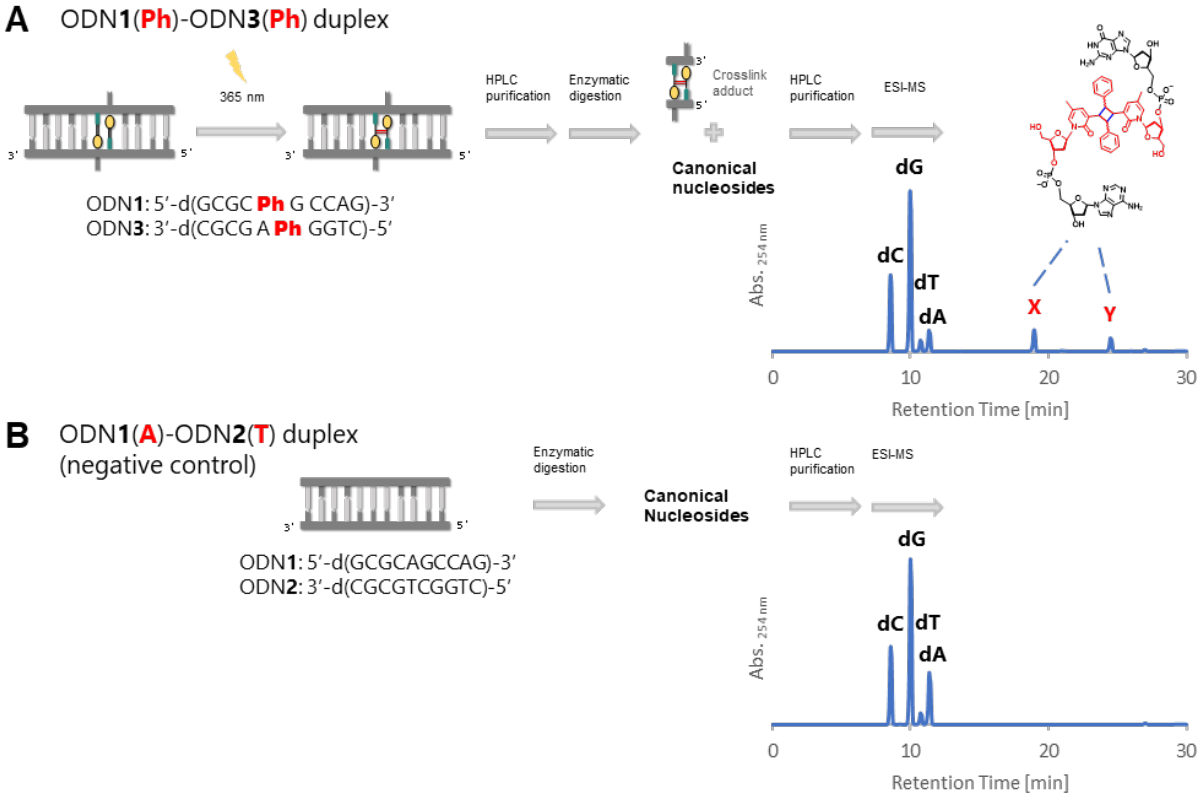

Figure 10. Enzymatic digestion and subsequent HPLC analysis of (A) ODN**1**(Ph)-ODN**3**(Ph) cross-linked duplex and (B) ODN**1**(A)-ODN**2**(T) duplex as a negative control.

nucleosides and cross-linked products present in the duplex. Subsequent HPLC and ESI-MS analyses of all the resulting products were performed (Figure 10). These analyses allowed the detection of two diastereomers corresponding to the Ph-Ph photocycloaddition product with the

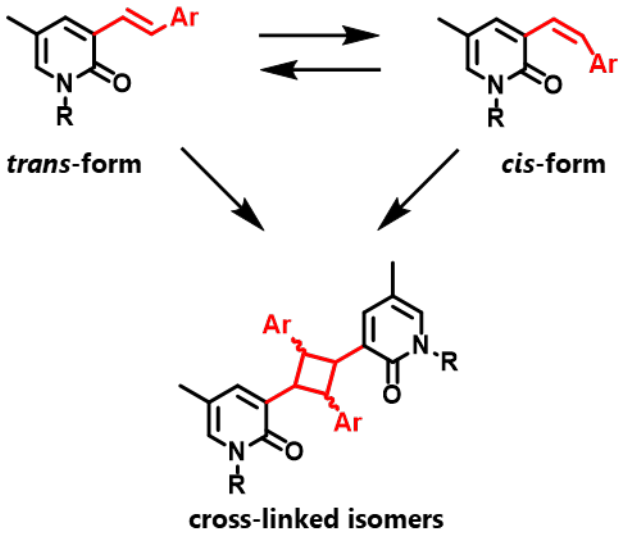

Figure 11. Assumed structures of isomers formed upon photoirradiation.

complementary nucleotides (dG and dA). The reason why these bases could not be cleaved by the enzyme may be due to their abnormal configuration resulting from the flipping-out of the helix. Whereas photoirradiation of the An-An, Ph-An and An-Ph combinations produced crosslink products in lower yields, 37%, 24% and 35%, respectively (Figure 6C-E). Unlike our previously reported alkyne-alkyne photo-cross-linking reaction in which hetero combinations were favorable[9], the Ph-Ph combination provided a high cross-linking yield within 10 sec. No significant change was observed in the degassing conditions by bubbling with argon gas,

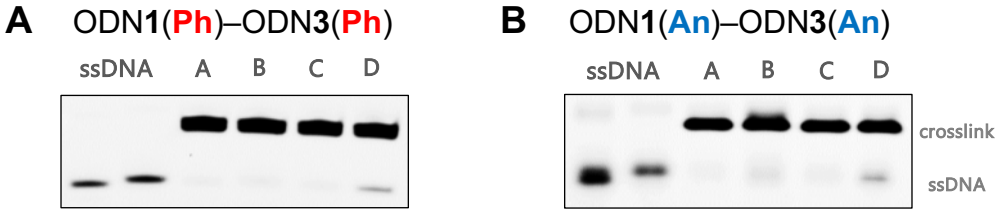

A. untreated crosslink
B. crosslink was irradiated for 10 sec
C. crosslink was incubated at 37 °C for 60 min
D. crosslink was incubated at 90 °C for 5 min

Figure 12. Investigation of the cross-linked product stability by PAGE analysis for HPLC-purified cross-linked product of **A**. ODN**1**(**X**=Ph)-ODN**3**(**Z**=Ph), **B**. ODN**1**(**X**=An)-ODN**3**(**Z**=An). (lane1) untreated crosslink product, (lane2) after photoirradiation (365 nm) for 10 sec, (lane3) incubation for 60 min at 37 °C and (lane4) incubation for 5 min at 90 °C. PAGE was carried out with cross-linked duplex (1.0 μM) in phosphate buffer (20 mM, pH 7.0) containing NaCl (100 mM).

suggesting that the expected [2+2] photocycloaddition reaction proceeded. Additionally, the Ph-An and An-Ph combinations provided two or three cross-linked product peaks with the same

MALDI-TOF MS value on the HPLC profile, suggesting that an isomerization occurred under the photo-irradiation conditions and the cross-linked isomers were produced (Figure 11). This isomerization is also supported by the enzymatic digestion of the Ph-Ph cross-linked product, which provided two diastereomeric peaks from one cross-linked product peak on the HPLC profile.

To investigate the stability of the Ph-Ph cross-linked product, aliquots of the HPLC-purified cross-linked product were photo-irradiated for another 10 sec, incubated at 37 °C for 1 h, or incubated at 90 °C for 5 min. A PAGE analysis showed sufficient stability of the cross-linked product (Figure 12A), indicating that this photo-cross-linking reaction is irreversible. On the other hand, for the An-An cross-linked product, a slight reverse reaction occurred after irradiation for 10 sec and after incubation at 90 °C for 5 min compared to Ph-Ph cross-linked product (Figure 12B). This observation might be one of the reasons for the modest yield of the An base-containing cross-linked product.

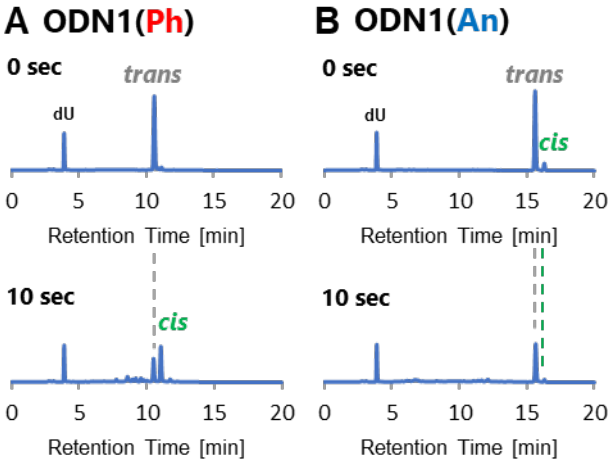

Figure 13. HPLC profiles of the Ph/An-containing single strand ODN**1**. ODN**1**(Ph) (A) or ODN**1**(An) (B) was photoirradiated by 365 nm UV light for 10 sec at 25 °C. The photoirradiation was carried out with ODN (5.0 μM) in phosphate buffer (20 mM, pH 7.0) containing NaCl (100 mM). The dU was used as an internal standard.

We investigated the possibility of an intermolecular [2+2] photocycloaddition reaction between the single-stranded ODNs (Figure 13). The Ph- or An-containing single-stranded ODNs, ODN**1**(**X** = Ph) and ODN**1**(**X** = An) were irradiated at 365 nm for 10 sec. For ODN**1**(**X**

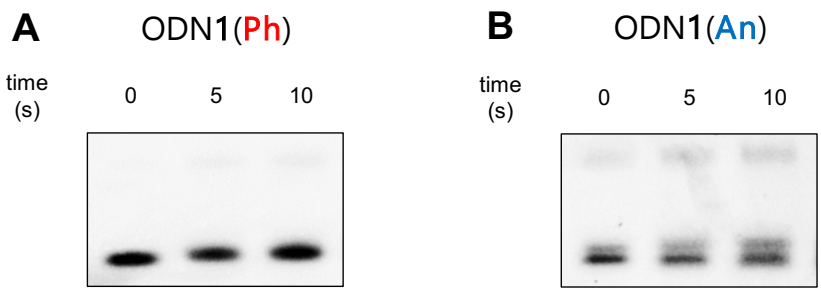

Figure 14. PAGE analysis for ssODN**1**(Ph) and ssODN**1**(An) before and after photoirradiation by 365 nm UV light at 25 °C. The photo irradiation was carried out with ODN (1.0 μM) in phosphate buffer (20 mM, pH 7.0) containing NaCl (100 mM). The electrophoresis was performed on a 16% denaturing polyacrylamide gel. The DNAs were stained by SYBR gold.

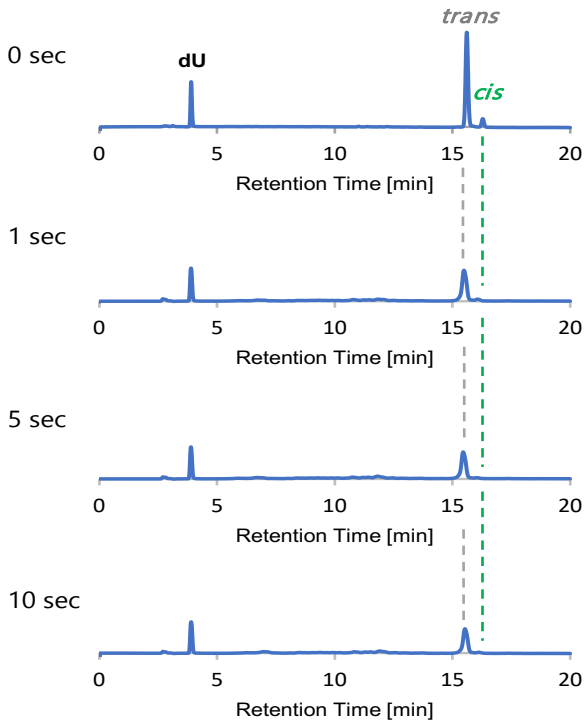

Figure 15. HPLC profiles of the An-containing single strand ODN**1**. ODN**1**(An) was photoirradiated by 365 nm UV light for 0, 1, 5, and 10 sec at 0 °C. The photo irradiation was carried out with ODN (5.0 μM) in phosphate buffer (20 mM, pH 7.0) containing NaCl (100 mM).

= Ph), a new peak with the same MALDI-TOF MS value as ODN**1**(**X** = Ph) appeared in the HPLC profile, indicating that photocycloaddition did not occur and isomerization to the *cis*-form took place instead (Figure 13A). PAGE analysis also showed no cross-linking reaction (Figure 14). For ODN**1**(**X** = An), the small peak with the mass number corresponding to the *cis*-isomer was observed on the HPLC profile before photo irradiation. After photo-irradiation, the HPLC and PAGE analyses showed no photocycloaddition (Figure 13B). Instead, a slight

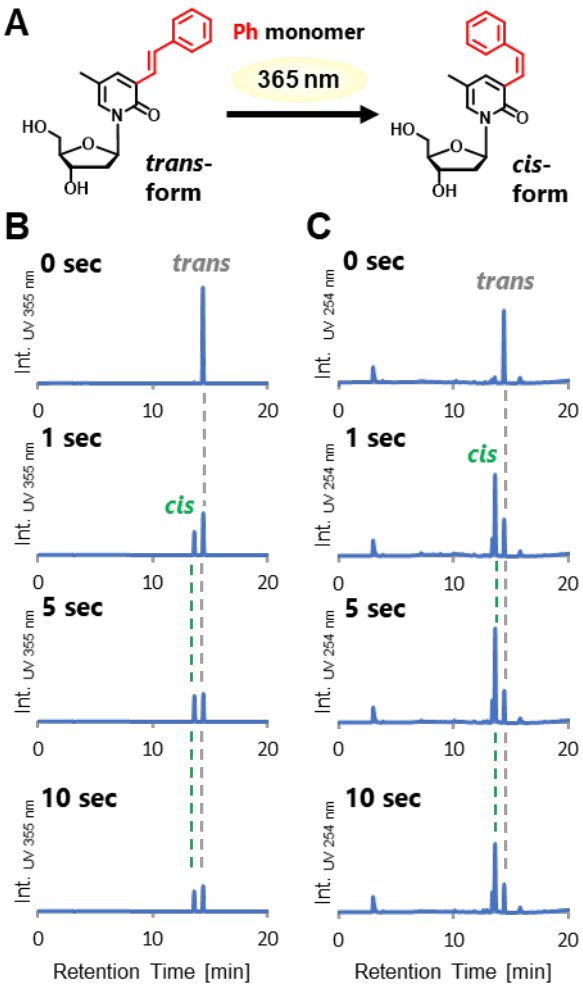

Figure 16. HPLC profiles of the Ph monomer before and after photoirradiation at the wavelength of 365 nm. (A) Scheme of the photoisomerization. (B and C) The HPLC profiles were recorded by UV detector at 355 nm (B) and 254 nm (C). The photoirradiation was carried out with **4-Ph** (50 μM) in phosphate buffer (20 mM, pH 7.0) containing 10% DMSO.

decrease in the peak intensity of ODN**1**(An) was recorded, probably due to the side reactions of the anthracenyl moiety. We attempted photoirradiation of ODN1(X = An) at 0 °C to suppress these side reactions and increase the *cis*-isomer, but no improvement was observed (Figure 15). This decrease in ODN**1**(An) would be the other reason for the modest cross-link yields with the An base. Also, the absence of the intermolecular [2+2] photocycloaddition reaction clarified the importance of the alkene-alkene proximity within the duplex to achieve that high yield photo-cross-linked product.

We also investigated the photochemical properties of the Ph diol monomer (**4-Ph**) (Figure 16).

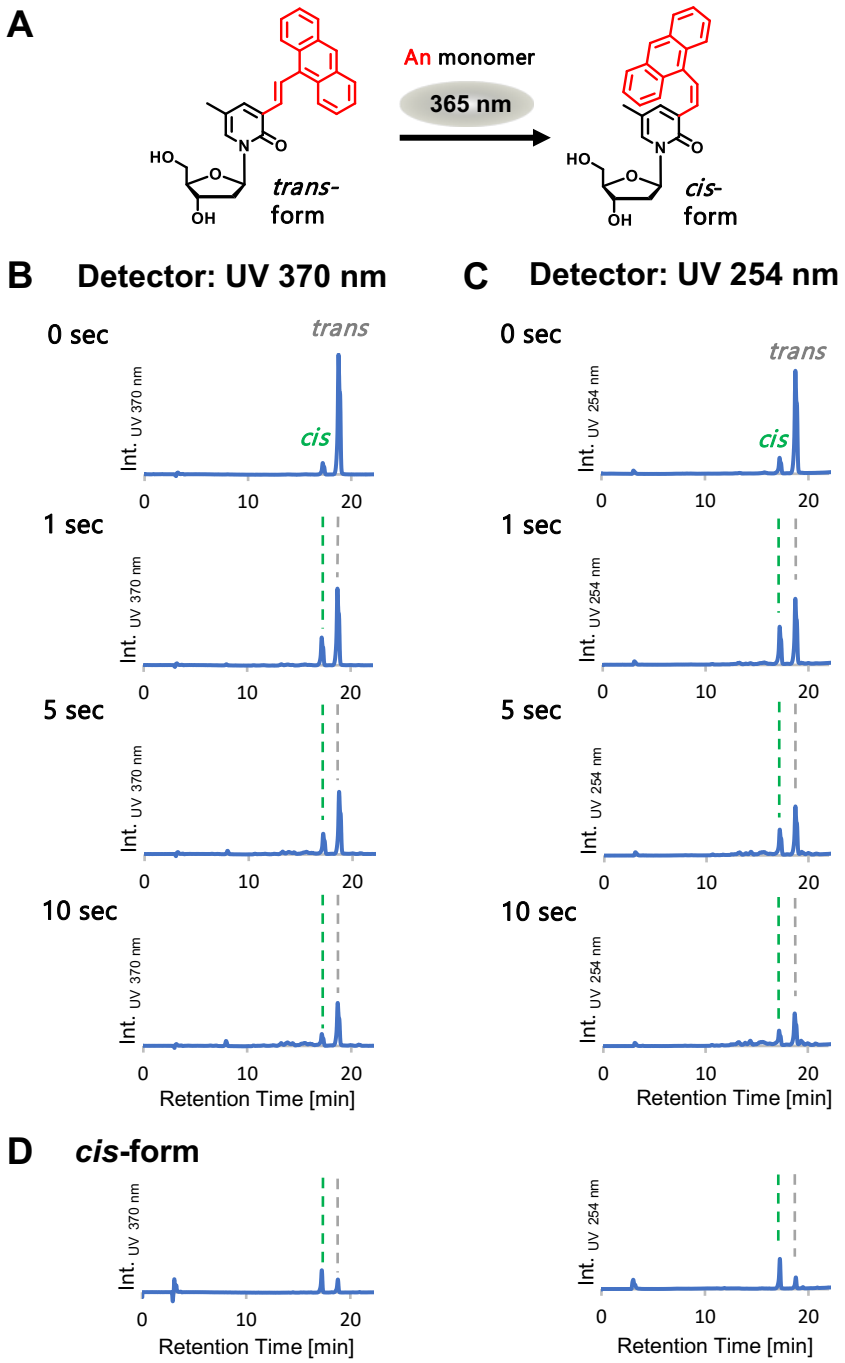

Figure 17. HPLC profiles of the **4-An** monomer before and after photoirradiation at wavelength 365 nm. (A) Scheme of the photoisomerization. (B and C) The HPLC profiles were recorded by UV detector at (B) 370 nm and (C) 254 nm. The photo irradiation was carried out with **4-An** (50 μM) in phosphate buffer (20 mM, pH 7.0) and 10% DMSO. (D) Analysis of the isolated *cis*-isomer. The HPLC profiles were recorded by UV detector at 370 nm (left) and 254 nm (right).

Upon irradiation at 365 nm, a new peak appeared on the HPLC profiles recorded by the UV detector at 355 nm and 254 nm. Its ESI-MS value was the same as the starting material. The ^{1}H

and ^{13}C NMR measurements indicated that the peak was the *cis*-isomer and suggested that the isomerization rapidly occurred from the *trans*- to *cis*-isomer. By increasing the irradiation to 10 sec, the [2+2] photocycloaddition product could not be observed under these reaction conditions due to the absence of the proximity effect. HPLC analysis of the An diol monomer (**4-An**) exhibited two peaks with the same ESI-MS number corresponding to the *cis*- and *trans*-

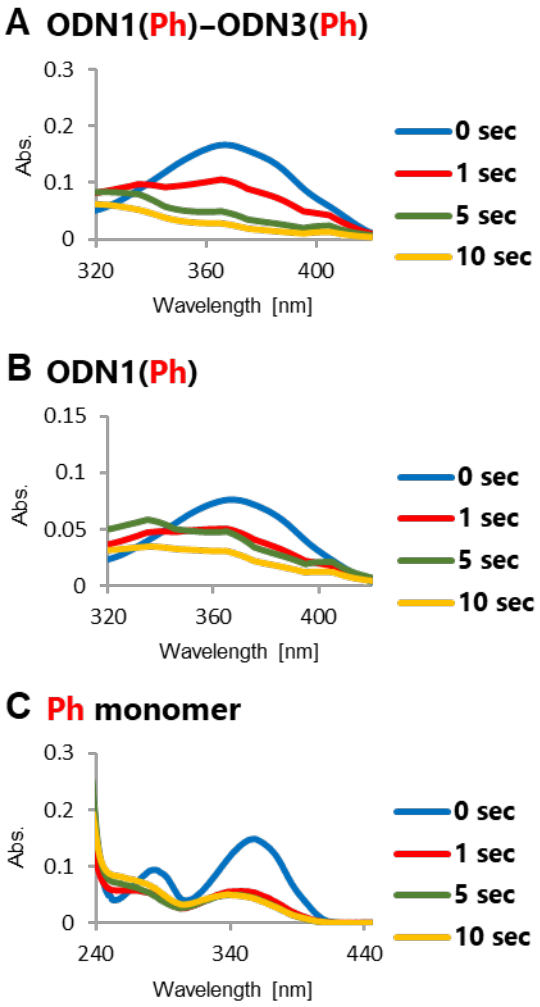

Figure 18. UV-vis spectra of (A) ODN**1**(Ph) – ODN**3**(Ph) duplex and (B) single strand ODN**1**(Ph) (C) Ph monomer before and after photoirradiation at 25 °C. For DNA, the solution conditions were 5.0 µM, 100 mM NaCl, 20 mM phosphate buffer (pH 7.0). For the monomer, the solution conditions were 10 µM, 20 mM phosphate buffer (pH 7.0) and 10% DMSO.

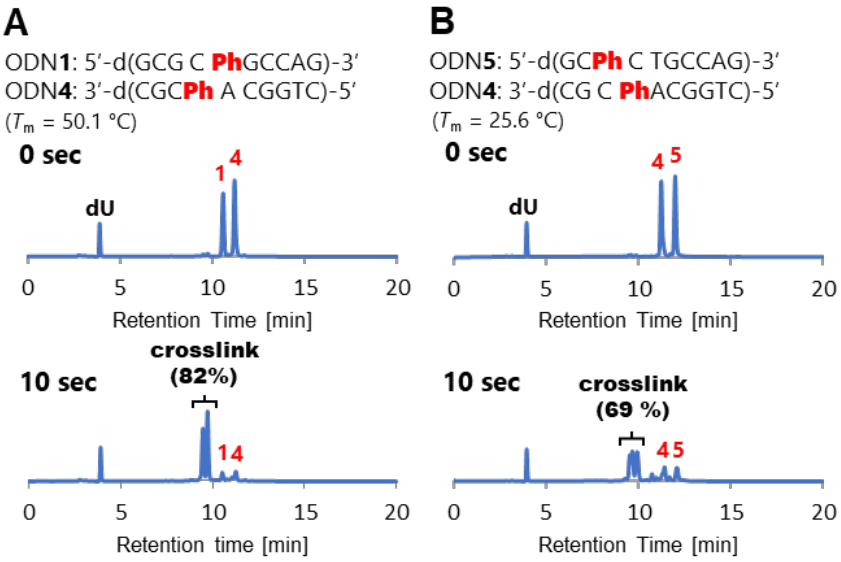

Figure 19. HPLC analysis for (A) ODN**1**(Ph)-ODN**4**(Ph) and (B) ODN**5**(Ph)-ODN**4**(Ph) duplexes before and after photoirradiation at 365 nm by UV light for 10 sec at 25 °C. For the HPLC analysis, the photoirradiation was carried out with ODN (5.0 μM) in phosphate buffer (20 mM, pH 7.0) containing NaCl (100 mM).

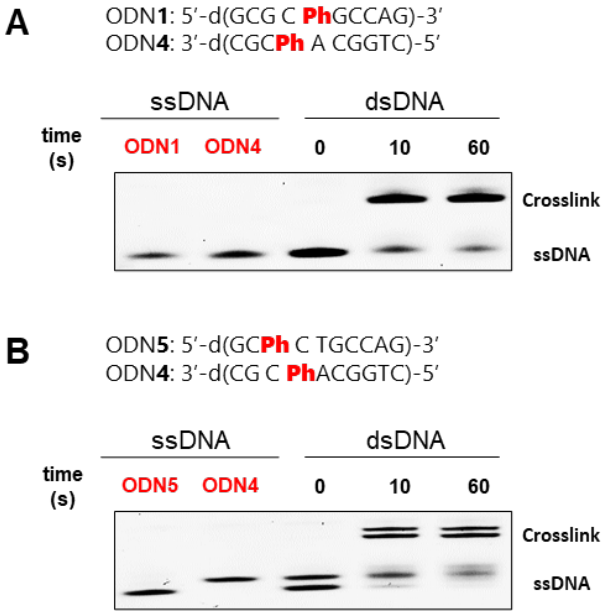

Figure 20. PAGE analysis of photo-cross-linking reaction. The reaction was carried out with (A) ODN**1**(Ph)-ODN**4**(Ph) (1.0 μM) and (B) ODN**5**(Ph)-ODN**4**(Ph) (1.0 μM) in phosphate buffer (20 mM, pH 7.0) containing NaCl (100 mM) under 365 nm photoirradiation at 25 °C. The electrophoresis was performed on a 20% denaturing polyacrylamide gel. The DNAs were stained by SYBR gold.

isomers (Figure 17). Upon irradiation at 365 nm for 1 sec, the *cis*-isomer peak increased, but further irradiation decreased both peaks. Subsequent HPLC analysis of the isolated *cis*-isomer afforded a mixture of both isomers, indicating low thermal stability of the *cis*-isomer. These

results suggest that the An base has isomerization properties and instability under photoirradiation conditions.

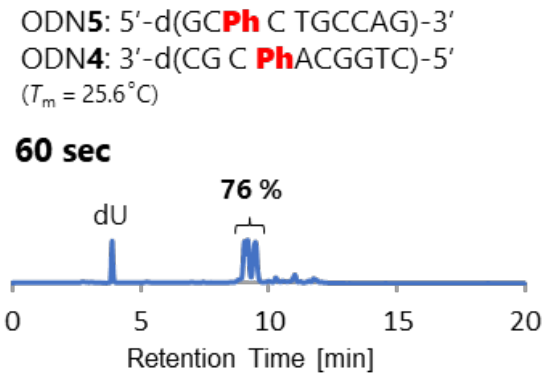

Figure 21. HPLC analysis for ODN**5**(Ph)-ODN**4**(Ph) duplex after photoirradiation (365 nm) for 60 sec at 0 °C. The photoirradiation was carried out with ODNs (5.0 μM) in phosphate buffer (20 mM, pH 7.0) containing NaCl (100 mM).

For further investigation of the Ph-Ph photo-cross-linking reaction of the ODN**1**(Ph)-ODN**3**(Ph) duplex and Ph isomerization of the single-stranded ODN**1** and monomer, we measured the UV-vis spectra before and after the photoirradiation (Figure 18). Before photoirradiation, the Ph bases exhibited a peak at around 370 nm for the π-π* transition of the *trans* isomer. Upon photoirradiation at 365 nm to the duplex for 10 sec, the peak of the Ph bases vanished without any peak shift of λ_{max}, suggesting that the [2+2] photoirradiation reaction occurred between the two Ph bases (Figure 18A). In contrast, the photoirradiation of the single-stranded ODN**1** caused a peak decrease at 370 nm with a slight hypsochromic shift which refers to the photoisomerization of the *cis*-form (Figure 18B). Regarding the Ph-monomer, two peaks of the Ph *trans*-form appeared at 286 and 363 nm before the photoirradiation. The photoirradiation for 10 sec at 365 nm caused a decrease in the peak intensities with a hypsochromic shift, 286 to 277 nm and 363 to 354 nm, respectively, with a similar tendency as the single-stranded ODN**1** (Figure 18C).

To investigate the generality of the Ph-Ph photo-cross-linking, we prepared ODN**1**(Ph)-ODN**4**(Ph) and ODN**5**(Ph)-ODN**4**(Ph) with the Ph-Ph overlapping at a different position on the duplex (Figure 19). The photo reaction of the ODN**1**-ODN**4** (Figure 19A) and ODN**5**-ODN**4** (Figure 19B) duplexes were analyzed by HPLC and PAGE analyses (Figure S20). Upon

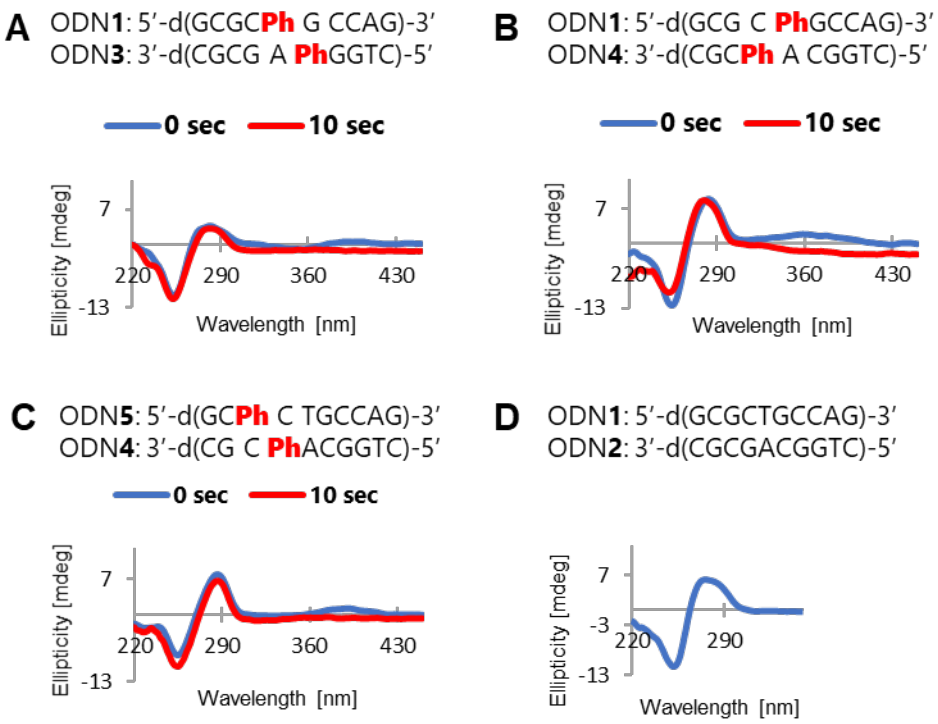

Figure 22. CD spectra of Ph-containing duplexes before (blue line) and after 10 sec photoirradiation (red line). Conditions are as follows: [ODN] = 4.0 μM, [NaCl] = 100 mM, 20 mM phosphate buffer (pH 7.0), 25 °C.

irradiation of the duplexes with 365 nm UV light at 25 °C for 10 sec, the peaks related to ODN**1**, ODN**4,** and ODN**5** decreased in the HPLC profile, and two or three new peaks appeared. The subsequent MALDI-TOF analysis of these peaks indicated the cross-linked products (Table 2). The multi-cross-linked products would be produced by isomerization, as shown in Figure 11. Furthermore, the interpretation that these new peaks correspond to the cross-linking products was supported by the PAGE analysis showing the expected low mobility bands corresponding to the cross-linked product (Figure 20). The photo-cross-linking yield of the ODN**1**-ODN**4** was 82%, almost the same as the yield of ODN**1**-ODN**3** duplex (83%). In contrast, the ODN**5**-ODN**4** duplex provided a lower yield (69%) due to the relatively low thermal stability (T_m = 25.6 °C). Therefore, photoirradiation was performed at 0 °C for 60 sec. The yield increased to 76% as the low temperature contributed to the proper formation of the duplex (Figure 21). This result suggests that the photo-cross-linking can proceed even with duplexes with a low T_m value.

The structural changes in the duplex were investigated by CD measurements before and after the photoirradiation for 10 sec using the native duplex and Ph-containing duplexes (Figure 22). Before the photoirradiation, the Ph-containing ODN**1**-ODN**3**, ODN**1**-ODN**4,** and ODN**5**-

ODN**4** duplexes showed the induced CD band in the region over 300 nm, suggesting that the Ph moiety is settled in the chiral environment of the duplex. After photoirradiation, the induced CD spectra disappeared due to the photocycloaddition. In addition, all the Ph-Ph combinations showed a CD similar to the native B-form duplex before the photoirradiation. After photoirradiation, no large differences were observed, indicating that the cross-linking reaction did not significantly change the duplex conformation.

Conclusion

In conclusion, we developed the base flip-inducing ODNs with the alkene-type Ph or An base, *i.e.*, the 5-methylpyridone derivatives linked to aromatic compounds with an alkene linker at the C3 position. Both the Ph and An bases flipped the complementary base on the DNA and RNA and stabilized the flipped-out structure by the stacking interaction. In addition, a rapid photo-cross-linking was realized by taking advantage of the formed specific reaction field. Especially the Ph-Ph combination provided a cross-linked product in a high yield by only a 10-sec photoirradiation. The highly efficient reaction enabled the forming of the cross-linked product even using the duplex with a low T_m value. This will be helpful in making short-strand cross-linkings. Recently, we reported that the anti-miRNA oligonucleotides (AMOs) containing the chemically cross-linked duplex at the terminal sequences and these AMOs showed a significantly high anti-miRNA activity.[95] Our alkene-alkene photo-cross-linking would be a new candidate to form cross-linked oligonucleotides in addition to our previous alkyne-alkyne photo-cross-linking. Further efforts are underway toward exploring the unique biological and nanomaterial functions of the flipped-out cross-linked nucleic acids.

Experimental data

General Materials and methods. The general chemicals were purchased from commercial suppliers (FUJIFILM Wako Pure Chemical, the Tokyo Chemical Industry, Kanto Chemical, Nacalai tesque or Aldrich) and used without further purification unless specifically mentioned. The target DNAs and RNAs were purchased from JBioS (Japan). The ^{1}H NMR spectra (400 MHz) were recorded by a Bruker AVANCE III 400 spectrometer. The ^{1}H NMR spectra (600 MHz) and ^{13}C NMR spectra (150 MHz) were recorded by a Bruker AVANCE III 600 spectrometer. The high-resolution electrospray mass analysis was performed by a Bruker MicrOTOFQ II. The HPLC purification was performed by a JASCO HPLC System (PU-4180, UV-4075, and CO-2067Plus). The MALDI-TOF MS measurements were performed by a

Bruker Autoflex speed instrument utilizing a 3-hydroxypicolinic acid/diammonium hydrogen citrate matrix.

General procedure for Heck coupling. A mixture of palladium acetate (7.4 mg, 0.033 mmol), triphenyl phosphine polymer-bound (22 mg, 0.066 mmol), and potassium carbonate (54.6 mg, 0.396 mmol) were added to a solution of **1**, previously reported,[91] (100 mg, 0.165 mmol) in anhydrous *N,N*-dimethylformamide (1.65 mL) under an argon atmosphere at room temperature and stirred for 30 min. An olefin (0.25 mmol) was then added to the reaction mixture, and the mixture was heated at 90 °C on an oil bath for 4 h. The produced suspension was cooled to room temperature, diluted with ethyl acetate, and filtered through Celite with ethyl acetate. The filtrate was evaporated under reduced pressure, and the residue was purified by flash column chromatography on silica gel (Kanto Chemical 60N) using hexane/ethyl acetate (1/3→2/3) to obtain the pure product.

*Compound **2-Ph***. Following the general method, the reaction of styrene (28 μL, 0.25 mmol) with **1** afforded **2-Ph** (60.3 mg, 58%) as a yellow foam.

^{1}H NMR (600 MHz, $CDCl_3$): δ 7.66 (m, 1H), 7.52 (d, J = 7.2 Hz, 2H), 7.49 (d, J = 16.2 Hz, 1H), 7.43 (dd, J = 7.8, 1.2 Hz, 2H), 7.41 (d, J = 2.4 Hz, 1H), 7.34-7.30 (m, 6H), 7.28 (t, J = 7.8 Hz, 2H), 7.23 (m, 3H), 6.83 (dd, J = 9.0, 1.8 Hz, 4H), 6.61 (t, J = 6.0 Hz, 1H), 4.52 (dt, J = 6.0, 4.2 Hz 1H), 4.15 (q, J = 3.6 Hz, 1H), 3.78 (s, 6H), 3.52 (dd, J = 10.8, 3.6 Hz, 1H), 3.39 (dd, J = 10.8, 3.6 Hz, 1H), 2.70 (ddd, J = 13.8, 6.0, 4.2 Hz, 1H), 2.52 (s, 1H), 2.27 (dt, J = 13.8, 6.0 Hz, 1H) , 1.84 (s, 3H). ^{13}C{^{1}H} NMR (150 MHz, $CDCl_3$): δ 160.3, 158.8, 144.7, 137.9, 137.9, 135.8, 135.8, 130.9, 130.2, 128.7, 128.7, 128.3, 128.1, 127.7, 127.3, 127.1, 126.8, 123.8, 115.3, 113.4, 86.9, 86.2, 72.3, 63.5, 55.4, 42.4, 17.5. HRMS (ESI): *m/z* calcd for $C_{40}H_{39}NO_6Na^+$ $[M+Na]^+$, 652.2670; found, 652.2682.

*Compound **2-An***. Following the general method, the reaction of 9-vinylanthracene (50.5 mg, 0.25 mmol) with **1** afforded **2-An** (46 mg, 38%) as a yellow foam.

^{1}H NMR (600 MHz, $CDCl_3$): δ 8.54 (d, J = 16.2 Hz, 1H), 8.41 (dd, J = 7.2, 1.2 Hz, 2H), 8.38 (s, 1H), 8.00-7.98 (m, 2H), 7.76 (d, J = 1.2 Hz, 1H), 7.46-7.42 (m, 7H), 7.33 (d, J = 9.0 Hz, 2H), 7.32 (d, J = 9.0 Hz, 2H), 7.28 (t, J = 7.2 Hz, 2H), 7.23 (t, J = 7.2 Hz, 1H), 6.98 (d, J = 16.2 Hz, 1H), 6.83 (d, J = 9.0 Hz, 2H), 6.82 (d, J = 9.0 Hz, 2H), 6.71 (t, J = 6.0 Hz, 1H), 4.54 (m, 1H), 4.17 (q, J = 3.6 Hz, 1H), 3.78 (s, 6H), 3.55 (dd, J = 10.8, 3.6 Hz, 1H), 3.39 (dd, J = 10.8, 3.6 Hz, 1H), 2.76 (ddd, J = 13.8, 6.0, 4.2 Hz, 1H), 2.46 (d, J = 3.6 Hz, 1H), 2.35 (dt, J = 13.8, 6.0 Hz, 1H), 1.88 (s, 3H). ^{13}C{^{1}H}NMR (150 MHz, $CDCl_3$): δ 160.4, 158.8, 144.7, 139.4, 135.8, 135.8, 133.7, 133.0, 131.7, 130.3, 129.7, 129.0, 128.7, 128.3, 128.3, 128.1, 127.2, 127.0, 126.4,

125.5, 125.3, 115.3, 113.4, 113.4, 86.9, 86.2, 86.1, 72.4, 63.5, 55.4, 42.4, 17.5. HRMS (ESI): *m/z* calcd for $C_{48}H_{43}NO_6Na^+$ $[M+Na]^+$, 752.2988; found, 752.2982.

General procedure for phosphitylation reaction. Compound **2** was co-evaporated with anhydrous acetonitrile (3 mL x 3) and dissolved in anhydrous dichloromethane. Then, *N,N*-diisopropylethylamine and 2-cyanoethyldiisopropylchlorophosphoroamidite were added to the solution under an argon atmosphere and stirred at room temperature. After 1 h, the reaction was quenched by adding methanol (50 μL) to the reaction mixture. The reaction mixture was diluted with a saturated aqueous sodium hydrogen carbonate solution (15 mL) and extracted with ethyl acetate (15 mL). The organic layer was washed with brine (15 mL), dried over anhydrous sodium sulfate, and the solvent was evaporated under reduced pressure. The residue was purified by silica gel column chromatography.

*Compound **3-Ph**.* Following the general procedure, a solution of **2-Ph** (25 mg, 0.040 mmol) in a dichloromethane solution (2.3 mL) was allowed to react with N, N-diisopropylethylamine (190 μL, 1.1 mmol) and 2-cyanoethyldiisopropylchlorophosphoroamidite (100 μL, 0.45 mmol). The residue was purified by silica gel column chromatography (Kanto Chemical 60N) using hexane/ethyl acetate (3/1) to provide **3-Ph** (94.2 mg, 63%) as a yellow foam.

^{31}P NMR (162 MHz, $CDCl_3$): δ 149.1, 148.3. HRMS (ESI): *m/z* calcd for $C_{49}H_{56}N_3O_7PNa^+$ $[M+Na]^+$, 852.3754; found, 852.3788.

*Compound **3-An**.* Following the general procedure, A solution of **2-An** (110 mg, 0.15 mmol) in dichloromethane solution (1.9 mL) was allowed to react with *N,N*-diisopropylethylamine (157 μL, 0.90 mmol), and 2-cyanoethyldiisopropylchlorophosphoroamidite (84 μL, 0.38 mmol). The residue was purified by silica gel column chromatography (Kanto Chemical 60N) using hexane/ethyl acetate = 1/1) to provide **3-An** (139 mg, 99%) as a yellow foam.

^{31}P NMR (162 MHz, $CDCl_3$): δ 149.0, 148.3. HRMS (ESI): *m/z* calcd for $C_{57}H_{60}N_3O_7PNa^+$ $[M+Na]^+$, 952.4067; found, 952.4088.

General procedure for diol formation. Trifluoroacetic acid was added to an anhydrous dichloromethane solution of **2-Ph or 2-An** at 0 °C under an argon atmosphere, and the mixture was stirred. The reaction mixture was quenched by a saturated aqueous sodium hydrogen carbonate solution (1 mL) and diluted with dichloromethane (15 mL). The mixture was washed with saturated aqueous sodium hydrogen carbonate (15 mL x 2), dried over anhydrous sodium sulfate, and the solvent was evaporated under reduced pressure. The residue was purified by silica gel column chromatography.

*Compound **4-Ph***. Following the general procedure, trifluoroacetic acid (7.5 μL, 0.098 mmol) was added to a solution of **2-Ph** (31 mg, 0.049 mmol) in anhydrous dichloromethane (817 μL), and the mixture was stirred for 1 h. The residue was purified by silica gel chromatography (Kanto Chemical 60N) using ethyl acetate to afford **4-Ph** (8.0 mg, 50%) as a white solid.

^{1}H NMR (400 MHz, $CDCl_3$): δ 7.88 (m, 1H), 7.69 (d, J = 2.4 Hz, 1H), 7.52 (d, J = 7.6 Hz, 2H), 7.45 (d, J = 16.4 Hz, 1H), 7.34 (t, J = 7.6 Hz, 2H), 7.27 (d, J = 16.4 Hz, 1H), 7.24 (t, J = 7.6 Hz, 1H), 6.52 (t, J = 6.4 Hz, 1H), 4.39 (dt, J = 6.4, 4.0 Hz 1H), 4.01 (q, J = 3.6 Hz, 1H), 3.86 (dd, J = 12.0, 3.6 Hz, 1H), 3.77 (dd, J = 12.0, 4.0 Hz, 1H), 2.51 (ddd, J = 13.6, 6.4, 4.0 Hz, 1H), 2.18 (s, 3H), 2.10 (dt, J = 13.6, 6.4 Hz, 1H). ^{13}C{^{1}H} NMR (150 MHz, $CDCl_3$): δ 159.9, 137.3, 137.0, 130.0, 128,6, 127.7, 126.8, 126.1, 125.6, 121.9, 115.7, 87.1, 85.4, 69.8, 60.6, 40.7, 15.5. HRMS (ESI): *m/z* calcd for $C_{19}H_{22}NO_4^+$ $[M+H]^+$, 328.1551; found, 328.1552.

*Compound **4-An***. Following the general procedure, trifluoroacetic acid (3.5 μL, 0.046 mmol) was added to a solution of **2-An** (16.6 mg, 0.023 mmol) in anhydrous dichloromethane (500 μL), and the mixture was stirred for 30 min. The residue was purified by silica gel chromatography (Kanto Chemical 60N) using hexane/ethyl acetate (1/2) to afford **4-An** (5.1 mg, 53%) as a white solid.

^{1}H NMR (600 MHz, MeOD-d_4): δ 8.43 (s, 1H), 8.40 (d, J = 16.8 Hz, 1H), 8.39-8.36 (m, 2H), 8.03 (dd, J = 6.0, 3.0 Hz, 2H), 7.97 (d, J =1.2 Hz, 1H), 7.83 (d, J = 1.8 Hz, 1H), 7.48-7.46 (m, 4H), 6.99 (d, J = 16.8 Hz, 1H), 6.58 (t, J = 6.0 Hz, 1H), 4.43 (dt, J = 6.0, 4.2 Hz, 1H) , 4.03 (q, J = 3.6 Hz, 1H), 3.89 (dd, J = 12.0, 3.6 Hz, 1H), 3.80 (dd, J = 12.0, 3.6 Hz, 1H), 2.56 (ddd, J = 13.2, 6.0, 4.2 Hz, 1H), 2.24 (s, 3H), 2.19 (dt, J = 13.2, 6.0 Hz, 1H) . ^{13}C{^{1}H} NMR (150 MHz, MeOD-d_4): δ 161.9, 140.6, 134.2, 133.4, 133.1, 131.1, 130.9, 129.8, 128.8, 127.8, 127.6, 127.3, 126.6, 126.2, 117.8, 89.1, 87.5, 71.7, 62.6, 42.8, 17.5. HRMS (ESI): *m/z* calcd for $C_{27}H_{26}NO_4^+$ $[M+H]^+$, 428.1864; found, 428.1859.

Preparation of DNA oligonucleotides. The DNA oligonucleotides were synthesized according to standard protocols (1.0 μmol scale) utilizing an Applied Biosystems model 392 DNA/RNA synthesizer. Deprotection and cleavage from the CPG support were carried out under ultra-mild conditions with a 28% ammonia solution at room temperature for 4 h. Next, the DMTr-ON oligonucleotides were purified by HPLC. The HPLC purification conditions were as follows: C-18 column (Nacalai tesque: COSMOSIL 5C_{18}-MS-II, 4.6ID x 250 mm) by a linear gradient of 10-40%/20 min acetonitrile in TEAA buffer (0.1 M) at the flow rate of 4 mL/min and 35 °C. Peaks were monitored by a UV detector (λ = 254 nm). Subsequently, the DMTr group was deprotected by 10% acetic acid at room temperature for 1 h. The

oligonucleotides were then purified by HPLC using the same conditions as mentioned above. The concentration of the ODNs was calculated by UV absorption at 260 nm.

Fluorescence measurement with 2-aminopurine-containing ODN. A mixture (50 μL) of the duplex (5.0 μM) in phosphate buffer (20 mM, pH 7.0) containing NaCl (100 mM) was transferred to a quartz cell with a 3-mm path length. The emission spectra were obtained with an excitation wavelength at 310 nm at 25 °C. The fluorescence measurement was performed by an FP-6500 (JASCO Corporation) equipped with a temperature controller.

Melting temperature (T_m) measurement. A mixture (100 μL) of the duplex (4.0 μM) in phosphate buffer (20 mM, pH 7.0) containing NaCl (100 mM) was transferred to a micro quartz cell with a 1-cm path length. The melting temperature was then measured under UV irradiation at 260 nm from 20 to 80 °C at the rate of 0.5 °C/min. The measurements were carried out three times per each sample and averaged for obtaining the final value. The melting temperature measurement was performed by a V-730 (JASCO Corporation) equipped with a temperature controller.

Photo-cross-linking reaction (HPLC analysis). A mixture (100 μL) of the duplex (5.0 μM) and dU (12.5 μM) as an internal standard in phosphate buffer (20 mM, pH 7.0) containing NaCl (100 mM) in a PCR tube (BIO-BIK) was exposed to 365 nm light (LED365–SPT/L stand lamp, 38 mW/cm^2) at room temperature. The distance between the lamp and sample was 50 mm. After 10 sec, the reaction mixture was analyzed by HPLC. HPLC analysis conditions were as follows: C-18 packed column (COSMOSIL 5C_{18}-MS-II, 4.6ID×250 mm) by a linear gradient of 10%-40%/20 min and 40%-100%/25 min acetonitrile in TEAA buffer (0.1 M) at the flow rate of 1mL/min and 35 °C. The peaks were monitored by a UV detector (= 254 nm).

Enzymatic digestion of photo-cross-linked product and HPLC analysis. A solution of the cross-linked product (17.0 μL, 500 pmol), prepared as already described, was mixed with the 10X nucleoside digestion mix reaction buffer (2.0 μL) and nucleoside digestion mix (New England Biolabs, 1.0 μL). The reaction mixture was incubated at 37 °C for 1 h. The sample was analyzed by HPLC. The HPLC analysis conditions were as follows: C-18 packed column (COSMOSIL 5C18-MS-II, 4.6ID×250 mm) by a linear gradient of 0%-40%/20 min and 40%-100%/25 min acetonitrile in ammonium formate buffer (50 mM) at the flow rate of 1mL/min and 35 °C. The peaks were monitored by a UV detector (= 254 nm). The two new peaks on a HPLC profile were separated, lyophilized, and analyzed by ESI-MS. HRMS (ESI): *m/z* calcd for $C_{58}H_{64}N_{12}O_{19}P_2^{2-}$ $[M-2H]^{-2}$, 647.1948; found, 647.1984 (peak X) and 647.1993 (peak Y).

Photo-cross-linking reaction (PAGE analysis). Aliquots (5.0 μL) of the duplex (1.0 μM) in phosphate buffer (20 mM) containing NaCl (100 mM) in a PCR tube (BIO-BIK) were exposed to 365-nm light (LED365–SPT/L stand lamp, 38 mW/cm^2) at room temperature. The distance between the lamp and sample was 50 mm. These aliquots were then quenched by the addition of a loading buffer (5 μL, 95% formamide, 50 mM EDTA pH 8.0). PAGE was performed by a 20% polyacrylamide gel electrophoresis with 1X TBE and 7.5 M urea at 300 V for 40 min. The gel was stained by SYBR gold, and the ODNs were visualized with FLA-5100 (Fujifilm Co., Tokyo, Japan).

Photoisomerization of compound 4-Ph (HPLC analysis). A 10% DMSO solution (100 μL) of Ph (1 mM) in phosphate buffer (20 mM, pH 7.0) in a PCR tube (BIO-BIK) was exposed to 365-nm UV light for 10 sec at 25 °C. The distance between the lamp and sample was 50 mm. The reaction mixture was analyzed by HPLC, and the *cis*-form was separated and lyophilized overnight. The HPLC analysis conditions were as follows: C-18 packed column (COSMOSIL 5C18-MS-II, 4.6ID×250 mm) by a linear gradient of 10%-100%/20 min and 100%/25 min acetonitrile in TEAA buffer (0.1 M) for analysis and ammonium formate buffer (50 mM) for purification of **4-Ph** (*cis*-isomer) at the flow rate of 1mL/min and 35 °C. The peaks were monitored by a UV detector (= 254 and 355 nm).

^{1}H NMR (600 MHz, DMSO-d_6): δ 7.68 (s, 1H), 7.29 (m, 4H), 7.23-7.21 (m, 1H), 7.11 (s, 1H), 6.62 (d, J = 12.6 Hz, 1H), 6.46 (d, J = 12.6 Hz, 1H), 6.39 (t, J = 6.6 Hz, 1H), 5.26 (s, 1H), 5.05 (s, 1H), 4.25-4.24 (m, 1H), 3.84-3.83 (m, 1H), 3.65-3.62 (m, 1H), 3.60-3.57 (m, 1H), 2.30-2.21 (m, 1H), 2.01-1.95 (m, 1H), 1.84 (s, 3H). ^{13}C{^{1}H} NMR (150 MHz, DMSO-d_6): δ 160.0, 140.1, 137.1, 130.9, 130.5, 128.9, 128.7, 127.8, 126.4, 125.6, 113.6, 88.1, 85.1, 70.7, 70.3, 61.6, 41.4, 17.4. HRMS (ESI): *m/z* calcd for $C_{19}H_{21}NO_4Na^+$ $[M+Na]^+$, 350.1369; found, 350.1357.

Stability checking for cross-linked products (PAGE analysis). Aliquots (5 μL) of the cross-linked product (1.0 μM) in phosphate buffer (20 mM) containing NaCl (100 mM) in a PCR tube (BIO-BIK) were exposed to our standard irradiation conditions for 10 sec, incubated at 37 °C for 60 mins, or incubated at 90 °C for 5 mins. These aliquots were then quenched by the addition of loading buffer (5 μL, 95% formamide, 50 mM EDTA pH 8.0). PAGE was performed by a 20% polyacrylamide gel electrophoresis with 1X TBE and 7.5 M urea at 300 V for 40 min. The gel was stained by SYBR gold, and the ODNs were visualized with FLA-5100 (Fujifilm Co., Tokyo, Japan).

CD measurements. A mixture (100 μL) of the duplex (4.0 μM) in phosphate buffer (20 mM, pH 7.0) containing NaCl (100 mM) was transferred to a micro quartz cell with a 1-cm path length. The CD spectra were measured at 25 °C by a J-720WI (JASCO Corporation) equipped

Chapter 5
Conclusion and future prospective

Oligonucleotides (ONs) have numerous utilities ranging from research to diagnostic applications and, recently therapeutics. The chemical modification of ONs or tethering reactive moieties into ONs can significantly expand their tasks and applications. The kind of modification depends on the purpose for which ONs will be used. ONs are short single-stranded DNA or RNA sequence which can recognize their target nucleic acid in a sequence-selective manner. In addition, some ONs with specific sequences can form secondary structures. Such structures can recognize by proteins. Hence, modifying ONs with reactive functional moieties can accelerate proximity-dependent chemical reactions near the reactive moiety upon binding with their targets. In this thesis, using chemically modified ONs, I developed a protein proximity labeling approach to interrogate nucleic acid-protein interactions. I also efficiently impeded the miR function using an anti-miR flanked by interstrand crosslinked duplex structures.

In my research, I developed ….

In chapter 3, I developed a highly efficient AVP-mediated 2'-OMe-RNA interstrand cross-linked (CL) anti-miRNA ONs (AMOs). It has been reported that miRNAs are overexpressed in many diseases, such as cancer. Chemically modified AMOs can interfere with these disease-relevant miRNAs and block them from binding to their mRNA targets. Komatsu's group reported that cross-linked duplexes flanking the single-stranded AMO inhibited the miRNA function more efficiently than AMOs with normal single or double strands. Here, I designed and synthesized AMOs flanked by native-like and less-distorted structures of interstrand cross-linked duplexes using the ONs containing 2-amino-6-vinylpurine (AVP). I expected the crosslinking to prevent the duplex structure from dissociation inside the cell. Also, the incorporation of the crosslinked duplexes was expected to facilitate the recognition of AMO by AGO proteins and increase the K_{ON} rate by pre-organizing the AMO conformation. As expected, using a dual luciferase system in cultured cells, these AMOs inhibited the miRNA function at a low nM concentration. Such inhibitory activity of CL AMOs was significantly higher than the inhibitory activity of the commercially available LNA-containing single-stranded AMO, indicating the importance of the cross-linked duplex structures. The structure-activity relationship study for the crosslinked duplex will be conducted to better understand its role.

In chapter 4, I designed and synthesized the artificial ON to induce the base flipping and accelerate the interstrand photo-cross-linking within the DNA duplex. The ONs containing properly designed artificial nucleic acids can induce base flipping and create specific fields for

various chemical reactions. Previously, our group found that the alkyne−alkyne photo-cross-linking rapidly proceeded by the use of the base-flipping-out field where two alkynes overlap each other. In this study, I designed the alkene-type analog having a 5-methyl pyridone derivative linked to Ph or An groups with an alkene linker at the C3 position. The specific field created by the designed alkene analogs accelerated the [2+2] photocycloaddition reaction in duplex DNA. The Ph-Ph combination provided a high yield, where 10 sec was enough to achieve more than 80% cross-link yield calculated from HPLC analysis.

Appendices

Chapter 3

NMR-spectra

Compound **2**

^{1}H NMR (400 MHz, $CDCl_3$)

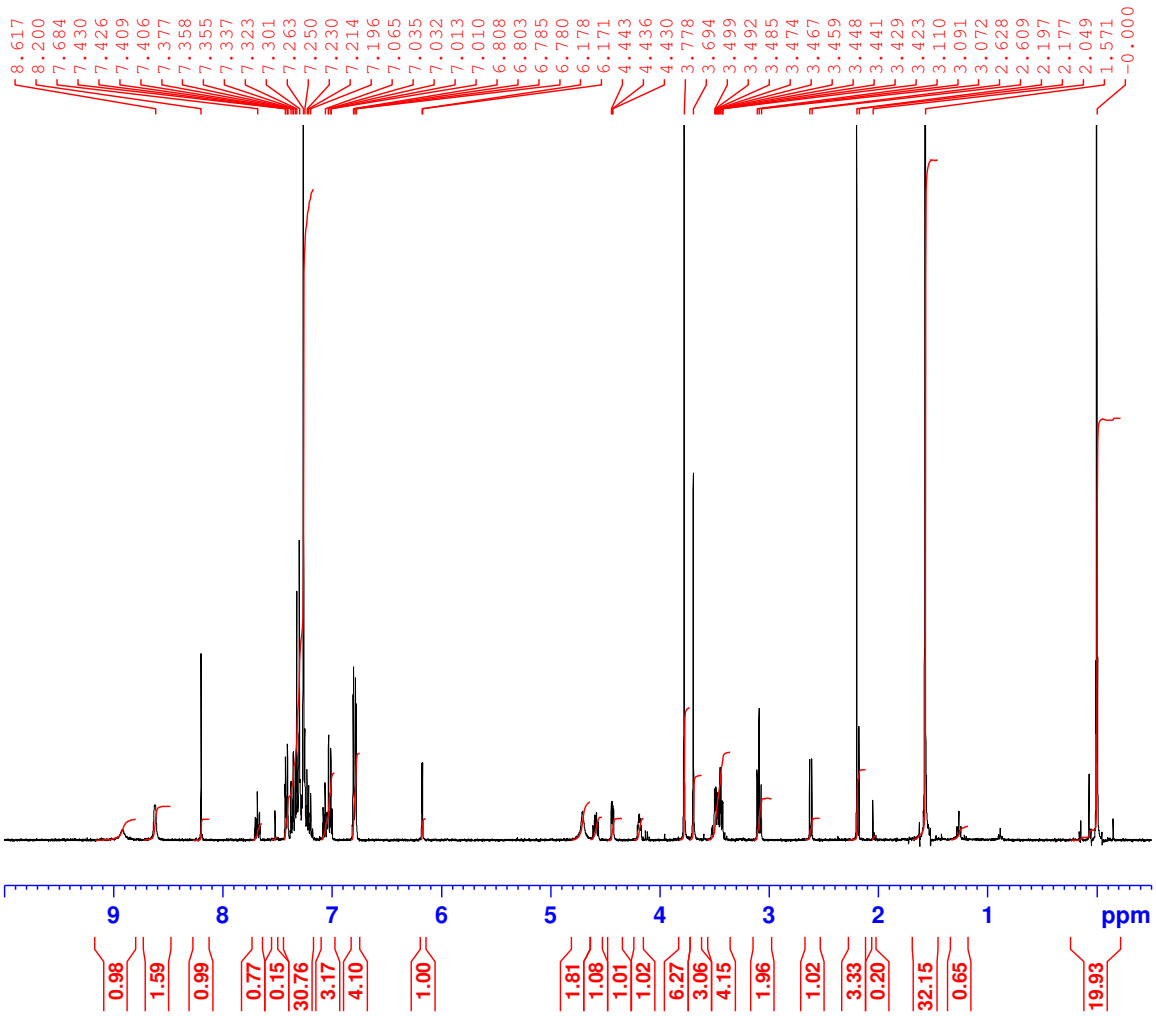

Compound **3**

^{1}H NMR (400 MHz, $CDCl_3$)

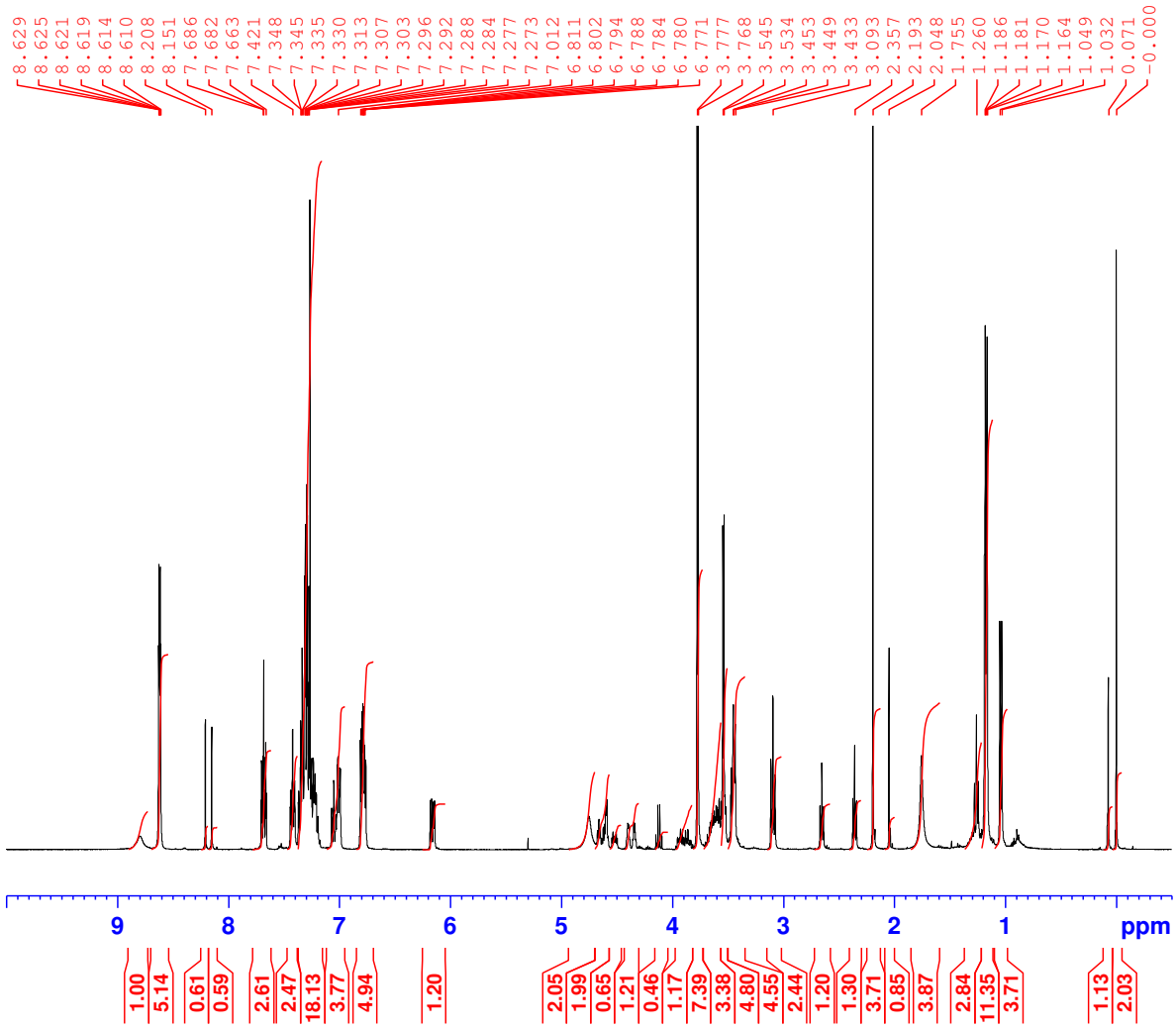

Compound **3**

^{31}P NMR (162 MHz, $CDCl_3$)

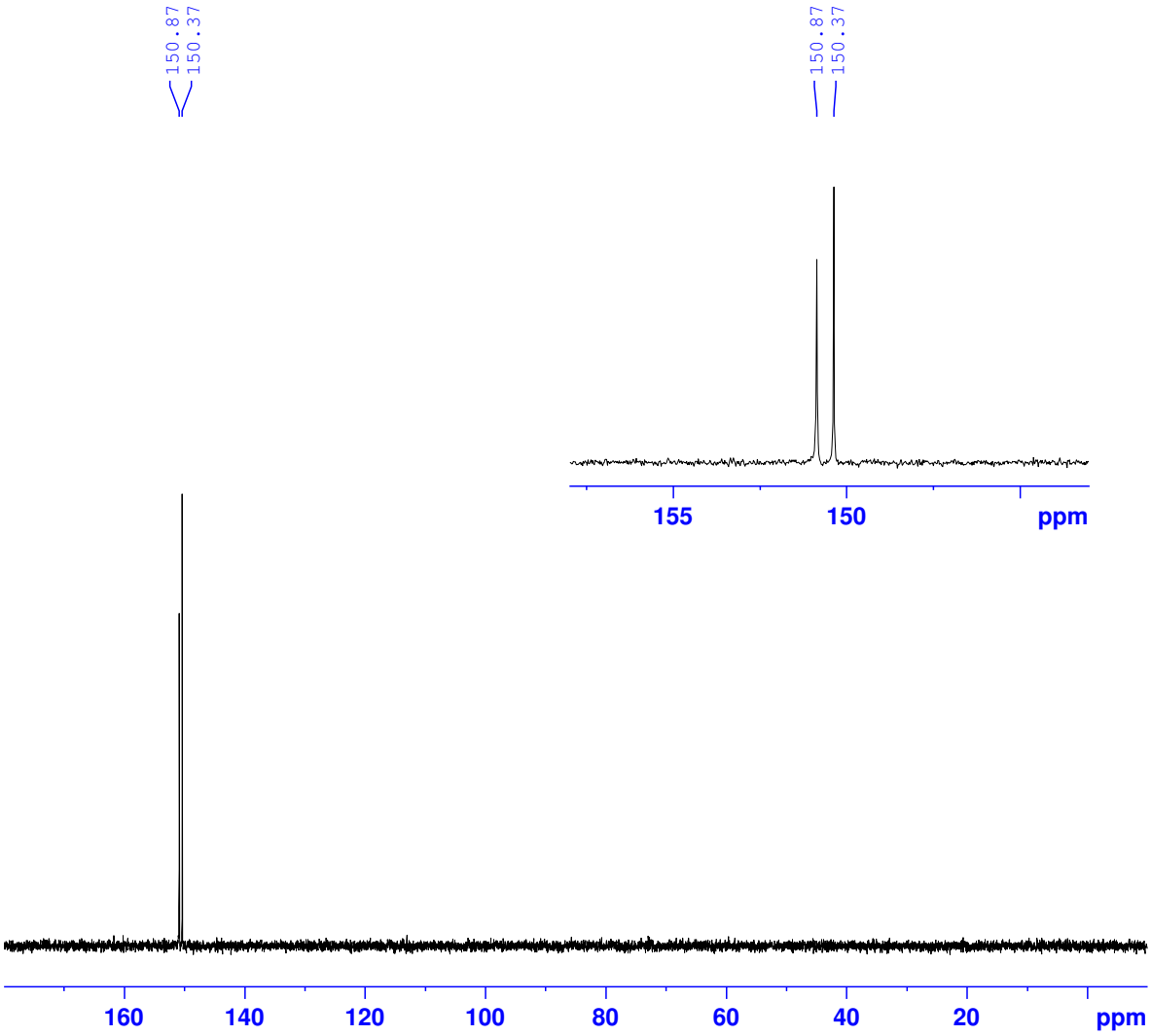

MALDI-TOF MS data

CFO (**6**)

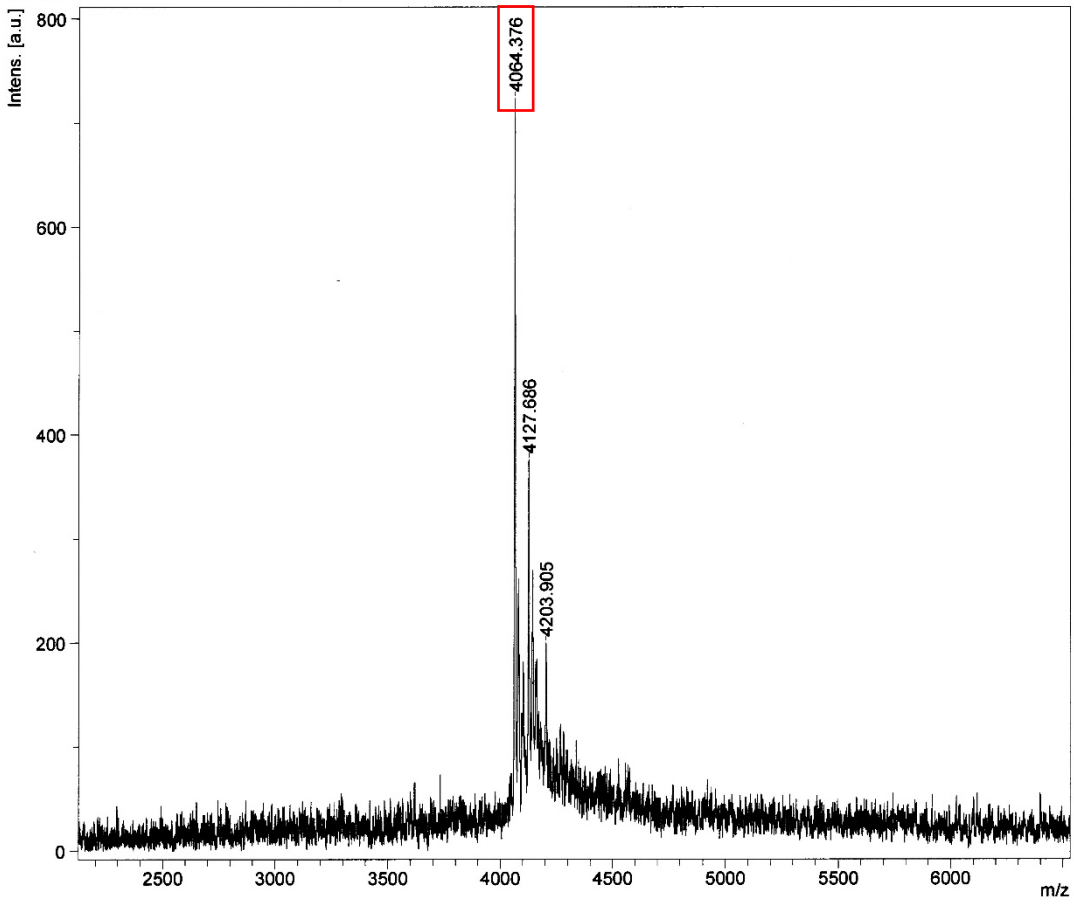

AMO**1** (1-CL)

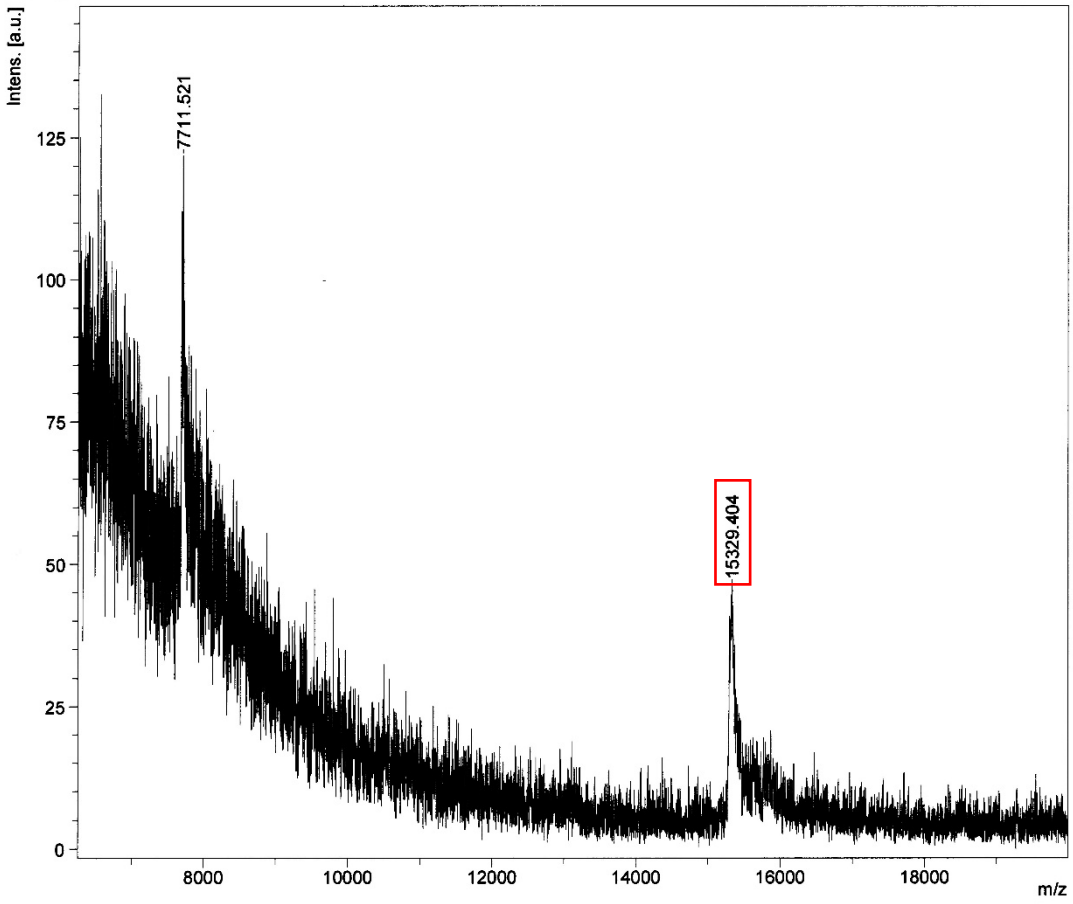
Intens. [a.u.]
125
100
75
50
25
0
7711.521
15329.404
8000
10000
12000
14000
16000
18000
m/z

AMO**2** (2-CL)

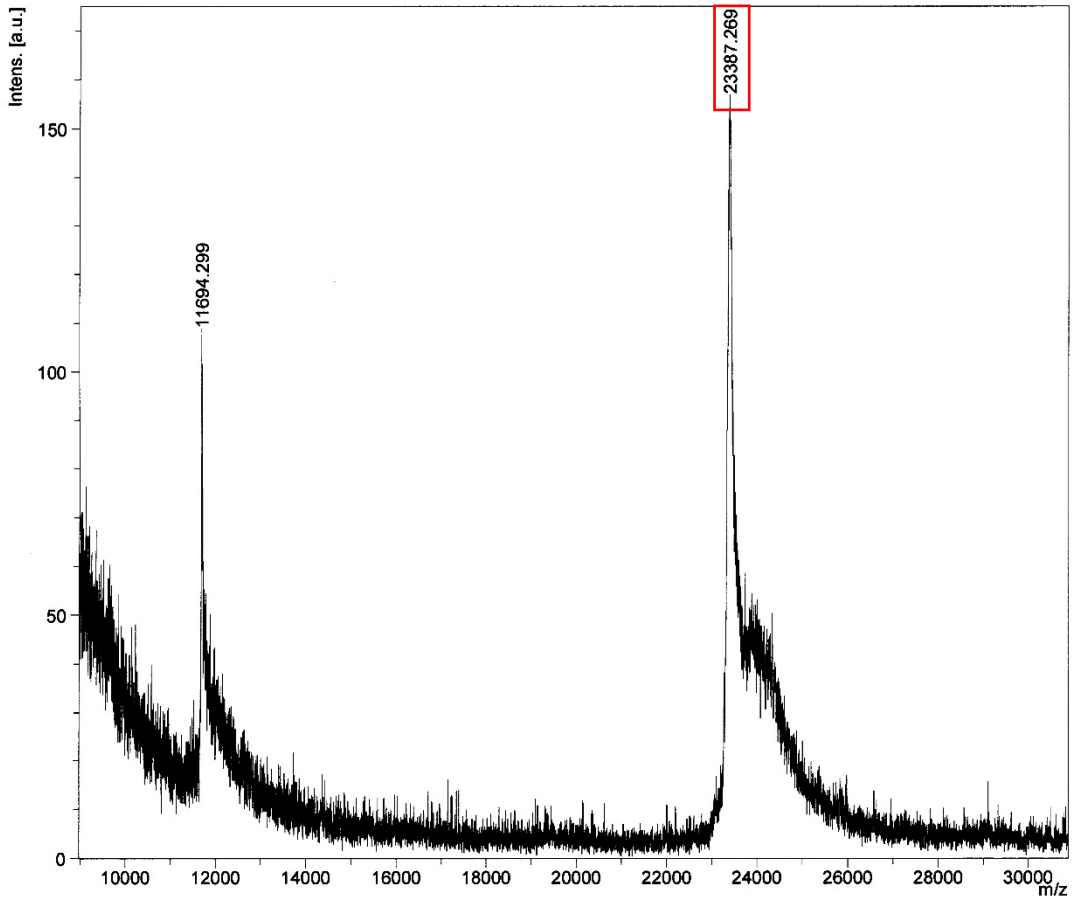
Intens. [a.u.]
150
100
50
0
11694.299
23387.269
10000
12000
14000
16000
18000
20000
22000
24000
26000
28000
30000
m/z

Chapter 4

NMR-spectra

Compound **1**

^{1}H NMR (600 MHz, $CDCl_3$)

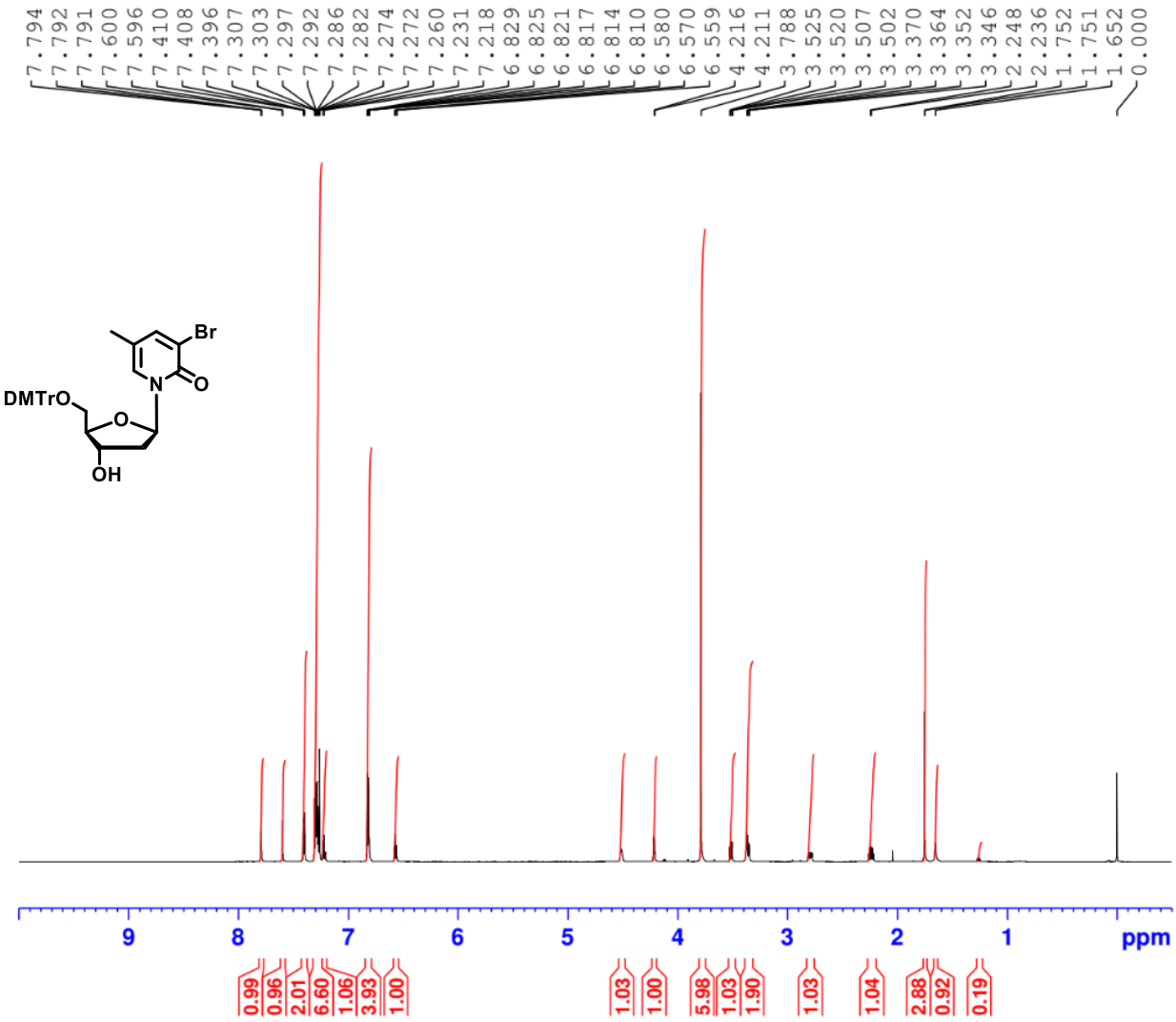

Compound **1**

$^{13}C\{^{1}H\}$ NMR (150 MHz, $CDCl_3$)

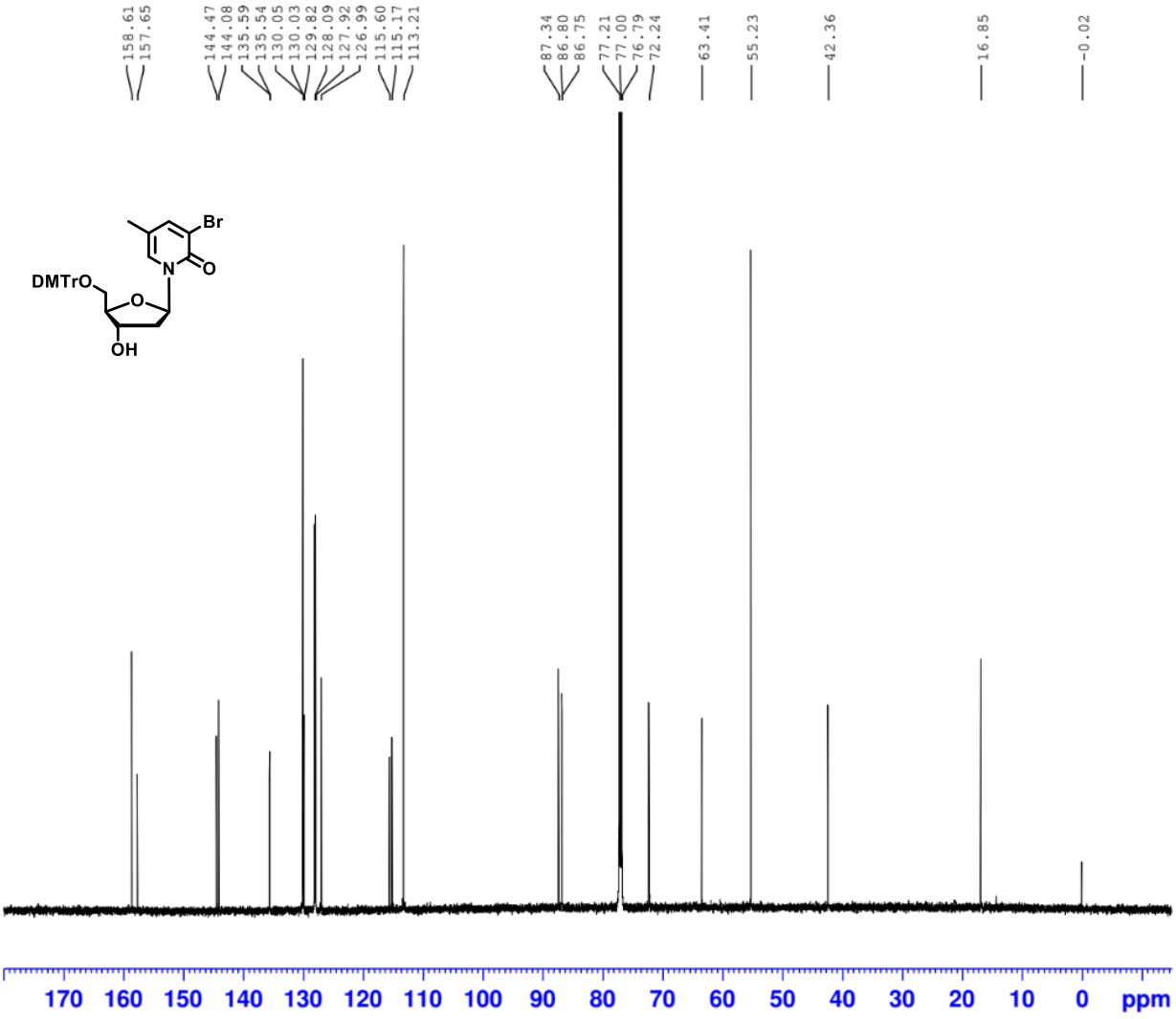

Compound **2-Ph**

^{1}H NMR (600 MHz, $CDCl_3$)

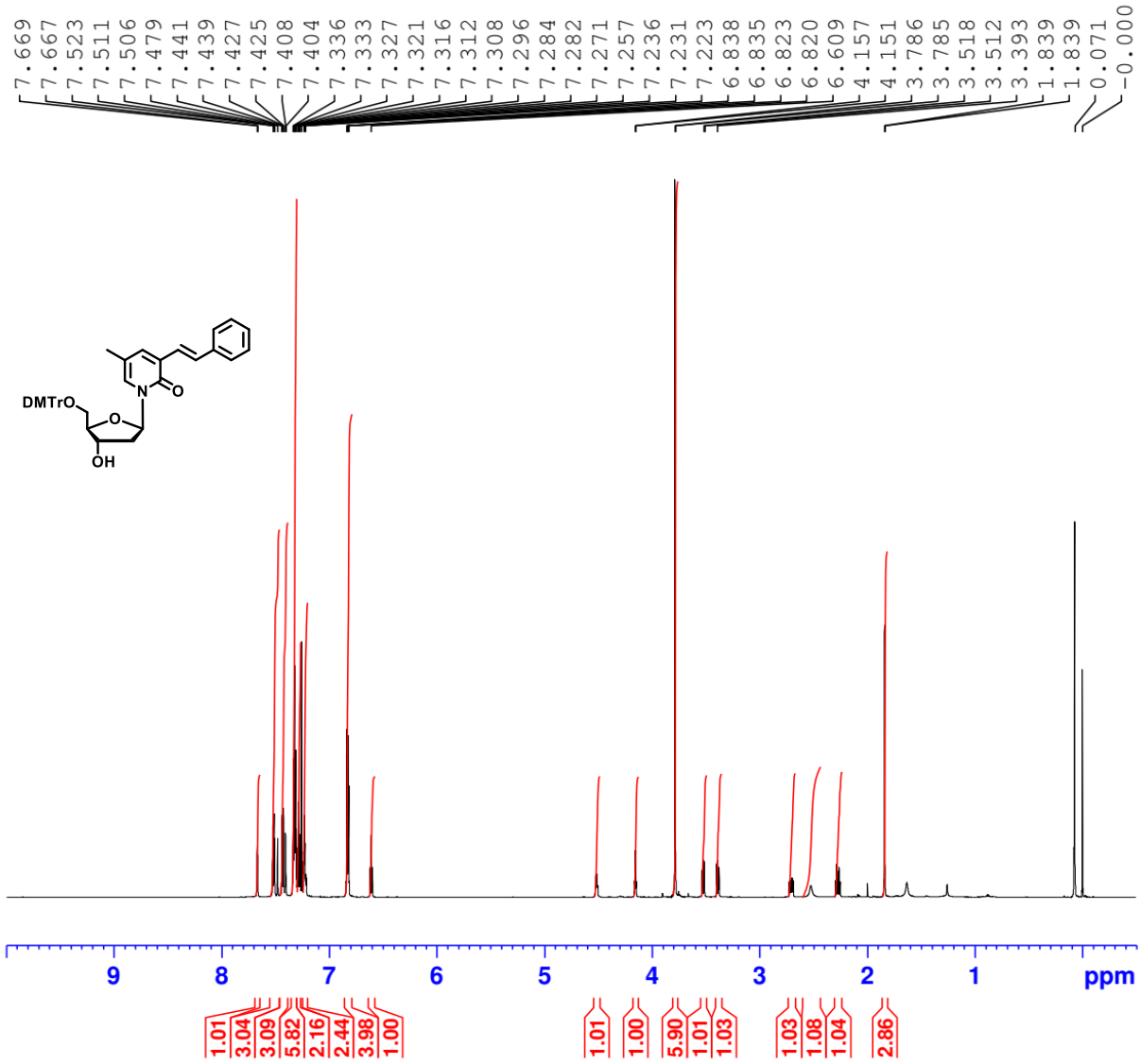

Compound **2-Ph**

$^{13}C\{^{1}H\}$ NMR (150 MHz, $CDCl_3$)

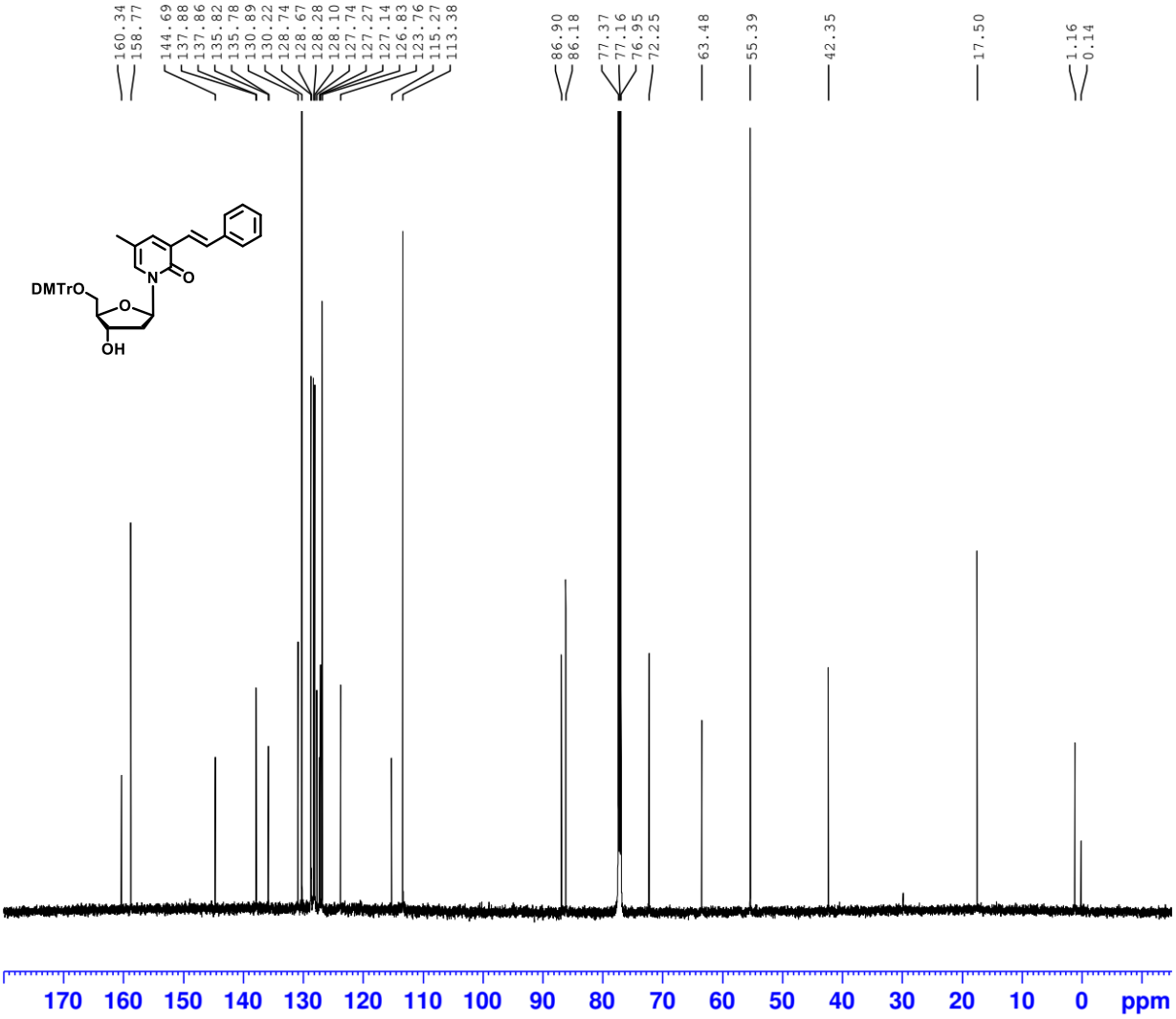

Compound **2-An**

^{1}H NMR (600 MHz, $CDCl_3$)

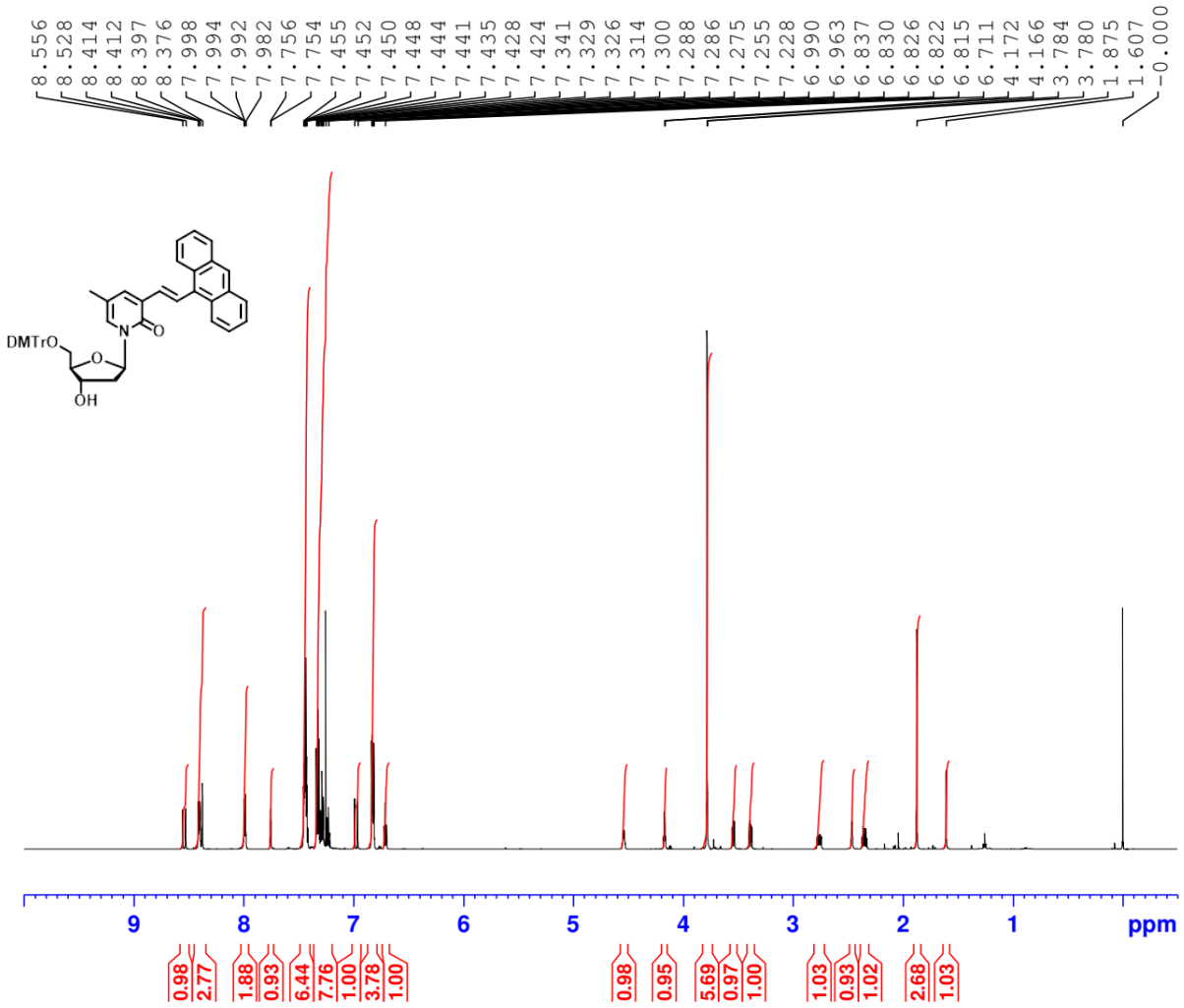

Compound **2-An**

$^{13}C\{^{1}H\}$ NMR (150 MHz, $CDCl_3$)

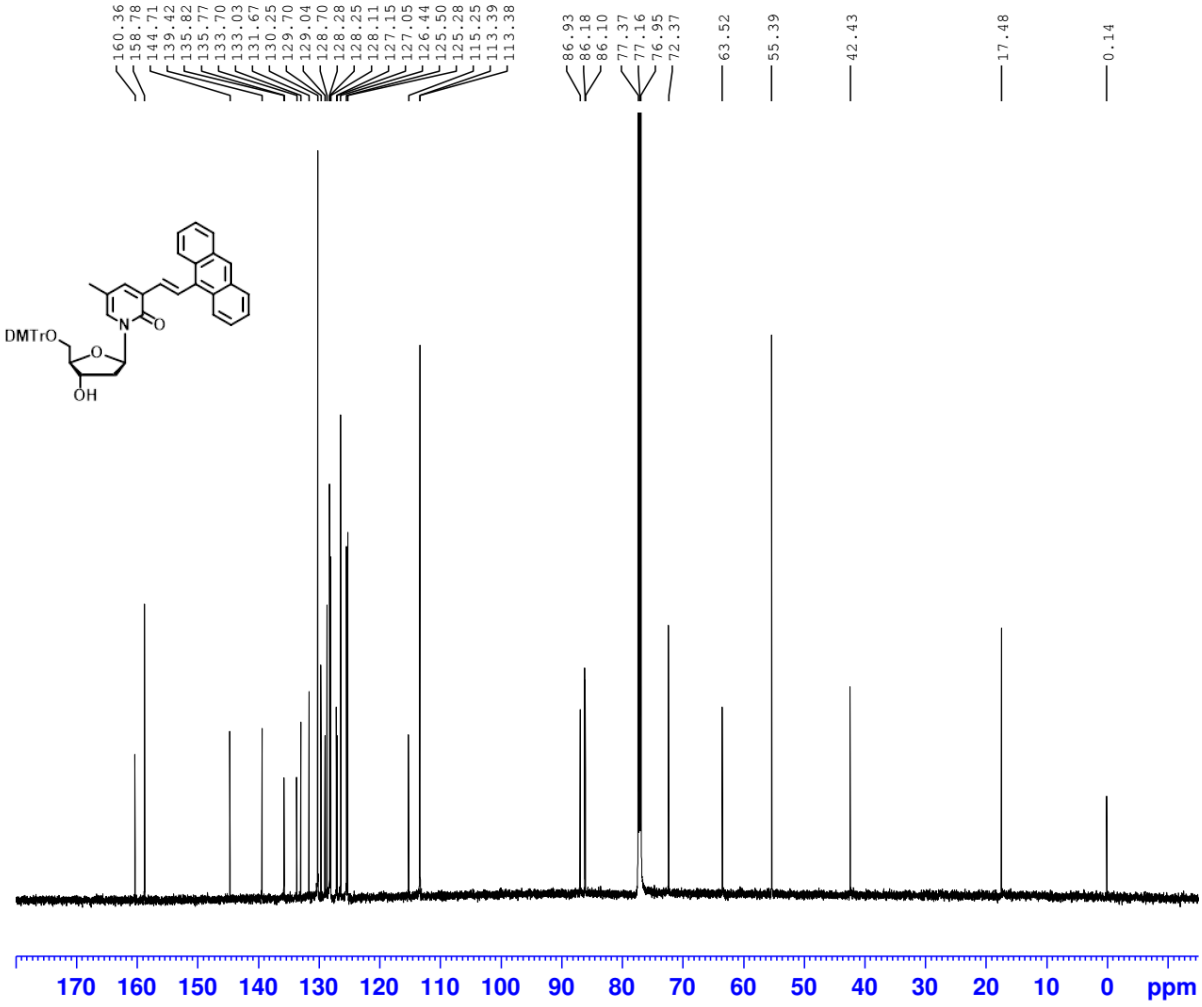

Compound **3-Ph**

^{31}P NMR (162 MHz, $CDCl_3$)

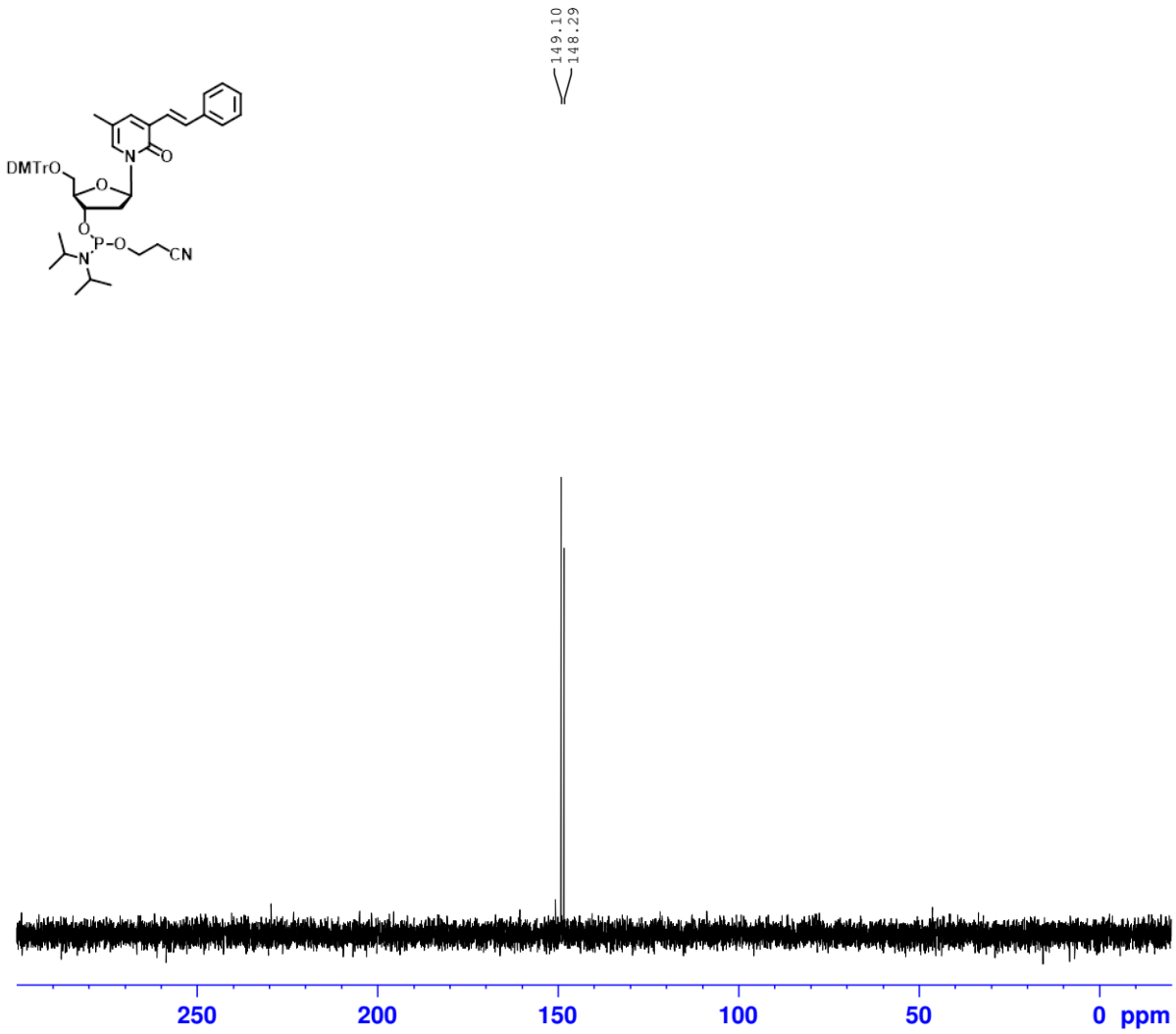

Compound **3-An**

^{31}P NMR (162 MHz, $CDCl_3$)

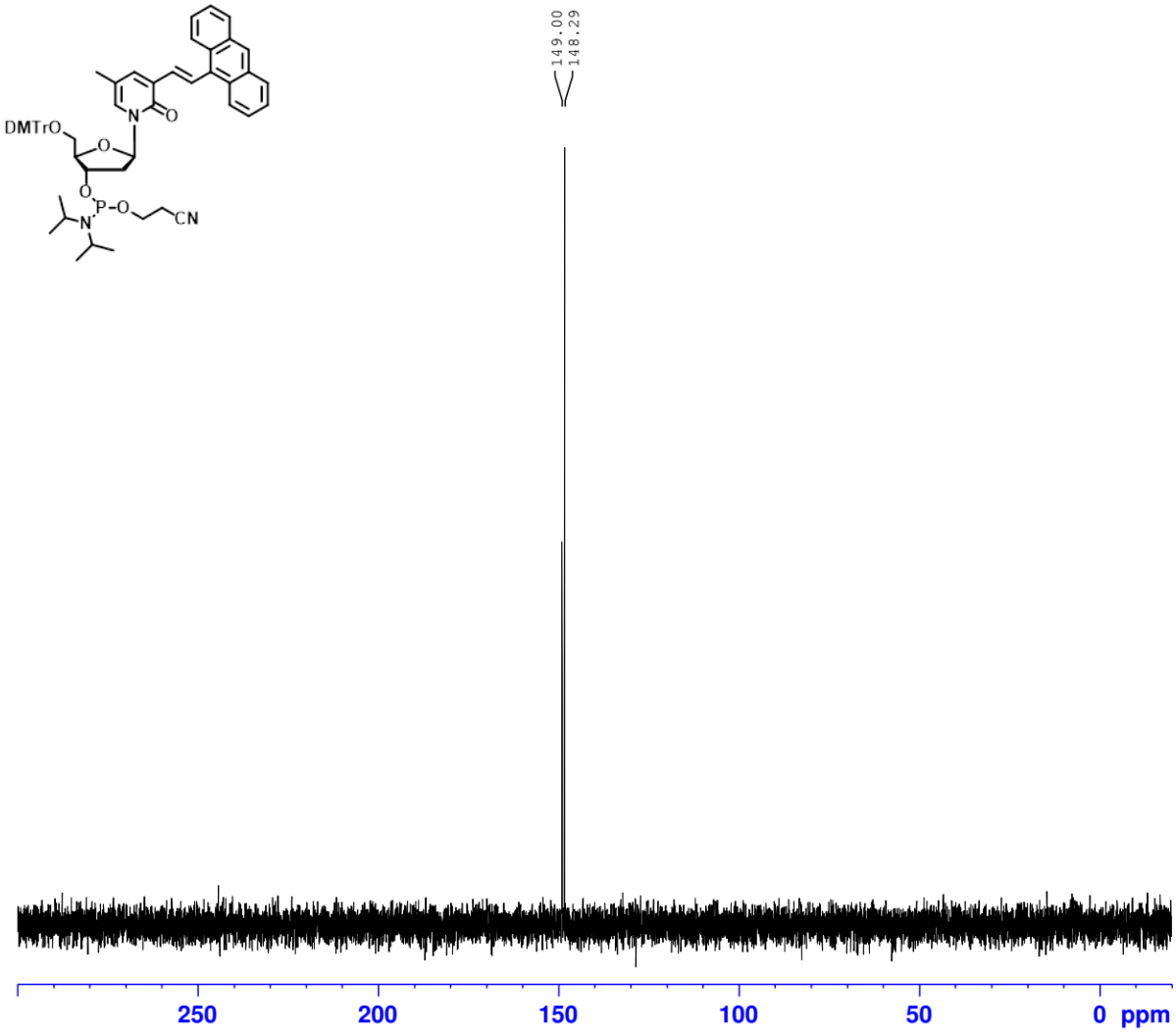

Compound **4-Ph** (*trans*-isomer)

^{1}H NMR (400 MHz, MeOD-d_4)

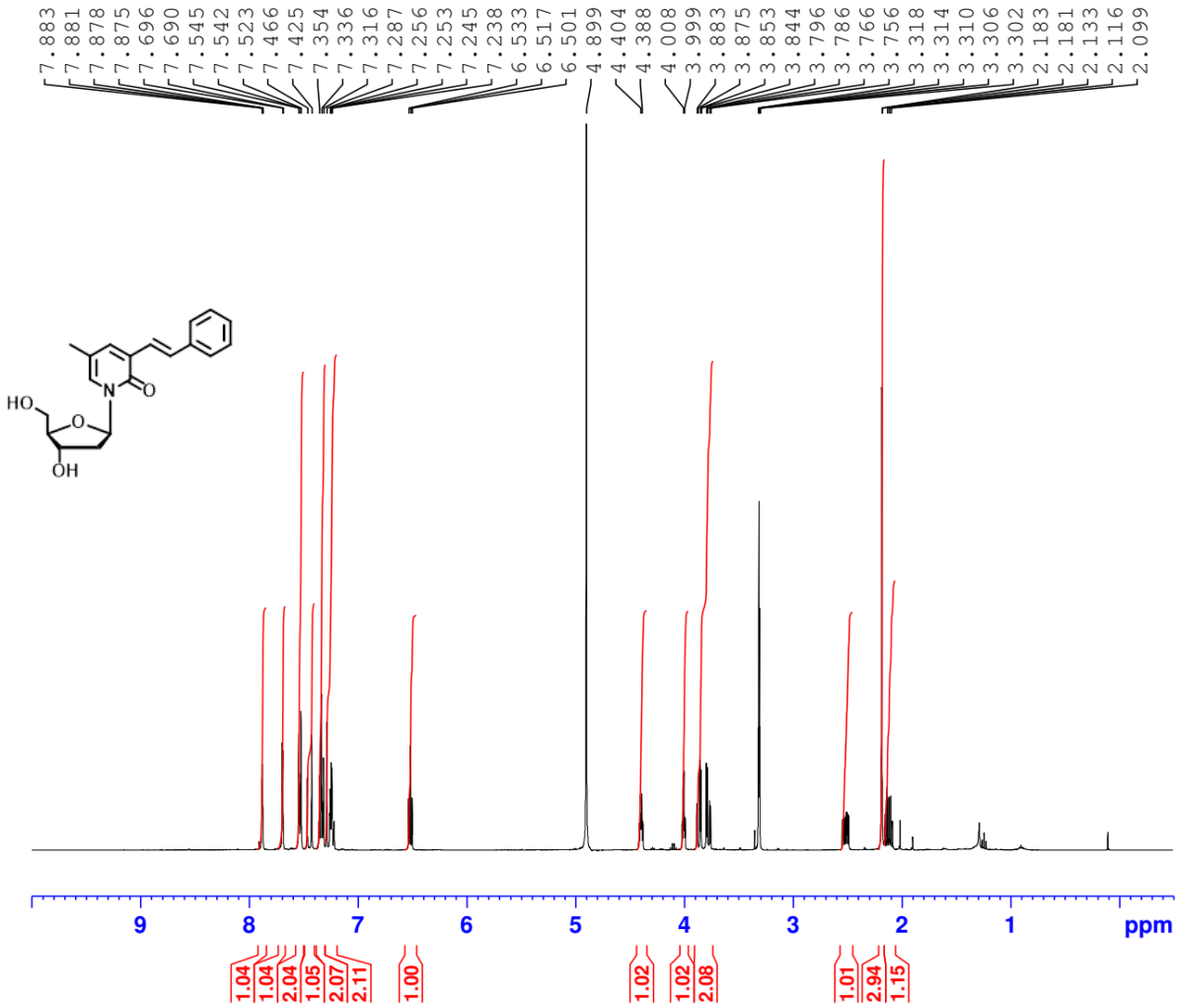

Compound **4-Ph** (*trans*-isomer)

$^{13}C\{^{1}H\}$ NMR (150 MHz, MeOD-d_4)

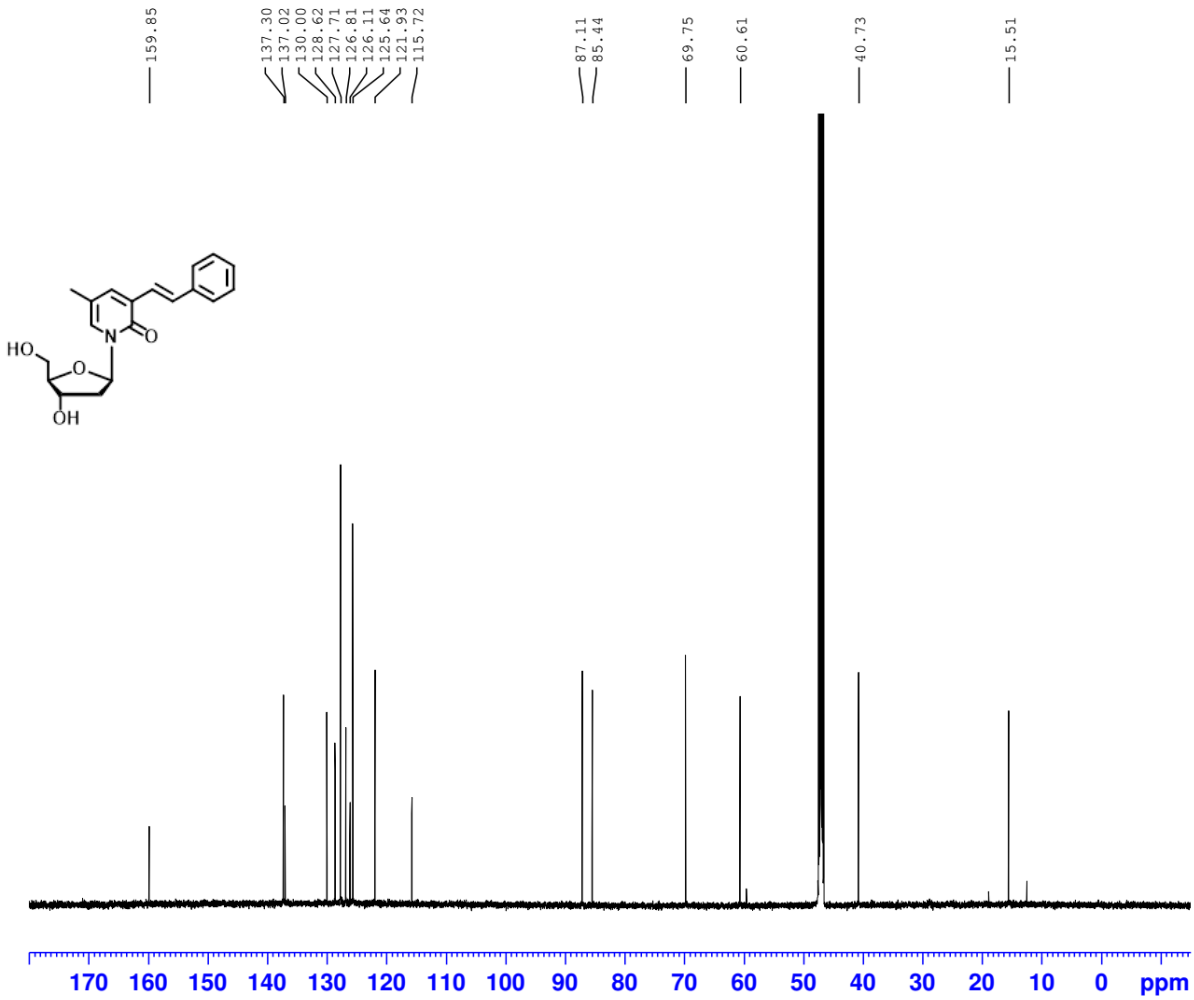

Compound **4-Ph** (*cis*-isomer)

^{1}H NMR (600 MHz, DMSO-d_6)

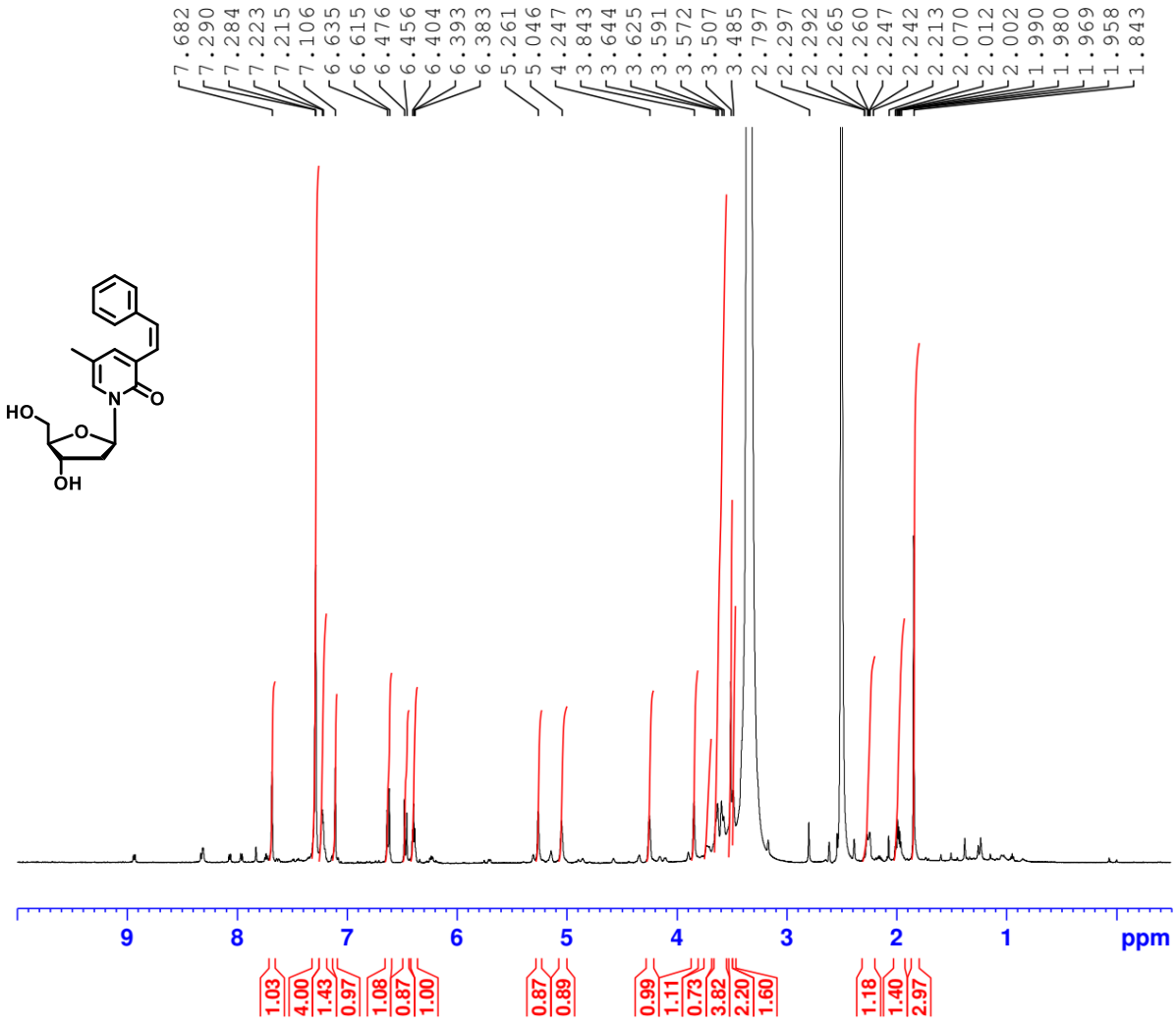

Compound **4-Ph** (*cis*-isomer)

$^{13}C\{^{1}H\}$ NMR (150 MHz, DMSO-d_6)

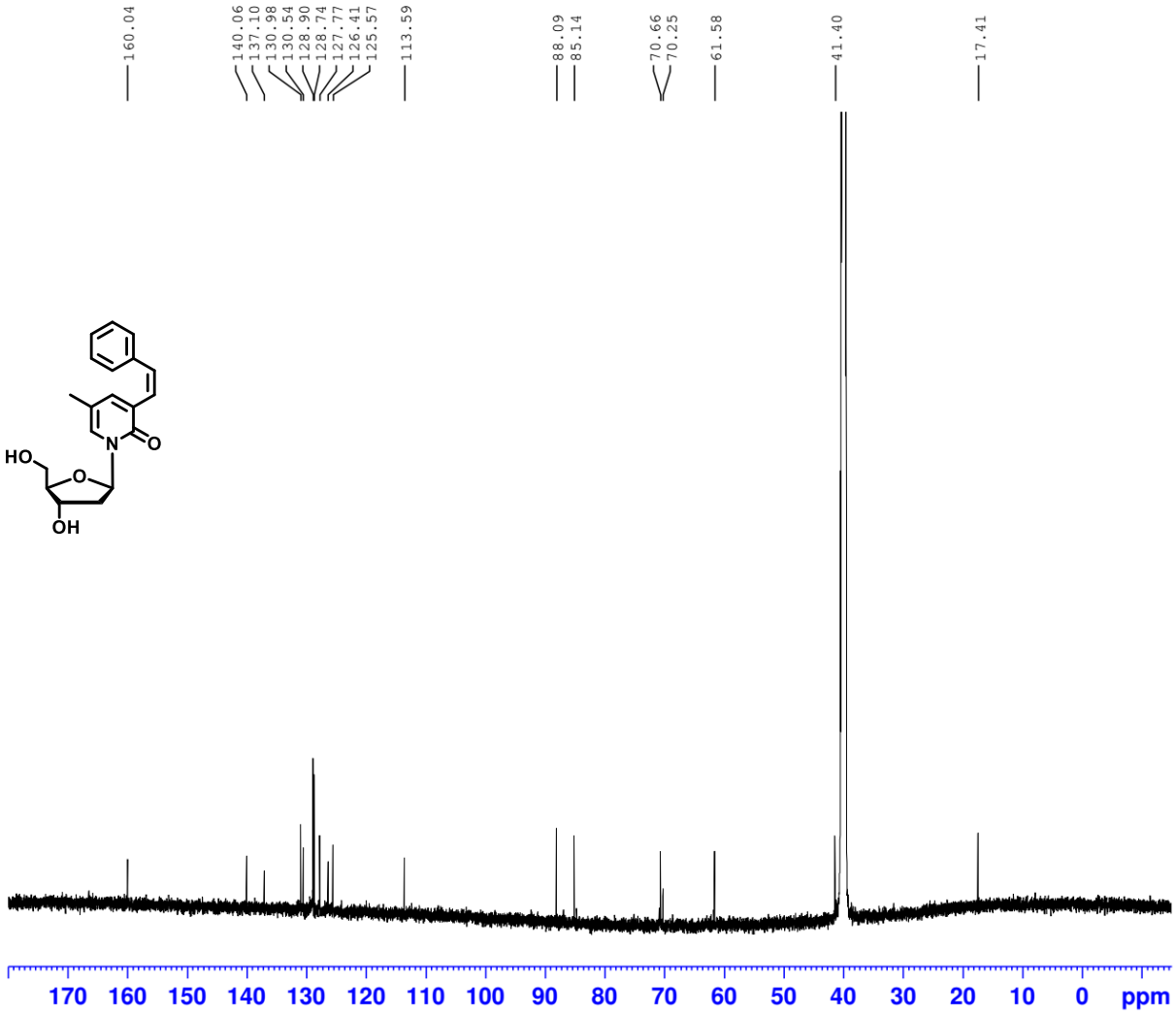

Compound **4-An**

^{1}H NMR (600 MHz, MeOD-d_4)

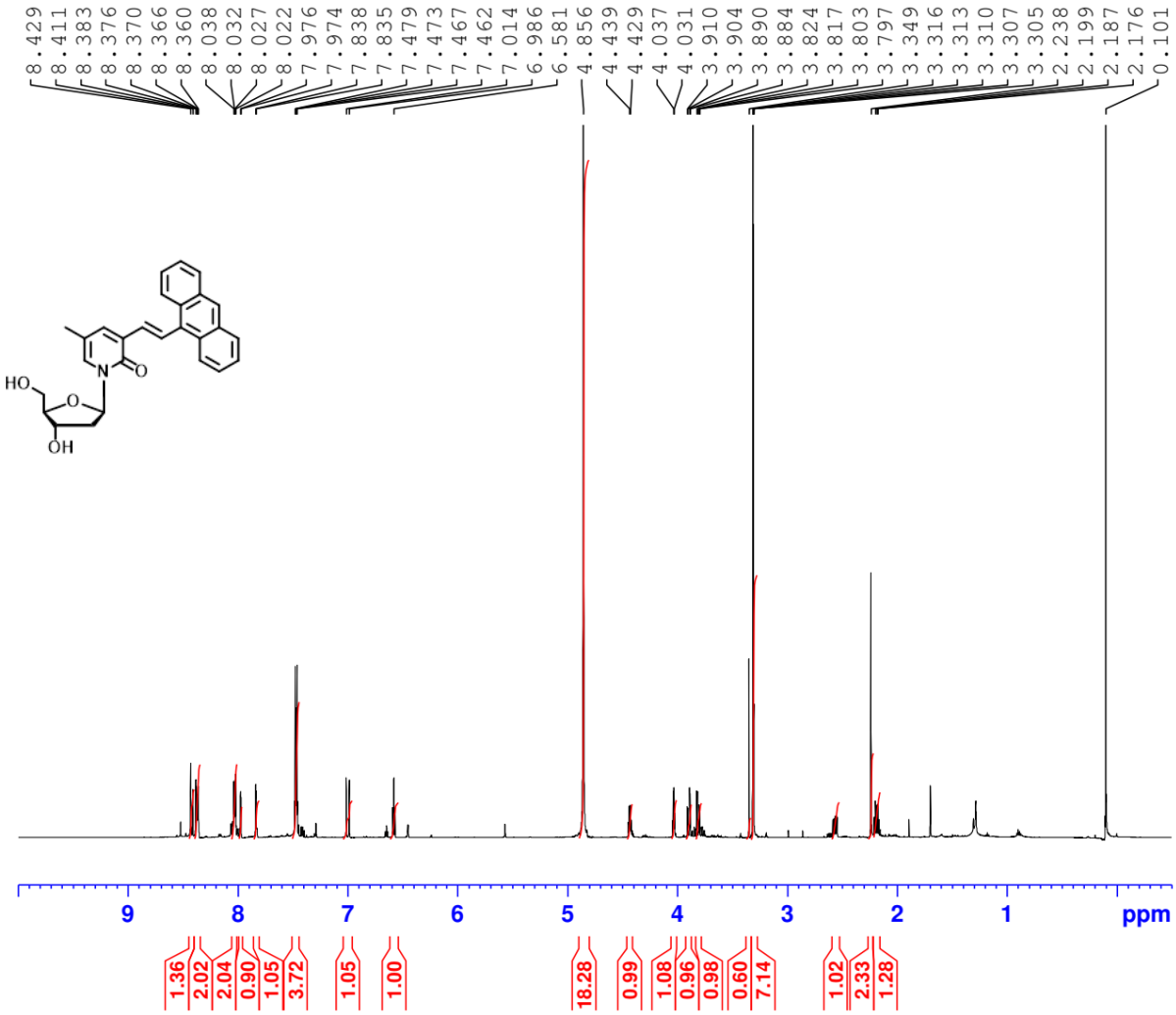

Compound **4-An**

$^{13}C\{^{1}H\}$ NMR (150 MHz, MeOD-d_4)

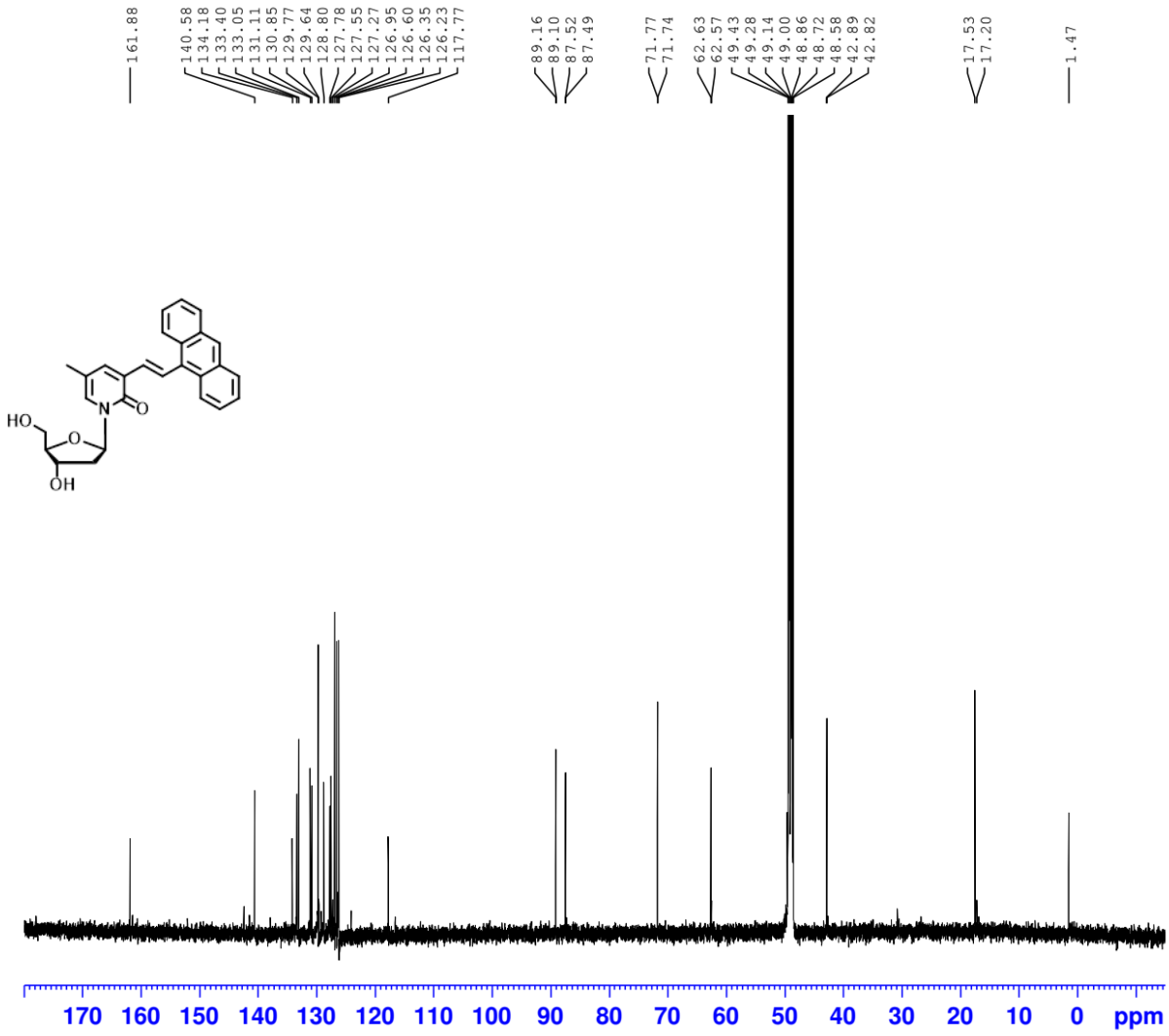

MALDI-TOF MS data

ODN**1**(Ph)

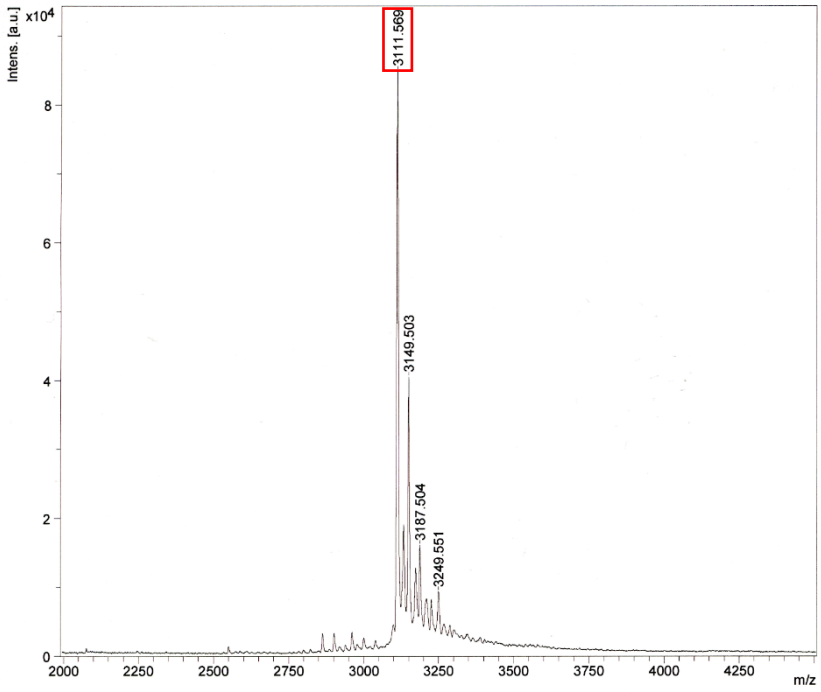

ODN**1**(An)

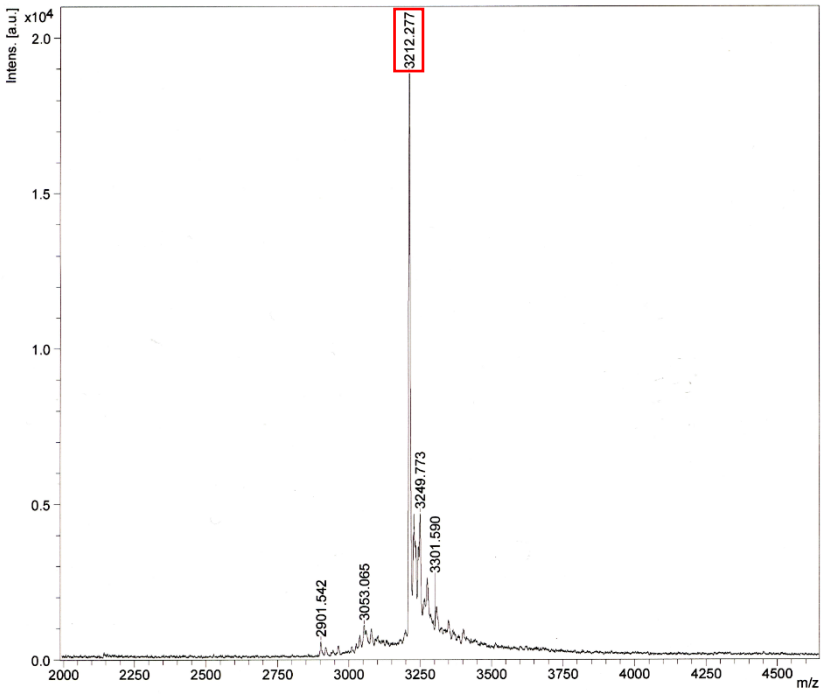

ODN**3**(Ph)

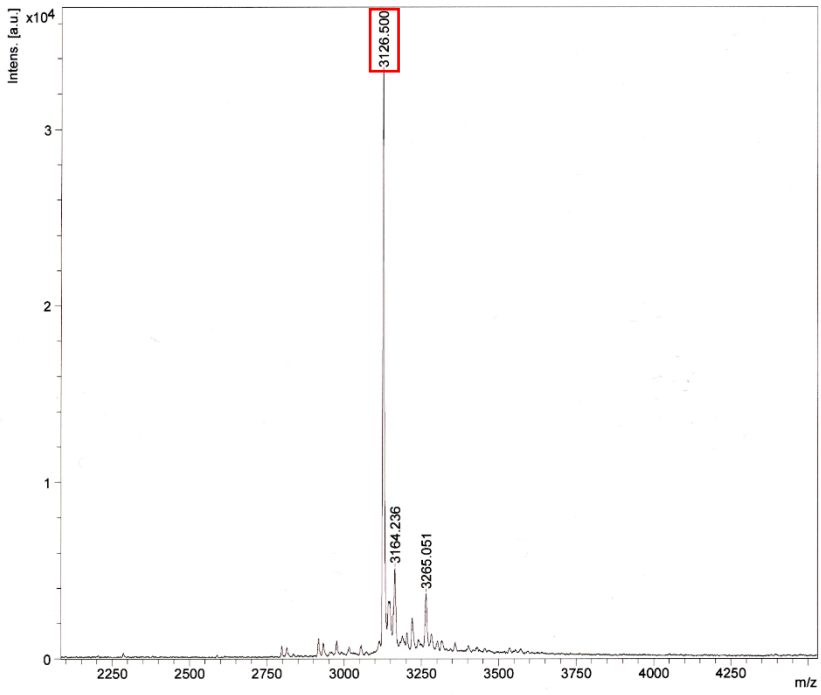

ODN**3**(An)

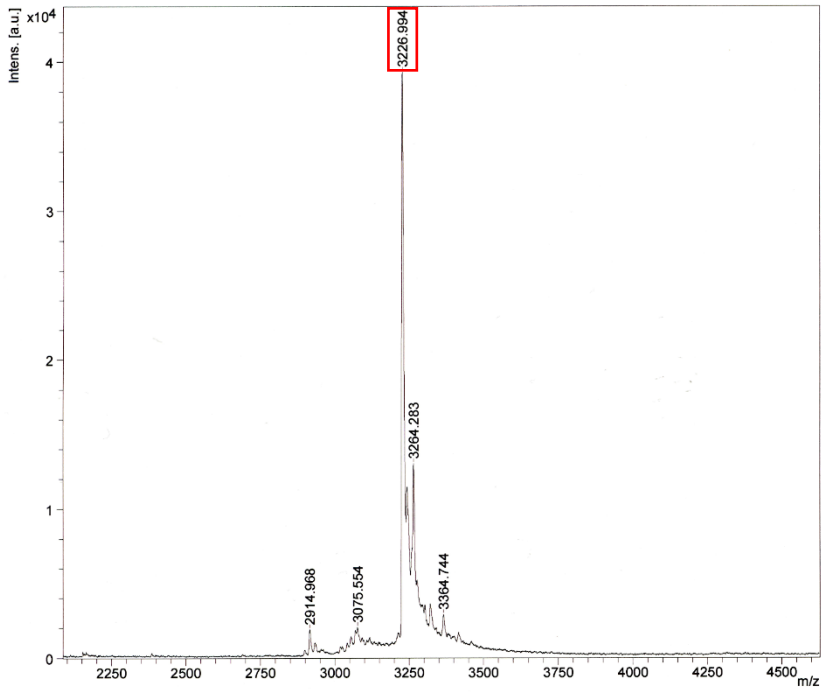

ODN**4**(Ph)

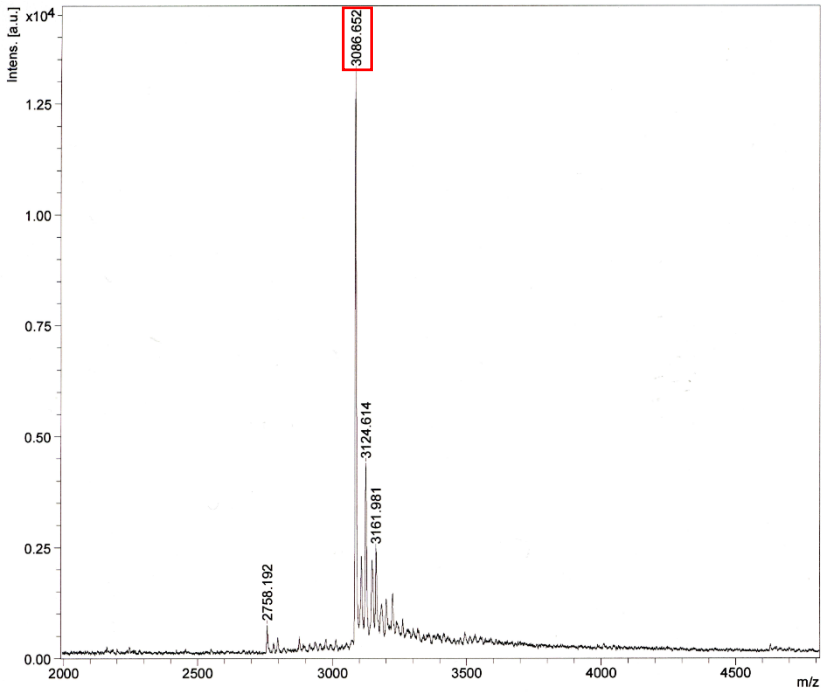

ODN**5**(Ph)

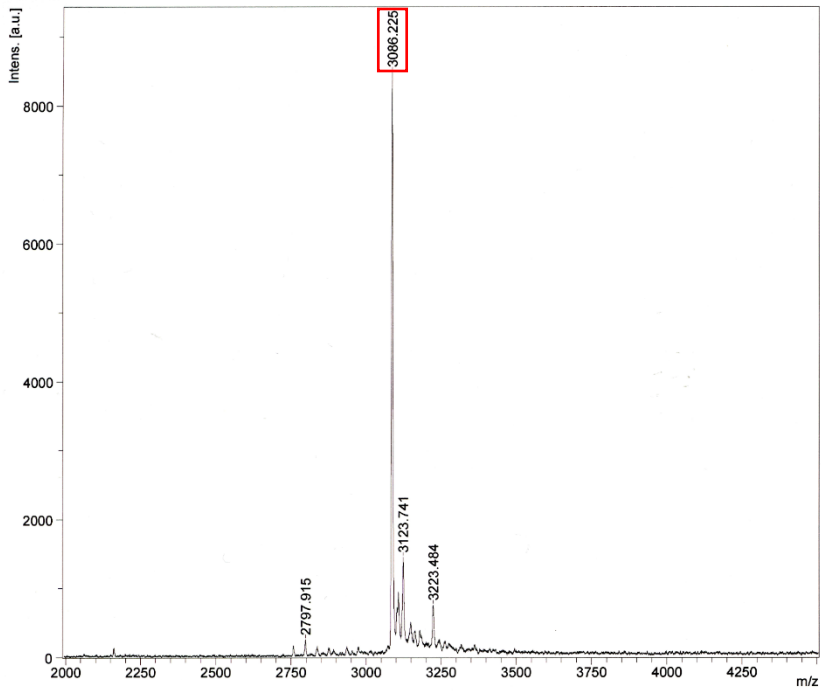

ODN**1**(Ph)-ODN**3**(Ph)

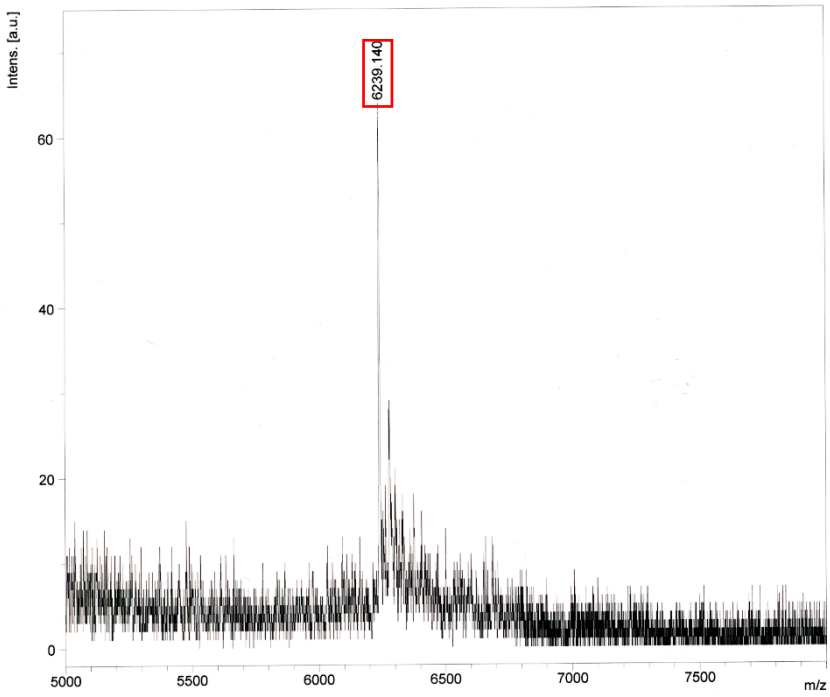

ODN**1**(An)-ODN**3**(An)

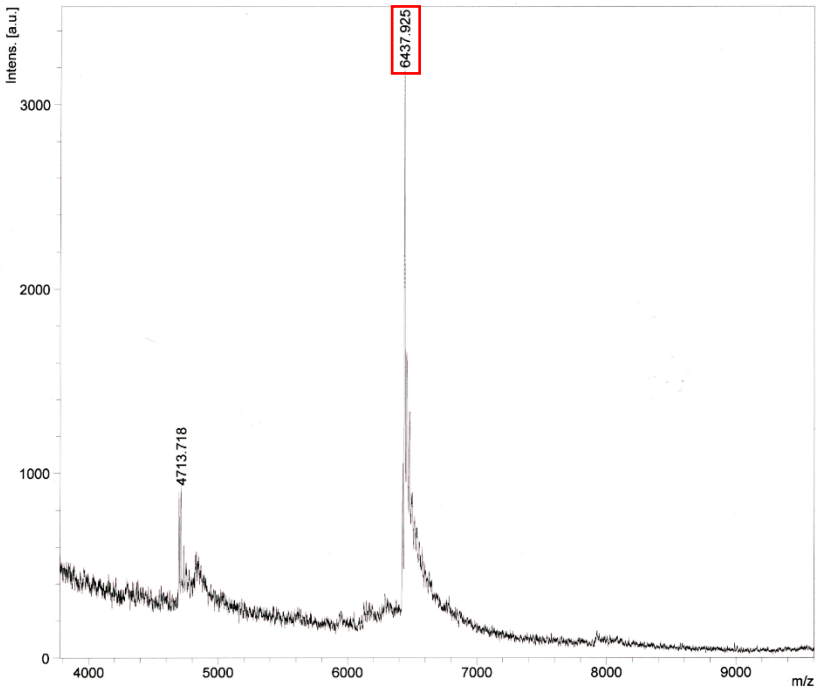

ODN**1**(Ph)-ODN**3**(An)

Crosslink1

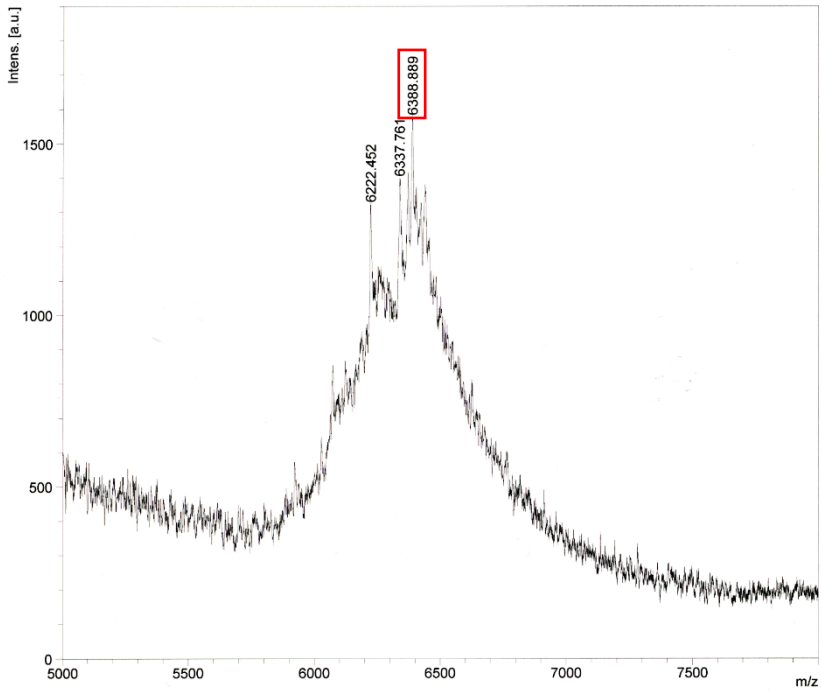

Crosslink2

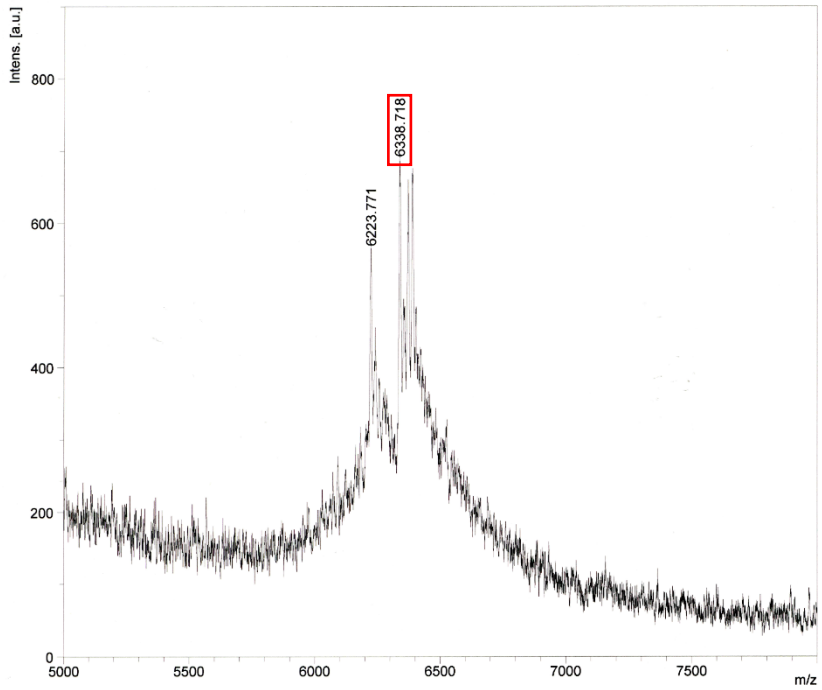

ODN**1**(An)-ODN**3**(Ph)

Crosslink1

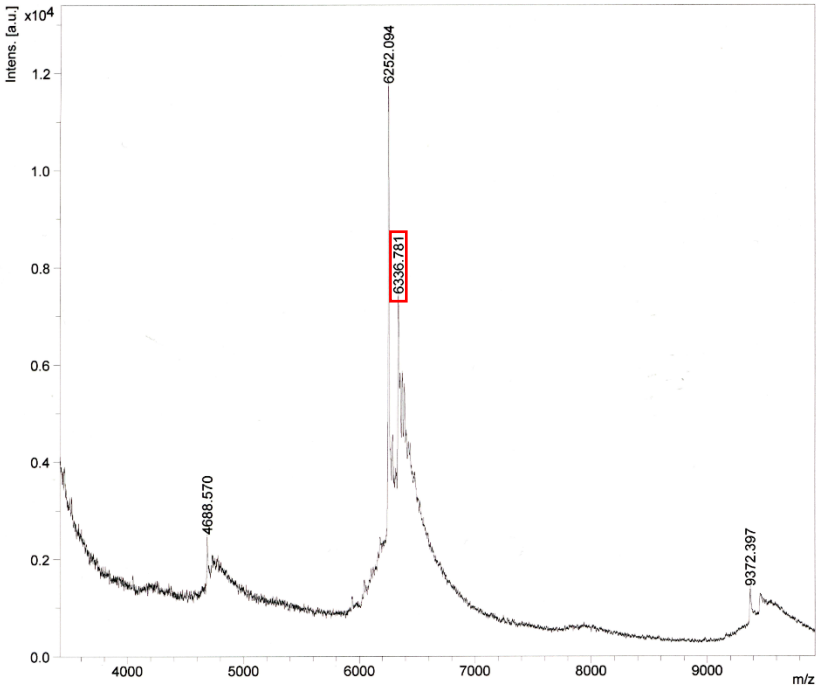

Crosslink2

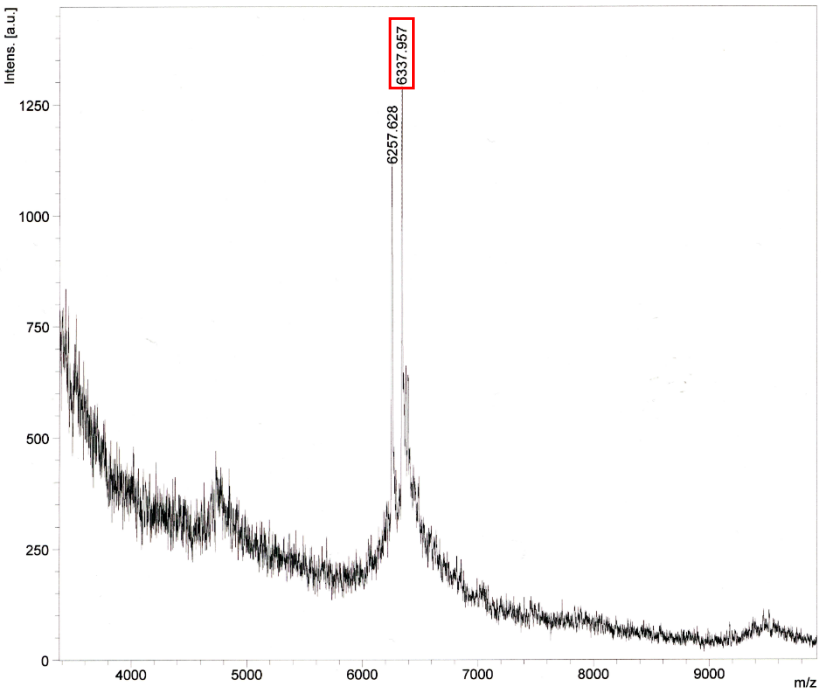

Crosslink3

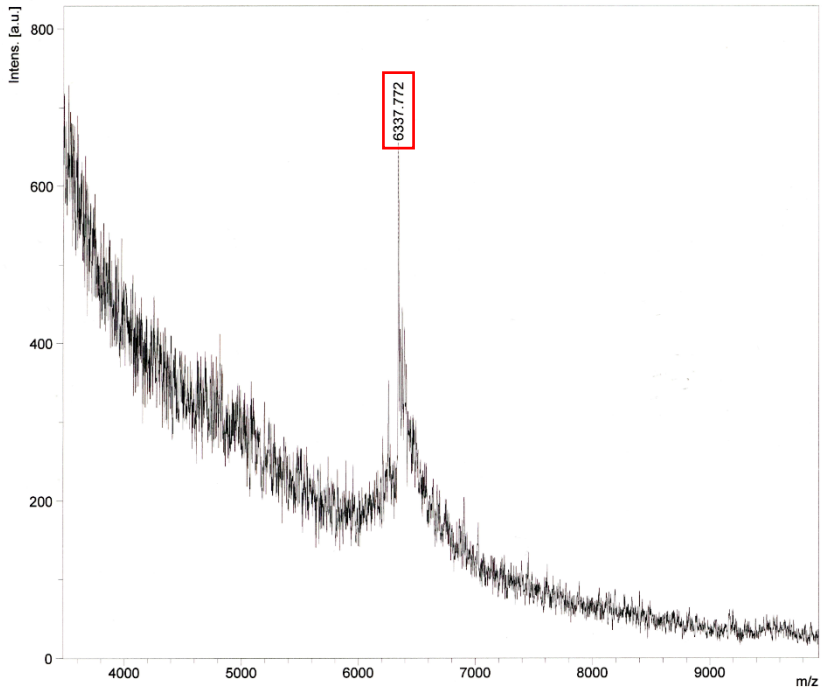

ODN**1**(Ph)-ODN**4**(Ph)

Crosslink1

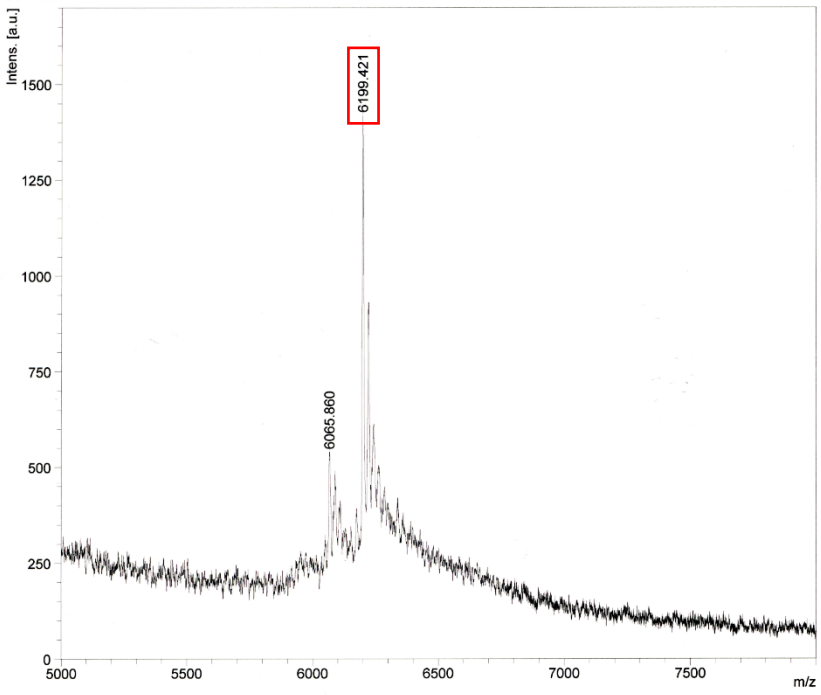

Crosslink2

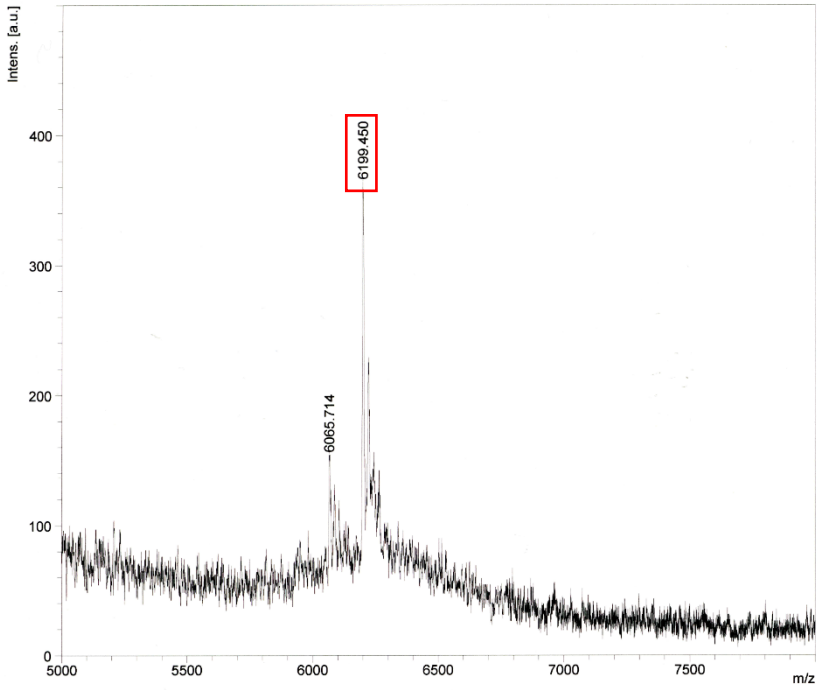

ODN**5**(Ph)-ODN**4**(Ph)

Crosslink1

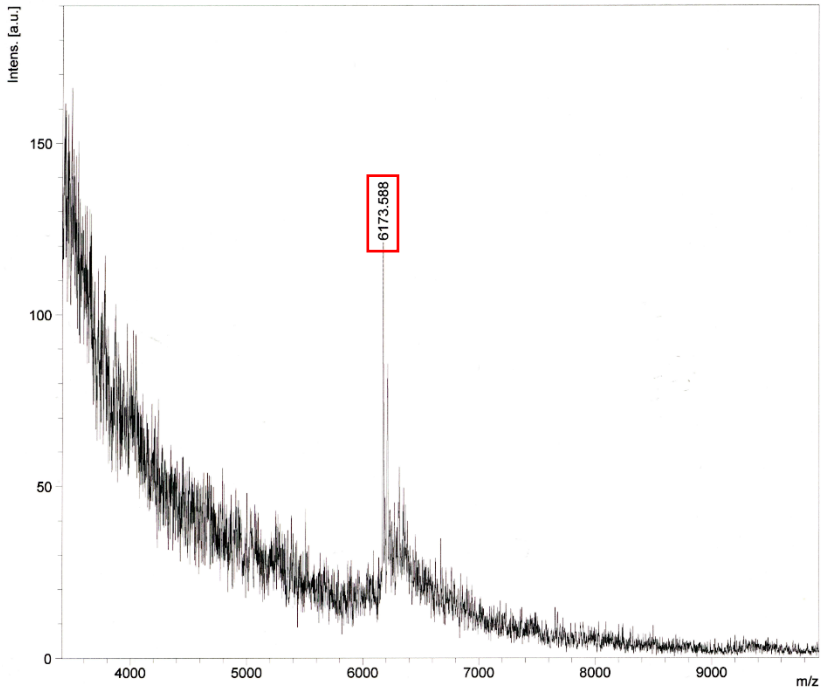

Crosslink2

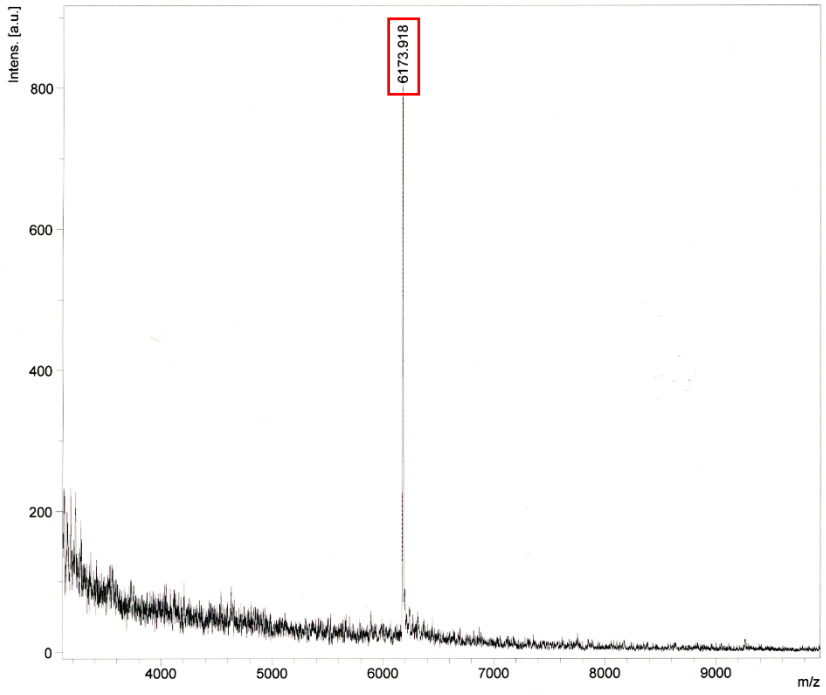

Crosslink3

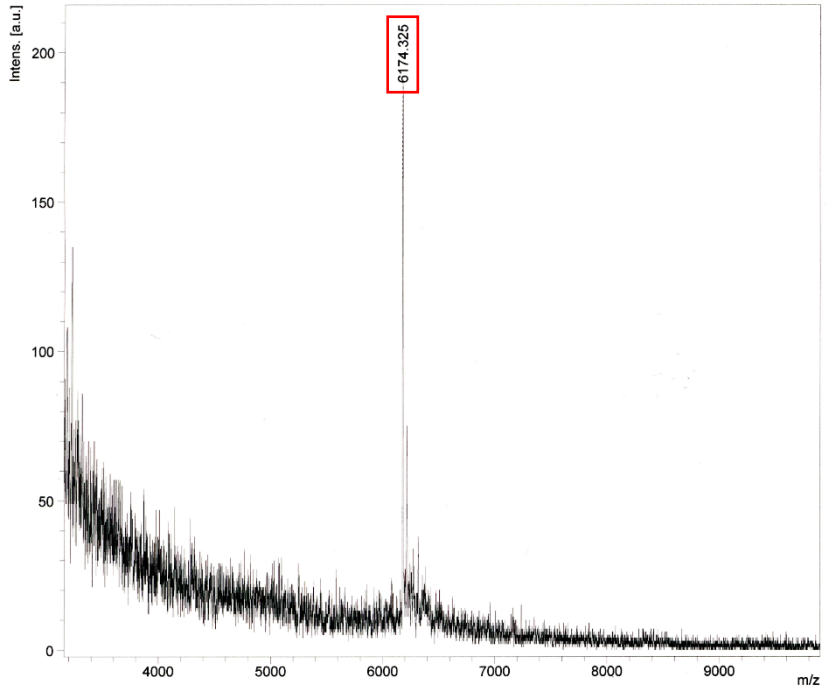

References

[1] W. H. Hudson, E. A. Ortlund, *Nat Rev Mol Cell Biol* **2014**, *15*, 749–760.

[2] R. Aebersold, M. Mann, *Nature* **2016**, *537*, 347–355.

[3] H. Ummethum, S. Hamperl, *Front Genet* **2020**, *11*, 450.

[4] C. Terada, S. Kawamoto, A. Yamayoshi, T. Yamamoto, *Pharmaceutics* **2022**, *14*, 2647.

[5] K. Kramer, T. Sachsenberg, B. M. Beckmann, S. Qamar, K. L. Boon, M. W. Hentze, O. Kohlbacher, H. Urlaub, *Nat Methods* **2014**, *11*, 1064–1070.

[6] J. W. Bae, S. C. Kwon, Y. Na, V. N. Kim, J. S. Kim, *Nat Struct Mol Biol* **2020**, *27*, 678–682.

[7] T. Malmqvist, C. Spickett, J. M. Gallo, K. Anthony, *Biol Methods Protoc* **2017**, *2*, DOI 10.1093/biomethods/bpx009.

[8] A. Panhale, F. M. Richter, F. Ramírez, M. Shvedunova, T. Manke, G. Mittler, A. Akhtar, *Nat Commun* **2019**, *10*, DOI 10.1038/s41467-019-10585-3.

[9] C. Costas, E. Yuriev, K. L. Meyer, T. S. Guion, M. M. Hanna, *Nucleic Acids Res* **2000**, *28*, 1849–1858.

[10] C. C. Smith, M. Hollenstein, C. J. Leumann, *RSC Adv* **2014**, *4*, 48228–48235.

[11] S. Kuboe, M. Yoda, A. Ogata, Y. Kitade, Y. Tomari, Y. Ueno, *Chemical Communications* **2010**, *46*, 7367–7369.

[12] H. S. Jeong, G. Hayashi, A. Okamoto, *ACS Chem Biol* **2015**, *10*, 1450–1455.

[13] F. Muttach, F. Mäsing, A. Studer, A. Rentmeister, *Chemistry - A European Journal* **2017**, *23*, 5988–5993.

[14] A. E. Arguello, A. N. Deliberto, R. E. Kleiner, *J Am Chem Soc* **2017**, *139*, 17249–17252.

[15] J. I. Perez-Perri, B. Rogell, T. Schwarzl, F. Stein, Y. Zhou, M. Rettel, A. Brosig, M. W. Hentze, *Nat Commun* **2018**, *9*, 4408.

[16] H. Luo, W. Tang, H. Liu, X. Zeng, W. S. C. Ngai, R. Gao, H. Li, R. Li, H. Zheng, J. Guo, F. Qin, G. Wang, K. Li, X. Fan, P. Zou, P. R. Chen, *Angewandte Chemie - International Edition* **2022**, *61*, e2022020.

[17] H. Luo, W. Tang, H. Liu, X. Zeng, W. S. C. Ngai, R. Gao, H. Li, R. Li, H. Zheng, J. Guo, F. Qin, G. Wang, K. Li, X. Fan, P. Zou, P. R. Chen, *Angewandte Chemie - International Edition* **2022**, *61*, DOI 10.1002/anie.202202008.

[18] M. C. Willis, B. J. Hicke, O. C. Uhienbeck, T. R. Cech, T. H. Koch, *Science (1979)* **1993**, *262*, 1255–1257.

[19] J. Dadová, P. Orság, R. Pohl, M. Brázdová, M. Fojta, M. Hocek, *Angewandte Chemie - International Edition* **2013**, *52*, 10515–10518.

[20] A. Olszewska, R. Pohl, M. Brázdová, M. Fojta, M. Hocek, *Bioconjug Chem* **2016**, *27*, 2089–2094.

[21] E. A. Raiber, G. Portella, S. Martínez Cuesta, R. Hardisty, P. Murat, Z. Li, M. Iurlaro, W. Dean, J. Spindel, D. Beraldi, Z. Liu, M. A. Dawson, W. Reik, S. Balasubramanian, *Nat Chem* **2018**, *10*, 1258–1266.

[22] S. Ji, I. Fu, S. Naldiga, H. Shao, A. K. Basu, S. Broyde, N. Y. Tretyakova, *Nucleic Acids Res* **2018**, *46*, 6455–6469.

[23] S. Ji, H. Shao, Q. Han, C. L. Seiler, N. Y. Tretyakova, *Angewandte Chemie* **2017**, *129*, 14318–14322.

[24] L. S. Runtsch, M. Stadlmeier, A. Schön, M. Müller, T. Carell, *Chemistry - A European Journal* **2021**, *27*, 12747–12752.

[25] F. Li, Y. Zhang, J. Bai, M. M. Greenberg, Z. Xi, C. Zhou, *J Am Chem Soc* **2017**, *139*, 10617–10620.

[26] M. Krömer, M. Brunderová, I. Ivancová, L. Poštová Slavětínská, M. Hocek, *Chempluschem* **2020**, *85*, 1164–1170.

[27] I. Ivancová, R. Pohl, M. Hubálek, M. Hocek, *Angewandte Chemie* **2019**, *131*, 13479–13482.

[28] D. L. Leone, R. Pohl, M. Hubálek, M. Kadeřábková, M. Krömer, V. Sýkorová, M. Hocek, *Chemistry - A European Journal* **2022**, *28*, DOI 10.1002/chem.202104208.

[29] D. L. Leone, M. Hubálek, R. Pohl, V. Sýkorová, M. Hocek, *Angewandte Chemie - International Edition* **2021**, *60*, 17383–17387.

[30] W. Dai, A. Li, N. J. Yu, T. Nguyen, R. W. Leach, M. Wühr, R. E. Kleiner, *Nat Chem Biol* **2021**, *17*, 1178–1187.

[31] Y. Liu, D. v Santi, C. T. Walsh, *PNAS* **2000**, *97*, 8263–8265.

[32] V. Khoddami, B. R. Cairns, *Nat Biotechnol* **2013**, *31*, 458–464.

[33] M. Brunderová, M. Krömer, M. Vlková, M. Hocek, *Angewandte Chemie International Edition* **2023**, DOI 10.1002/anie.202213764.

[34] K. Onizuka, Y. Yamano, A. M. Abdelhady, F. Nagatsugi, *Org Biomol Chem* **2022**, *20*, 4699–4708.

[35] S. Imoto, T. Hori, S. Hagihara, Y. Taniguchi, S. Sasaki, F. Nagatsugi, *Bioorg Med Chem Lett* **2010**, *20*, 6121–6124.

[36] S. Hagihara, S. Kusano, W. C. Lin, X. G. Chao, T. Hori, S. Imoto, F. Nagatsugi, *Bioorg Med Chem Lett* **2012**, *22*, 3870–3872.

[37] S. Hagihara, W. C. Lin, S. Kusano, X. guang Chao, T. Hori, S. Imoto, F. Nagatsugi, *ChemBioChem* **2013**, *14*, 1427–1429.

[38] F. Nagatsugi, S. Imoto, *Org Biomol Chem* **2011**, *9*, 2579–2585.

[39] A. Nishimoto, D. Jitsuzaki, K. Onizuka, Y. Taniguchi, F. Nagatsugi, S. Sasaki, *Nucleic Acids Res* **2013**, *41*, 6774–6781.

[40] K. Yamada, Y. Abe, H. Murase, Y. Ida, S. Hagihara, F. Nagatsugi, *J Org Chem* **2018**, *83*, 8851–8862.

[41] K. Hattori, T. Hirohama, S. Imoto, S. Kusano, F. Nagatsugi, *Chemical Communications* **2009**, 6463–6465.

[42] Y. Taniguchi, Y. Kurose, T. Nishioka, F. Nagatsugi, S. Sasaki, *Bioorg Med Chem* **2010**, *18*, 2894–2901.

[43] S. Kusano, T. Sakuraba, S. Hagihara, F. Nagatsugi, *Bioorg Med Chem Lett* **2012**, *22*, 6957–6961.

[44] T. Akisawa, Y. Ishizawa, F. Nagatsugi, *Molecules* **2015**, *20*, 4708–4719.

[45] S. Kusano, S. Ishiyama, S. L. Lam, T. Mashima, M. Katahira, K. Miyamoto, M. Aida, F. Nagatsugi, *Nucleic Acids Res* **2015**, *43*, 7717–7730.

[46] S. Kusano, T. Haruyama, S. Ishiyama, S. Hagihara, F. Nagatsugi, *Chemical Communications* **2014**, *50*, 3951–3954.

[47] T. Akisawa, K. Yamada, F. Nagatsugi, *Bioorg Med Chem Lett* **2016**, *26*, 5902–5906.

[48] K. Kikuta, H. Piao, J. Brazier, Y. Taniguchi, K. Onizuka, F. Nagatsugi, S. Sasaki, *Bioorg Med Chem Lett* **2015**, *25*, 3307–3310.

[49] N. Sato, G. Tsuji, Y. Sasaki, A. Usami, T. Moki, K. Onizuka, K. Yamada, F. Nagatsugi, *Chemical Communications* **2015**, *51*, 14885–14888.

[50] N. Sato, S. Takahashi, H. Tateishi-karimata, M. E. Hazemi, T. Chikuni, K. Onizuka, N. Sugimoto, F. Nagatsugi, *Org Biomol Chem* **2018**, *16*, 1436–1441.

[51] K. Onizuka, A. Usami, Y. Yamaoki, T. Kobayashi, M. E. Hazemi, T. Chikuni, N. Sato, K. Sasaki, M. Katahira, F. Nagatsugi, *Nucleic Acids Res* **2018**, *46*, 1059–1068.

[52] M. E. Hazemi, K. Onizuka, T. Kobayashi, A. Usami, N. Sato, F. Nagatsugi, *Bioorg Med Chem* **2018**, *26*, 3551–3558.

[53] K. Onizuka, M. E. Hazemi, N. Sato, G. I. Tsuji, S. Ishikawa, M. Ozawa, K. Tanno, K. Yamada, F. Nagatsugi, *Nucleic Acids Res* **2019**, *47*, 6578–6589.

[54] K. Onizuka, E. Ganbold, Y. Ma, S. Sasaki, M. E. Hazemi, Y. Chen, N. Sato, M. Ozawa, K. Nagasawa, F. Nagatsugi, *Org Biomol Chem* **2021**, *19*, 2891–2894.

[55] F. Nagatsugi, K. Onizuka, *Chem Lett* **2020**, *49*, 771–780.

[56] K. Onizuka, M. E. Hazemi, J. M. Thomas, L. R. Monteleone, K. Yamada, S. Imoto, P. A. Beal, F. Nagatsugi, *Bioorg Med Chem* **2017**, *25*, 2191–2199.

[57] K. Ichikawa, N. Kojima, Y. Hirano, T. Takebayashi, K. Kowata, Y. Komatsu, *Chemical Communications* **2012**, *48*, 2143–2145.

[58] Y. Mie, Y. Hirano, K. Kowata, A. Nakamura, M. Yasunaga, Y. Nakajima, Y. Komatsu, *Mol Ther Nucleic Acids* **2018**, *10*, 64–74.

[59] Y. Hirano, Y. Komatsu, *RSC Adv* **2022**, *12*, 24471–24477.

[60] M. I. Nejad, N. E. Price, T. Haldar, C. Lewis, Y. Wang, K. S. Gates, *ACS Chem Biol* **2019**, *14*, 1481–1489.

[61] J. Gamboa Varela, K. S. Gates, *Angewandte Chemie* **2015**, *127*, 7776–7779.

[62] N. E. Price, K. M. Johnson, J. Wang, M. I. Fekry, Y. Wang, K. S. Gates, *J Am Chem Soc* **2014**, *136*, 3483–3490.

[63] S. Dutta, G. Chowdhury, K. S. Gates, *J Am Chem Soc* **2007**, *129*, 1852–1853.

[64] K. M. Johnson, N. E. Price, J. Wang, M. I. Fekry, S. Dutta, D. R. Seiner, Y. Wang, K. S. Gates, *J Am Chem Soc* **2013**, *135*, 1015–1025.

[65] A. H. Kellum, D. Y. Qiu, M. W. Voehler, W. Martin, K. S. Gates, M. P. Stone, *Biochemistry* **2021**, *60*, 41–52.

[66] A. H. El-Sagheer, T. Brown, *Chem Soc Rev* **2010**, *39*, 1388–1405.

[67] N. Z. Fantoni, A. H. El-Sagheer, T. Brown, *Chem Rev* **2021**, *121*, 7122–7154.

[68] J. Gierlich, G. A. Burley, P. M. E. Gramlich, D. M. Hammond, T. Carell, *Org Lett* **2006**, *8*, 3639–3642.

[69] H. Peacock, O. Maydanovych, P. A. Beal, *Org Lett* **2010**, *12*, 1044–1047.

[70] K. Onizuka, A. Shibata, Y. Taniguchi, S. Sasaki, *Chemical Communications* **2011**, *47*, 5004–5006.

[71] K. Onizuka, J. G. Harrison, A. A. Ball-Jones, J. M. Ibarra-Soza, Y. Zheng, D. Ly, W. Lam, S. Mac, D. J. Tantillo, P. A. Beal, *J Am Chem Soc* **2013**, *135*, 17069–17077.

[72] P. Kočalka, A. H. El-Sagheer, T. Brown, *ChemBioChem* **2008**, *9*, 1280–1285.

[73] M. Nakane, S. Ichikawa, A. Matsuda, *Journal of Organic Chemistry* **2008**, *73*, 1842–1851.

[74] Y. Yoshimura, K. Fujimoto, *Org Lett* **2008**, *10*, 3227–3230.

[75] T. Sakamoto, Y. Tanaka, K. Fujimoto, *Org Lett* **2015**, *17*, 936–939.

[76] K. Fujimoto, S. Sasago, J. Mihara, S. Nakamura, *Org Lett* **2018**, *20*, 2802–2805.

[77] A. Shigeno, T. Sakamoto, Y. Yoshimura, K. Fujimoto, *Org Biomol Chem* **2012**, *10*, 7820–7825.

[78] K. Fujimoto, H. Yang-Chun, S. Nakamura, *Chem Asian J* **2019**, DOI 10.1002/asia.201801917.

[79] K. Fujimoto, K. Konishi-Hiratsuka, T. Sakamoto, Y. Yoshimura, *Chemical Communications* **2010**, *46*, 7545–7547.

[80] S. Nakamura, K. Ishino, K. Fujimoto, *ChemBioChem* **2020**, *21*, 3067–3070.

[81] K. Fujimoto, K. Toyosato, S. Nakamura, T. Sakamoto, *Bioorg Med Chem Lett* **2016**, *26*, 5312–5314.

[82] K. Fujimoto, M. Hashimoto, N. Watanabe, S. Nakamura, *Bioorg Med Chem Lett* **2019**, *29*, 2173–2177.

[83] K. Fujimoto, N. Watanabe, *ChemistrySelect* **2020**, *5*, 14670–14676.

[84] D. Kandatsu, K. Cervantes-Salguero, I. Kawamata, S. Hamada, S. ichiro M. Nomura, K. Fujimoto, S. Murata, *ChemBioChem* **2016**, 1118–1121.

[85] T. Gerling, H. Dietz, *Angewandte Chemie* **2019**, *58*, 2680–2684.

[86] M. M. Haque, H. Sun, S. Liu, Y. Wang, X. Peng, *Angewandte Chemie - International Edition* **2014**, *53*, 7001–7005.

[87] H. Kashida, T. Doi, T. Sakakibara, T. Hayashi, H. Asanuma, *J Am Chem Soc* **2013**, *135*, 7960–7966.

[88] T. Doi, H. Kawai, K. Murayama, H. Kashida, H. Asanuma, *Chemistry - A European Journal* **2016**, *22*, 10533–10538.

[89] Y. Kamiya, K. Iishiba, T. Doi, K. Tsuda, H. Kashida, H. Asanuma, *Biomater Sci* **2015**, *3*, 1534–1538.

[90] Y. Zhou, C. Li, J. Peng, L. Xie, L. Meng, Q. Li, J. Zhang, X. D. Li, X. Li, X. Huang, X. Li, *J Am Chem Soc* **2018**, *140*, 15859–15867.

[91] K. Onizuka, K. Ishida, E. Mano, F. Nagatsugi, *Org Lett* **2019**, *21*, 2833–2837.

[92] H. J. Shine, D.-C. Zhao, *J. Org. Chem* **1990**, *55*, 4086–4089.

[93] D. Wei, F. Liang, *Org Lett* **2016**, *18*, 5860–5863.

[94] K. M. Chan, D. K. Kölmel, S. Wang, E. T. Kool, *Angewandte Chemie* **2017**, *129*, 6597–6601.

[95] A. M. Abdelhady, Y. Hirano, K. Onizuka, H. Okamura, *Bioorg Med Chem Lett* **2021**, *48*, 128257.

[96] A. Abdelhady, K. Onizuka, K. Ishida, S. Yajima, E. Mano, F. Nagatsugi, *J Org Chem* **2022**, *87*, 2267–2276.

[97] D. P. Bartel, *Cell* **2018**, *173*, 20–51.

[98] K. N. Ivey, D. Srivastava, *Cold Spring Harb Perspect Biol* **2015**, *7*, 1–9.

[99] D. Sayed, M. Abdellatif, *Physiol Rev* **2011**, *91*, 827–887.

[100] M. Jovanovic, M. O. Hengartner, *Oncogene* **2006**, *25*, 6176–6187.

[101] Z. Su, Z. Yang, Y. Xu, Y. Chen, Q. Yu, *Oncotarget* **2015**, *6*, 8474–8490.

[102] P. Hydbring, Y. Wang, A. Fassl, X. Li, V. Matia, T. Otto, Y. J. Choi, K. E. Sweeney, J. M. Suski, H. Yin, R. L. Bogorad, S. Goel, H. Yuzugullu, K. J. Kauffman, J. Yang, C. Jin, Y. Li, D. Floris, R. Swanson, K. Ng, E. Sicinska, L. Anders, J. J. Zhao, K. Polyak, D. G. Anderson, C. Li, P. Sicinski, *Cancer Cell* **2017**, *31*, 576-590.e8.

[103] M. J. Bueno, M. Malumbres, *Biochimica et Biophysica Acta* **2011**, *1812*, 592–601.

[104] R. Garzon, G. Marcucci, C. M. Croce, *Nat Rev Drug Discov* **2010**, *9*, 775–789.

[105] S. M. Hammond, *Curr Opin Genet Dev* **2006**, *16*, 4–9.

[106] P. T. Nelson, W. X. Wang, B. W. Rajeev, *Brain Pathology* **2008**, *18*, 130–138.

[107] N. Bushati, S. M. Cohen, *Curr Opin Neurobiol* **2008**, *18*, 292–296.

[108] T. Thum, D. Catalucci, J. Bauersachs, *Cardiovasc Res* **2008**, *79*, 562–570.

[109] C. Xiao, K. Rajewsky, *Cell* **2009**, *136*, 26–36.

[110] J. F. Lima, L. Cerqueira, C. Figueiredo, C. Oliveira, N. F. Azevedo, *RNA Biol* **2018**, *15*, 338–352.

[111] K. A. Lennox, M. A. Behlke, *Pharm Res* **2010**, *27*, 1788–1799.

[112] Y. Kamiya, Y. Donoshita, H. Kamimoto, K. Murayama, J. Ariyoshi, H. Asanuma, *ChemBioChem* **2017**, *18*, 1917–1922.

[113] S. Obad, C. O. dos Santos, A. Petri, M. Heidenblad, O. Broom, C. Ruse, C. Fu, M. Lindow, J. Stenvang, E. M. Straarup, H. F. Hansen, T. Koch, D. Pappin, G. J. Hannon, S. Kauppinen, *Nat Genet* **2011**, *43*, 371–380.

[114] A. Vermeulen, B. Robertson, A. B. Dalby, W. S. Marshall, J. Karpilow, D. Leake, A. Khvorova, S. Baskerville, *RNA* **2007**, *13*, 723–730.

[115] T. Haraguchi, H. Nakano, T. Tagawa, T. Ohki, Y. Ueno, T. Yoshida, H. Iba, *Nucleic Acids Res* **2012**, *40*, e58.

[116] J. Elskens, A. Madder, *RSC Chem Biol* **2021**, *2*, 410–422.

[117] M. H. Y. S. A. K. T. Y. T. S. A. M. Asako Yamayoshi, *Nucleosides Nucleotides Nucleic Acids* **2020**, *39*, 119–130.

[118] M. Higuchi, A. Kobori, A. Yamayoshi, A. Murakami, *Bioorg Med Chem* **2009**, *17*, 475–483.

[119] Z. Qiu, L. Lu, X. Jian, C. He, *J Am Chem Soc* **2008**, *130*, 14398–14399.

[120] K. Nakamoto, Y. Ueno, *Journal of Organic Chemistry* **2014**, *79*, 2463–2472.

[121] K. Fujimoto, T. Yamaguchi, T. Inatsugi, M. Takamura, I. Ishimaru, A. Koto, S. Nakamura, *RSC Adv* **2019**, *9*, 30693–30697.

[122] K. Fujimoto, S. Sasago, J. Mihara, S. Nakamura, *Org Lett* **2018**, *20*, 2802–2805.

[123] Y. Sugihara, Y. Nakata, A. Yamayoshi, A. Murakami, A. Kobori, *Journal of Organic Chemistry* **2016**, *81*, 981–986.

[124] Q. Zhou, S. E. Rokita, *Proc Nat Acad Sci USA* **2003**, *100*, 15452–15457.

[125] E. G. N. D. L. A. M. L.L.G. Carrette, *Chem Commun* **2016**, *52*, 1539–1554.

[126] L. L. G. Carrette, E. Gyssels, J. Loncke, A. Madder, *Org Biomol Chem* **2014**, *12*, 931–935.

[127] M. op de Beeck, A. Madder, *J Am Chem Soc* **2012**, *134*, 10737–10740.

[128] M. O. de Beeck, A. Madder, *J Am Chem Soc* **2011**, *133*, 796–807.

[129] A. M. Abdelhady, Y. Hirano, K. Onizuka, H. Okamura, Y. Komatsu, F. Nagatsugi, *Curr Protoc* **2022**, e386.

[130] T. Kawasaki, F. Nagatsugi, M. M. Ali, M. Maeda, K. Sugiyama, K. Hori, S. Sasaki, *Journal of Organic Chemistry* **2005**, *70*, 14–23.

[131] B. L. Bass, *Annu Rev Biochem* **2002**, *71*, 817–846.

[132] M. M. Matthews, J. M. Thomas, Y. Zheng, K. Tran, K. J. Phelps, A. I. Scott, J. Havel, A. J. Fisher, P. A. Beal, *Nat Struct Mol Biol* **2016**, *23*, 426–433.

[133] V. Blanc, N. O. Davidson, *Journal of Biological Chemistry* **2003**, *278*, 1395–1398.

[134] S. I. Nakano, Y. Uotani, K. Uenishi, M. Fujii, N. Sugimoto, *J Am Chem Soc* **2005**, *127*, 518–519.

[135] S. I. Nakano, Y. Uotani, K. Uenishi, M. Fujii, N. Sugimoto, *Nucleic Acids Res* **2005**, *33*, 7111–7119.

[136] S. I. Nakano, H. Oka, Y. Uotani, K. Uenishi, M. Fujii, N. Sugimoto, *Biochemistry* **2009**, *48*, 11304–11311.

[137] S. I. Nakano, M. Fujii, N. Sugimoto, *J Nucleic Acids* **2011**, *2011*, 967098.

[138] H. Xiong, F. Seela, *Bioconjug Chem* **2012**, *23*, 1230–1243.

[139] S. Hentschel, J. Alzeer, T. Angelov, O. D. Schärer, N. W. Luedtke, *Angewandte Chemie - International Edition* **2012**, *51*, 3466–3469.

[140] S. Ghosh, M. M. Greenberg, *Journal of Organic Chemistry* **2014**, *79*, 5948–5957.

[141] F. Fakhari, S. E. Rokita, *Nat Commun* **2014**, *5*, 5591.

[142] T. Nishioka, I. Oshiro, K. Onizuka, Y. Taniguchi, S. Sasaki, *Chem. Pharm. Bull* **1315**, *64*, 1315–1320.

[143] M. Tera, Z. Harati Taji, N. W. Luedtke, *Angewandte Chemie* **2018**, *130*, 15631–15635.

[144] Y. Matsuyama, A. Yamayoshi, A. Kobori, A. Murakami, *Bioorg Med Chem* **2014**, *22*, 1003–1007.

[145] K. Kikuta, Y. Taniguchi, S. Sasaki, *Chem. Pharm. Bull* **2019**, *67*, 877–883.

[146] A. Rajendran, M. Endo, Y. Katsuda, K. Hidaka, H. Sugiyama, *J Am Chem Soc* **2011**, *133*, 14488–14491.

[147] T. Gerling, M. Kube, B. Kick, H. Dietz, *Sci Adv* **2018**, *4*, eaau1157.

[148] F. D. Lewis, T. Wu, E. L. Burch, D. M. Bassani, J.-S. Yang, S. Schneider, W. Jager, R. L. Letsinger, *Am. Chem. Soc* **1995**, *117*, 8785–8792.

[149] T. Doi, H. Kashida, H. Asanuma, *Org Biomol Chem* **2015**, *13*, 4430–4437.

[150] B. Holz, S. Klimasauskas, S. Serva, E. Weinhold, *Nucleic Acids Res* **1998**, *26*, 1076–1083.

[151] J. Qiu, A. Wilson, A. H. El-Sagheer, T. Brown, *Nucleic Acids Res* **2016**, *44*, 1–12.